Dissertation

Dennis Getzkow

Development and Test of an FPGA-based Readout System of a Silicon Pixel Detector with High Bandwidth

Justus-Liebig-Universität
Gießen

Development and Test of an FPGA-based Readout System of a Silicon Pixel Detector with High Bandwidth

Inauguraldissertation

zur Erlangung des Doktorgrades der Naturwissenschaften (Dr. rer. nat.)

Justus-Liebig-Universität
Fachbereich 07 - Mathematik und Informatik, Physik, Geographie

II. Physikalisches Institut
Heinrich-Buff-Ring 16
35392 Gießen

vorgelegt von

Dennis Getzkow

Dekan:	Prof. Dr. Stefan Hennemann
Gutachter:	apl. Prof. Dr. Jens Sören Lange
Gutachterin:	Prof. Dr. Claudia Höhne

Selbstständigkeitserklärung

Ich erkläre: Ich habe die vorgelegte Dissertation selbständig und ohne unerlaubte fremde Hilfe und nur mit den Hilfen angefertigt, die ich in der Dissertation angegeben habe. Alle Textstellen, die wörtlich oder sinngemäß aus veröffentlichten Schriften entnommen sind, und alle Angaben, die auf mündlichen Auskünften beruhen, sind als solche kenntlich gemacht. Bei den von mir durchgeführten und in der Dissertation erwähnten Untersuchungen habe ich die Grundsätze guter wissenschaftlicher Praxis, wie sie in der „Satzung der Justus-Liebig-Universität Gießen zur Sicherung guter wissenschaftlicher Praxis“ niedergelegt sind, eingehalten.[1]

Datum

Unterschrift

[1] Der Wortlaut der Erklärung wurde der Promotionsordnung [1, S. 15] entnommen.

Zusammenfassung

Das Online Selection Nodes (ONSEN)-System ist Teil der Datenverarbeitung des Belle II Experiments und basiert auf FPGA-Technologien. Es filtert bzw. reduziert die Daten eines neuartigen Pixeldetektors (PXD) in Echtzeit. Der PXD ist der Teil des Belle II Detektors mit der geringsten Nähe zum Kollisionspunkt des Elektron-Positron-Beschleunigers SuperKEKB.

Die erwartete Datenrate (PXD nach ONSEN) beträgt bis zu 20 GB/s, was eine Datenselektion erforderlich macht. Daher werden Regionen-von-Interesse (RoIs) auf den sensitiven Bereichen des PXD durch die Systeme HLT und DATCON ermittelt. PXD-Daten außerhalb von RoIs werden von ONSEN verworfen. Das ONSEN reduziert die Datenrate somit voraussichtlich um Faktor ~ 30 durch Berücksichtigung der RoIs (Faktor 10) und Verwerfung kompletter Events (Faktor 3).

Ein Schwerpunkt dieser Arbeit lag auf Tests der ONSEN-Datenverarbeitung. Von besonderem Interesse waren dabei Bedingungen, die zu einer fehlerhaften Datenverarbeitung führen könnten. In Testkampagnen, die 2016 und 2017 am DESY durchgeführt wurden, wurden u.a. unerwartete Temperaturabhängigkeiten und fehlerhaftes Verhalten bei der Verarbeitung invalider Daten beobachtet. Die Erkenntnisse aus den Tests wurden von den ONSEN-Entwicklern für Firmwareoptimierungen genutzt, um eine stabile Datenerfassung und -verarbeitung am KEK, dem Standort des Belle II Detektors, zu gewährleisten.

Daten der Testkampagne am DESY von 2017 wurden ebenfalls untersucht. Anhand von 5 Millionen Events (genommen mit Elektronenstrahl (3 GeV) und Magnetfeld (1 T)) wurde ein ONSEN-Pixeldatenreduktionsfaktor von 10,38 ermittelt, mit bis zu drei RoIs auf jeder der beiden für diese Tests verfügbaren PXD-Modulen und ohne Event-Verwerfung. Die Abweichung zwischen Pixelzeilen- und -spaltenkoordinaten und den entsprechenden RoI-Zentren in Zeilen- und Spaltenrichtung betrug $\sim 0{,}64$ Pixel mit $\sigma \approx 3{,}41$ Pixel (Spalten, Modul der inneren PXD-Schicht), $\sim 0{,}92$ Pixel mit $\sigma \approx 1{,}22$ Pixel (Zeilen, Modul der inneren PXD-Schicht), $\sim 2{,}23$ Pixel mit $\sigma \approx 0{,}90$ Pixel (Spalten, Modul der äußeren PXD-Schicht) und $\sim 0{,}16$ Pixel mit $\sigma \approx 0{,}69$ Pixel (Zeilen, Modul der äußeren PXD-Schicht).

Eine ONSEN-interne RoI-Verteilung wurde entwickelt und mit einer für Testzwecke angepassten Firmware getestet. Im Zeitrahmen dieser Arbeit wurde das ONSEN in die Belle II Datenerfassungssysteme am KEK integriert. Dadurch konnte die Verteilung mit Triggerraten von bis zu 20 kHz am KEK erfolgreich getestet werden. Andere Firmware-Anpassungen konzentrierten sich auf die Verarbeitung von fehlerhaften, sowie von HLT-verworfenen Events.

Abstract

The Online Selection Nodes (ONSEN) system is part of Belle II data acquisition and is based on FPGA technologies. It filters and reduces the recorded data from a novel Belle II Pixel Detector (PXD) in real time. The PXD is the part of the Belle II detector with the least proximity to the interaction point of the electron-positron collider SuperKEKB.

The expected data rate (PXD to ONSEN) is up to 20 GB/s in total which makes data selection necessary. Therefore, Regions of Interest (RoIs) on the sensitive areas of the PXD are determined by the systems HLT and DATCON. PXD data outside any RoIs is discarded by the ONSEN. The ONSEN is expected to reduce the data rate by a factor $\sim$ 30 by applying RoIs (factor 10) and the rejection of complete events (factor 3).

One focus of this work was on ONSEN data processing tests. Of particular interest were conditions which could lead to incorrect data processing. In test campaigns carried out at DESY in 2016 and 2017, unexpected temperature dependencies and incorrect behaviour in case of invalid data input were observed, among others. The results from the tests were used by the ONSEN developers for firmware optimisations to ensure stable data acquisition and processing at KEK, where the Belle II detector is located.

Data of the test campaign at DESY from 2017 was also analysed. Using a sample of 5 million events (collected with electron beam (3 GeV) and magnetic field (1 T)), the ONSEN pixel data reduction factor was found to be 10.38 with up to three RoIs on each of the two PXD modules available for these tests and w/o event rejection. The deviation between the pixel row and column coordinates and the corresponding RoI centres in row and column direction were found to be $\sim$ 0.64 pixel with $\sigma \approx$ 3.41 pixel (columns, inner PXD layer), $\sim$ 0.92 pixel with $\sigma \approx$ 1.22 pixel (rows, inner PXD layer), $\sim$ 2.23 pixel with $\sigma \approx$ 0.90 pixel (columns, outer PXD layer) and $\sim$ 0.16 pixel with $\sigma \approx$ 0.69 pixel (rows, outer PXD layer).

An ONSEN-internal RoI distribution was developed and tested using firmware adapted for the tests. At the time of this work, the ONSEN was integrated into the Belle II data acquisition systems at KEK. The distribution feature could therefore be successfully tested at trigger rates of up to 20 kHz at KEK. Other firmware adjustments addressed processing of faulty events and handling of events rejected by the HLT system.

Contents

Chapter 1

Motivation

There are many challenges for particle physicists. The Standard Model of particle physics was verified in many aspects by numerous experiments in the last decades. However, in recent years many particles have been discovered which were not covered by Standard Model predictions. The model also lacks an explanation for the matter-antimatter asymmetry in the universe or how Dark Matter and Dark Energy interact with ordinary matter. Addressing those and other questions requires huge efforts from several collaborations worldwide, including the Belle II collaboration.

Belle II predecessor Belle accumulated a data sample with an integrated luminosity of 1,041 fb^{-1} from asymmetric electron-positron collisions at the KEKB collider (Tsukuba, Japan) during one decade of operation [2]. As modern challenges in particle physics require state-of-the-art particle detection and vertex resolution, the Belle detector was decommissioned in 2010 [2] to make way for the construction of its successor.

The Belle II detector consists of several subdetectors, inter alia, a novel silicon Pixel Detector (PXD) situated closely to the interaction point. Various subdetector and data acquisition (DAQ) upgrades were implemented. The KEKB collider was upgraded to the SuperKEKB collider. It adopted a nanobeam collision scheme which is discussed in more detail in section 3.3. The nanobeam collision scheme enables to achieve an unprecedented level of luminosity and thus state-of-the-art physics data generation and accumulation. Details about that can be found in the comprehensive *Belle II Technical Design Report* [3], among others.

The PXD is expected to operate with output data rates of up to 20 GB/s [4]. The large volume of data makes data selection a necessity. The Belle II team at Justus-Liebig-University (JLU) has contributed to this by developing and testing a dedicated system for this purpose based on Field Programmable Gate Arrays (FPGAs): the Online Selection Nodes (ONSEN).

The ONSEN filters the PXD data based on Regions of Interest (RoIs), areas on the sensitive area of the PXD modules. The RoIs are determined by two independent systems: the High Level Trigger (HLT) and the Data Acquisition Tracking Concentrator Online Node (DATCON). Both systems perform track extrapolation and determine PXD data which must be stored for physics analyses. All data not covered by at least one Region of Interest is considered irrelevant for physics analyses (background data) and therefore is discarded by ONSEN. The RoI approach alone is expected to achieve a data reduction factor of 10 [5]. An additional rejection of two out of three events is expected, thus, the total data reduction factor is 30 [4].

The ONSEN had to be thoroughly tested before integration into the DAQ systems at the High Energy Accelerator Research Organization (KEK) in Tsukuba, Japan. The tests were mainly carried out at JLU. Systems like HLT (RoI source), event-builder-2 (EB2) (receiver of ONSEN data) and Data Handling Hub (DHH) (forwards zero-suppressed PXD data to ONSEN) were not available at JLU. Therefore, the tests carried out at the JLU laboratories made use of the ONSEN system and commercially available PCs as substitutes for systems which were not available. Tests to verify proper data readout and processing including the actual (but scaled-down) Belle II DAQ systems were carried out in several test campaigns at the Deutsches Elektronen-Synchrotron (DESY) and KEK.

The work on this thesis contributed to the firmware development and testing of the ONSEN at JLU, DESY and KEK. The firmware development addressed optimisations of the distribution of RoIs in ONSEN and processing of faulty or rejected data.

Note that this thesis has a similar structure and introductions to particle physics, the ONSEN etc. as dissertations like *Development of FPGA-Based Algorithms for the Data Acquisition of the Belle II Pixel Detector* [6] and *Development of the Online Data Reduction System and Feasibility Studies of 6-Layer Tracking for the Belle II Pixel Detector* [7] which were written by students from the same Belle II research group at JLU I was a member of while working on this thesis.

Chapter 2

Physics Introduction

2.1 Standard Model of Particle Physics

The Standard Model (SM) of particle physics is a fascinating subject of modern science. The term "particle zoo" is often used for the time period in the mid-20th century when physicists had to face a variety of particles with different properties. The theory of a SM – which assumes just a few elementary particles – was an approach to explain the observations. As of now, the SM is the most suitable theory in particle physics for the description of elementary particles and interactions between them.

The SM provides good explanations for observations in particle physics but there are still blind spots. Those become clear, for example, when it comes to explaining the matter-antimatter asymmetry in the universe, or which processes or particles are involved in the interactions of Dark Matter and Dark Energy with ordinary matter. Although many particles can be well described with SM elementary particles and interactions, observations of particles and phenomena not predicted by the SM are yet to be understood.

The following sections will provide a brief overview of the SM particles and their interactions. The introduction of particle physics in this chapter refers mainly to basic topics covered in various textbooks. Thus, more comprehensive introductions to particle physics and the corresponding history can be found in textbooks like *Elementare Teilchen* [8] (in German; author: J. Bleck-Neuhaus) and *Particles and Nuclei* [9] (in English; authors: B. Povh, K. Rith, C. Scholz and F. Zetsche).

In chapter 3, the focus will shift to the Belle II experiment and to a selection of physics topics that will be addressed by it.

2.2 Quarks

In the early 20th century the constituents of "normal" matter, thus matter we can see with the naked eye, were already discovered to be the proton (p), the neutron (n) and the electron (e^-). Naively one might assume that p and n are elementary particles as they form the atomic nuclei but this is not the case. In the last century, it became evident that p and n are actually composed of other particles and therefore cannot be elementary particles on their own. Instead, the elementary particles are the point-like quarks.

Overview of Quark Properties						
	Generation					
	First		Second		Third	
Name	Up	Down	Strange	Charm	Bottom	Top
Symbol	u	d	s	c	b	t
Mass in [MeV] (u,d,s)/ [GeV] (c,b,t)	$2.16^{+0.49}_{-0.26}$	$4.67^{+0.48}_{-0.17}$	$93.4^{+8.6}_{-3.4}$	1.27 ± 0.02	$4.18^{+0.03}_{-0.02}$	172.69 ± 0.30
Electric Charge in [e]	$2/3$	$-1/3$	$-1/3$	$2/3$	$-1/3$	$2/3$
I_Z	$+1/2$	$-1/2$	0	0	0	0
Strangeness	0	0	-1	0	0	0
Charm	0	0	0	$+1$	0	0
Bottom	0	0	0	0	-1	0
Top	0	0	0	0	0	$+1$

Table 2.1: Properties of the six Standard Model quarks as listed in *Review of Particle Physics* [12, p. 32].

The concept of quarks was introduced by M. Gell-Mann in *A Schematic Model of Baryons and Mesons* [10] and G. Zweig in *An SU_3 Model for strong Interaction Symmetry and its breaking*[1] [11] at about the same time in 1964. Today, six flavours of quarks are known. They can be separated into three families or generations each consisting of two quarks with specific flavours. Quarks of the first generation form ordinary matter. Thus, for example, the p constituents are two up- (u) and one down-quark (d) while the n consists of two down- and one up-quark. The strange (s) and charm (c) quarks are categorized to the second generation while the third generation includes the heaviest quarks, the bottom (b) and top (t) quarks. All quarks are fermions, thus, they carry spin $\pm 1/2$.

An overview of the properties of the six quark flavours as provided in *Review of Particle Physics* [12, p. 32] is given in table 2.1. As stated there, a particular quantum number is assigned to each quark corresponding to its flavour. The first generation is an exception for historical reasons: up and down quarks carry isospin $I = 1/2$ and $I_z = \pm 1/2$. The flavour quantum numbers of the remaining four quarks are strangeness ($S = -1$ for s-quarks), charm ($C = +1$ for c-quarks), bottom ($B = -1$ for b-quarks) and top ($T = +1$ for t-quarks).

Quarks are sensitive to strong, electromagnetic and weak forces. They carry electric charge of $-1/3\,e$ or $+2/3\,e$. Accordingly, antiquarks carry an electric charge of $+1/3\,e$ or $-2/3\,e$. Systems made of (anti-)quarks always carry zero or integer electric charge ($0\,e$, $\pm 1\,e$, ...).

As explained in Ref. [10], quark systems can be mesons or baryons. The mesons are

[1] G. Zweig used the name "aces" for the concept.

made of an even number of quarks, antiquarks or a combination of both. Baryons on the other hand are always composed of an odd number of (anti-)quarks. Thus, the constituents of mesons and baryons are at least two and three (anti-)quarks, respectively, but are not limited to those numbers. In recent years, several particles were observed which might be mesons or baryons made of more than the minimum number of (anti-)quarks. Examples for those are discussed in section 3.2.1.

2.3 Leptons

Leptons are another type of elementary fermions. Unlike quarks, leptons do not couple to the strong force. However, all leptons are sensitive to weak interactions. They carry zero or integer electric charge of $-1\,\mathrm{e}$ while the corresponding antiparticles carry opposite electric charge. Leptons with non-zero electric charge are also sensitive to electromagnetic interactions.

Leptons can be categorized into three generations like the quarks. The elementary leptons of the first generation are the electron (e^-, another part of ordinary matter) and the electric neutral ($0\,\mathrm{e}$) electron neutrino ν_e. The constituents of the second and third generation, respectively, are the muon (μ^-) and the tau (τ^-) and their corresponding electric neutral neutrinos ν_μ and ν_τ. The properties of the elementary leptons are listed in table 2.2[2].

It should be noted that neutrinos have very low but non-zero masses. This was proven in 1998 when the Super-Kamiokande collaboration reported an observation consistent with $\nu_\mu \leftrightarrow \nu_\tau$ oscillations and a non-vanishing squared mass difference of neutrino mass eigenstates in *Evidence for Oscillation of Atmospheric Neutrinos* [13]. This was awarded the Nobel Prize in 2015 [14].

[2]Note that Ref. [12, pp. 1274-1275] lists masses for $\overline{\nu}_e$ and ν_e. For the latter there are two values available in the reference. Table 2.2 lists the value with 95% confidence level. The listed $\overline{\nu}_e$ mass is just $< 1.1\,\mathrm{eV}$. There is no distinction between the other (anti-)neutrino masses.

Overview of Lepton Properties						
	Generation					
	First		Second		Third	
Name	Electron	Electron-Neutrino	Muon	Muon-Neutrino	Tau	Tau-Neutrino
Symbol	e^-	ν_e	μ^-	ν_μ	τ^-	ν_τ
Mass in [MeV] except ν_e: [eV]	≈ 0.511	<225	≈ 105.658	<0.19	1776.86	<18.2
Electric Charge in [e]	-1	$< 4 \times 10^{-35}$	-1	$< 4 \times 10^{-35}$	-1	$< 4 \times 10^{-35}$

Table 2.2: Properties of the six Standard Model leptons. Source for e^-, μ^- and τ^- masses: *Review of Particle Physics* [12, pp. 1239-1240, 1245], source for neutrino properties: [12, pp. 1274-1275, 1278]. In this table rounded mass values are shown. For more accurate values incl. uncertainties the reader is referred to Ref. [12]. Note that listings in Ref. [12, pp. 1274-1275] distinguish between the ν_e and $\overline{\nu}_e$ masses.

2.4 Number of Generations

In the last sections the three generations of quarks and leptons were discussed. The number of lepton flavours can be derived from the decay width of the Z^0 boson (see section 2.5.2). The decay width has been determined in Large Electron Positron Collider (LEP) experiments which lead to the number of light neutrinos $N_\nu = 2.9840 \pm 0.0082$ as reported in *Precision Electroweak Measurements on the Z Resonance* [15]. Further studies on the Bhabha cross section at LEP in Ref. [16] even resulted in $N_\nu = 2.9963 \pm 0.0074$[3]. Those results are consistent with a number of generations of three as stated above. Thus, there is no indication for a fourth light neutrino and therefore for no indication for a fourth light lepton generation as well.

Assuming that the number of quark generations is the same as the number of lepton generations leads to the conclusion that the number of quark generations is confirmed by the number of light neutrinos as well. However, the existence of a (heavy) fourth quark or lepton generation might be unlikely as of now but it is not excluded. Therefore searches for such a fourth generation are subject of research. *Review of Particle Physics* [12, pp. 1337-1340] lists the mass limits for a possibly existing fourth quark generation (b' and t'). It is worth mentioning that most limits are well above 100 GeV or even 1,000 GeV.

[3]The results mentioned here as well as other results are also discussed / listed e.g. in Ref. [12, pp. 1282-1284].

2.5 Standard Model Interactions

2.5.1 Strong Interactions

Bound systems like the p exist because of the strong interaction between its constituents (quarks). The strong force is mediated by the massless boson gluon (g), which carries both a colour and an anticolour charge. (Anti-)quarks also carry (anti-)colour and therefore gluons can couple to the (anti-)colour of (anti-)quarks and also to other gluons. One can distinguish between three colours, for example red, blue and green. The corresponding anticolours are anti-red, anti-blue and anti-green.

When all (anti-)colours are combined, the result is colourlessness. Particles composed of quarks are always colourless. For example, a J/ψ ($c\overline{c}$) consists of a c with a certain colour and a $\overline{c}$ with the corresponding anticolour. A particle with colour cannot be observed as a single particle. Thus, as soon as the $c\overline{c}$ pair gets separated, the colourlessness is maintained by additional (anti-)quarks with proper (anti-)colours. Eventually one would end up with two separate and colourless mesons. This property of carriers of (anti-)colour charge is called *confinement*.

Colourless systems can also be made of baryons. As stated in section 2.2 baryons are composed of an odd number of (anti-)quarks (at least three of them). A baryon composed of three quarks would carry all three colours and therefore would be colourless. Examples for such baryons are the p and n. Their corresponding antiparticles, the antiproton ($\overline{p}$) and the antineutron ($\overline{n}$), carry anticolour instead of colour and therefore are colourless as well. Systems with more than three (anti-)quarks are subject of research and will be briefly discussed in section 3.2.1. A possible combination of colours in a system composed of two quarks and two antiquarks could be green, anti-green, red and anti-red. Similarly, the constituents of a system of five quarks could carry the colours red, green, blue, red and anti-red.

2.5.2 Electromagnetic and Weak Interactions

The massless photon (γ) is the mediator of the electromagnetic force even though it does not carry electric charge. Carrier of electric charge can participate in electromagnetic interactions, thus, the photon can couple to quarks, e^-, μ^-, τ^-, their antiparticles and the $W^\pm$ bosons, mediators of weak interactions.

Besides the electric charged $W^\pm$ bosons, the electric neutral Z^0 boson is another mediator of weak interactions. $W^\pm$ and Z^0 bosons carry mass which limits the range of the force significantly. Weak interactions affect also neutrinos and can change the flavour of quarks. The interaction violates parity P, charge-conjugation C as well as the combination charge-conjugation parity (CP). This is discussed in section 2.6.

The properties of the elementary bosons as listed in Ref. [12] are shown in table 2.3.

Overview of Elementary Boson Properties					
	Interactions				
	Electro-magnetic	Weak		Strong	Higgs Mechanism
Name	Photon	$W^{\pm}$ Boson	Z^0 Boson	Gluon	Higgs Boson
Symbol	γ	$W^{\pm}$	Z^0	g	H^0
Mass	$< 10^{-18}$ eV	80.377 ± 0.012 GeV	91.1876 ± 0.0021 GeV	0 eV	125.25 ± 0.17 Gev
Electric Charge in [e]	$< 10^{-35}$	±1	0	0	0

Table 2.3: Properties of the SM gauge bosons and the Higgs boson. Source for boson properties: *Review of Particle Physics* [12, pp. 1141-1143, 1156, 1175]

2.5.3 Higgs Boson

The mass of particles (for example the $W^{\pm}$ and Z bosons) can be explained by a certain mechanism which also implies the existence of an observable boson. In 2012, the discovery of the Higgs boson was reported by the Large Hadron collider (LHC) experiments CMS and Atlas in *Observation of a new boson at a mass of 125 GeV with the CMS experiment at the LHC* [17] and in *Observation of a new particle in the search for the Standard Model Higgs boson with the ATLAS detector at the LHC* [18] after extensive searches.

The theory behind this mechanism was already introduced in the 1960s by F. Englert and R. Brout in *Broken Symmetry and the Mass of Gauge Vector Mesons* [19] and P. Higgs in *Broken Symmetries and the Masses of Gauge Bosons* [20] independently of each other as stated in Nobel Prize announcement [21]. F. Englert and P. Higgs were awarded the Nobel Prize in 2013, shortly after the discovery of the Higgs boson [22]. The properties of the boson are listed in table 2.3 (see column "Higgs Mechanism").

2.6 CP Violation

2.6.1 Overview

The parity P (space mirroring), charge-conjugation C (transformation from one particle to its antiparticle) as well as the combination of both, the CP symmetry, is not conserved in weak interactions.

In the following, a brief history of those symmetry violations will be provided as an overview. The publications (from Gell-Mann and Pais, Lee and Yang, Wu, and Christenson, Cronin, Fitch and Turlay) and Nobel Prizes mentioned in the following,

were identified using information provided in textbook Ref. [8, pp. 535-559] where a more comprehensive overview can be found. The topic is continued in section 3.2.3.

2.6.2 History

In 1954, M. Gell-Mann and A. Pais discussed in *Behavior of Neutral Particles under Charge Conjugation* [23] the neutral kaon[4]. They addressed phenomena which, as we now today, involved the s quark[5]. They explained that the virtual transition $K^0 \leftrightarrow \overline{K^0}$ might be possible due to weak interactions. They also explained that K^0 might be a mixture consisting of two parts with different decay modes and different lifetimes.

As we know today, there are two mass eigenstates of the K^0 which can be distinguished: the short living K_S^0 (K-short; $\tau_{K_S^0} \approx 0.9 \cdot 10^{-10}$ s) the long living K_L^0 (K-long; $\tau_{K_L} \approx 5 \cdot 10^{-8}$ s). The mass difference Δm of the mass eigenstates is in the order of 10^{-12} MeV. The K^0-decay into two or three pions can be understood as $K_S^0 \to \pi\pi$ with CP eigenvalue +1, and $K_L^0 \to \pi\pi\pi$ with CP eigenvalue −1, respectively. The information about the neutral Kaon properties were taken from Ref. [12, pp. 40-41].

In 1956, T.D. Lee and C.N. Yang had proposed several experiments in *Question of Parity Conservation in Weak Interactions* [24] to test the parity conservation. Shortly after that, results published in *Experimental Test of Parity Conservation in Beta Decay* [25] (C. S. Wu et. al., 1957) indicated that weak interactions in β decays of polarized cobalt-60 violate P and C conservations. T.D. Lee and C.N. Yang were awarded the Nobel Prize in 1957 [26].

In 1964, the observation of the decay $K_L^0 \to \pi\pi$ and thus a violation of CP symmetry in K_L^0 decay was reported by J.H. Christenson, J.W. Cronin, V.L. Fitch and R. Turlay in *Evidence for the* 2π *Decay of the* K_2^0 *Meson* [27]. This decay occurs rarely with $\Gamma_i/\Gamma \sim 10^{-3}$ [12, p. 41] and showed that K_L^0[6] is not a pure CP eigenstate [27]. J.W. Cronin and V.L. Fitch were awarded the Nobel Prize in 1980 [28].

CP violating processes are still subject of research. Even though more than 50 years have passed since the publications mentioned in this section. In experiments such as Belle II, the analysis of CP violating processes is continued.

2.7 The CKM Matrix

Weak interactions can change the quark flavour. The probability for a certain quark flavour to transit into another is described by the Cabibbo-Kobayashi-Maskawa

[4] In Ref. [23] it is not called K^0. Instead the authors used the term θ^0 for the particle. In this work I will use names as commonly used today.

[5] Reminder: the introduction of quarks by M. Gell-Mann was in 1964 [10].

[6] In Ref. [27] referred to as K_2^0

(CKM) matrix. For example, the probability of a transition of $u \rightarrow d$ (up to down quark) in weak interactions is described by $|V_{ud}|^2$.

The underlying theory was discussed by M. Kobayashi and T. Maskawa in *CP-Violation in the Renormalizable Theory of Weak Interaction* [29]. The discussion of CP violation included a model that assumed three generations of quarks as early as 1973 – even though only three quarks (u, d and s) had been discovered at that time. In 2008, M. Kobayashi and T. Maskawa were awarded the Nobel Prize [30].

According to Ref. [12, pp. 261-267], the CKM matrix can be written as:

$$V_{CKM} = \begin{pmatrix} 1 - \lambda^2/2 & \lambda & A\lambda^3(\rho - i\eta) \\ -\lambda & 1 - \lambda^2/2 & A\lambda^2 \\ A\lambda^3(1 - \rho - i\eta) & -A\lambda^2 & 1 \end{pmatrix} + O(\lambda^4) \tag{2.1}$$

$$= \begin{pmatrix} V_{ud} & V_{us} & V_{ub} \\ V_{cd} & V_{cs} & V_{cb} \\ V_{td} & V_{ts} & V_{tb} \end{pmatrix} \tag{2.2}$$

$$|V_{CKM}| = \begin{pmatrix} 0.97435 \pm 0.00016 & 0.22500 \pm 0.00067 & 0.00369 \pm 0.00011 \\ 0.22486 \pm 0.00067 & 0.97349 \pm 0.00016 & 0.04182^{+0.00085}_{-0.00074} \\ 0.00857^{+0.00020}_{-0.00018} & 0.04110^{+0.00083}_{-0.00072} & 0.999118^{+0.000031}_{-0.000036} \end{pmatrix} \tag{2.3}$$

Equation 2.1 represents the Wolfenstein parametrization of the matrix. This was introduced in *Parametrization of the Kobayashi-Maskawa Matrix* [31].

The diagonal entries $|V_{ud}|$, $|V_{cs}|$ and $|V_{tb}|$ indicate that transitions between quarks of the same generation are the most likely ones. As clearly visible in the Wolfenstein parametrization, the CKM elements contain complex numbers. The phases of those numbers enable CP violations in the SM.

The CKM matrix is unitary ($VV^\dagger = 1$) which results in nine independent equations, including

$$V_{ud}^* V_{ub} + V_{cd}^* V_{cb} + V_{td}^* V_{tb} = 0$$

as the most relevant one for B physics [32, p. 115].

The CKM matrix can be visualized as a triangle with the angles shown in the following [12, p. 264]:

$$\beta = \phi_1 = \arg\left(-\frac{V_{cd}V_{cb}^*}{V_{td}V_{tb}^*}\right)$$

$$\alpha = \phi_2 = \arg\left(-\frac{V_{td}V_{tb}^*}{V_{ud}V_{ub}^*}\right)$$

$$\gamma = \phi_3 = \arg\left(-\frac{V_{ud}V_{ub}^*}{V_{cd}V_{cb}^*}\right)$$

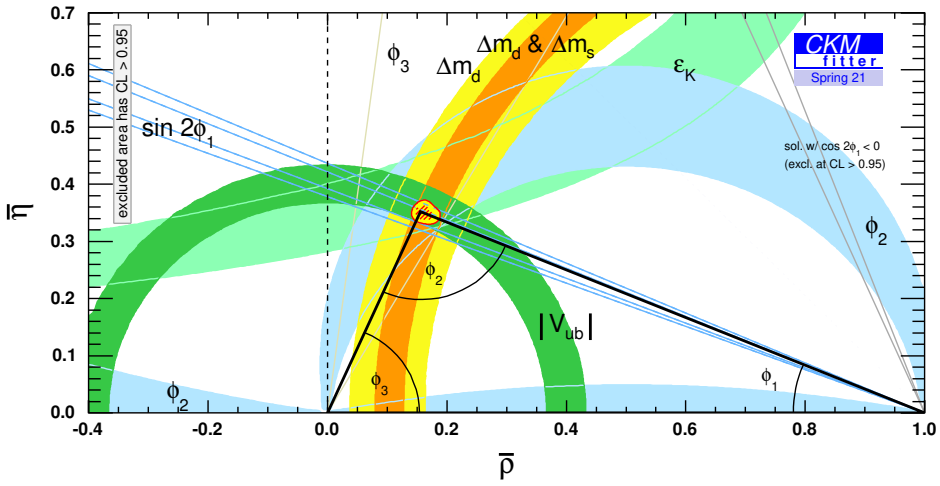

Figure 2.1: Unitarity Triangle in $\overline{\rho}-\overline{\eta}$ plane in ϕ_1, ϕ_2, ϕ_3 convention. Figure source: *CKMfitter* [33]

A possible way of presentation of this unitarity triangle is shown in figure 2.1. It represents the $\overline{\rho}-\overline{\eta}$ plane with

$$\overline{\rho}+i\overline{\eta} = -\frac{V_{ud}V_{ub}^*}{V_{cd}V_{cb}^*}$$
$$1-(\overline{\rho}+i\overline{\eta}) = -\frac{V_{td}V_{tb}^*}{V_{cd}V_{cb}^*},$$

as stated in Ref. [32, p. 115].

Improving the accuracy of ϕ_1, ϕ_2 and ϕ_3 is currently subject of research. In section 3.2.4 the determination of the angles is briefly discussed.

Chapter 3

The Belle II Experiment

3.1 Overview

The Belle II experiment, located at the KEK in Tsukuba, Japan, addresses important questions in the field of particle physics. Data needed for this purpose is collected by the Belle II detector which is situated around the interaction point (IP) of the SuperKEKB electron-positron collider.

The operation of predecessor experiment Belle ended in June 2010 [2]. In 2018, after several years of preparation, the first collision runs for Belle II were performed with a near-final Belle II detector setup. The total integrated luminosity recorded so far is listed on Confluence page [34]. According to that, a total integrated luminosity of 427.79 fb^{-1} was recorded until August 2022, just before a long shutdown. It is expected that a total integrated luminosity of 50 ab^{-1} will be accumulated [35].

The detector operation and data analyses are carried out by dedicated collaborators from all over the world. The Belle II research group at JLU, Gießen, is one of the collaborating groups.

Section 3.2 will provide a selection of physics topics relevant for Belle II . After that, the focus will be on the SuperKEKB collider, the Belle II detector components and its DAQ systems.

3.2 Belle II Physics Program

The Belle II Physics Book [32] covers the Belle II physics program in detail and provides information about simulations, "golden" decay modes, machine parameters of the detector etc. The following is just a selection of information to give a brief introduction to the topic.

There are two approaches to collect data for particle physics experiments as stated in Ref. [32, pp. 18-19]. The first one is collecting data at very high energies – the "energy frontier" – which is the approach of experiments at the proton-proton collider LHC which operates at centre-of-mass energies of up to 14 TeV. The Belle II experiment follows the second approach by collecting data at the "intensity frontier".

SuperKEKB operates near the $\Upsilon(4S)$ resonance (see e.g. Ref. [35]) which is just above the $B\overline{B}$ threshold ($m_{B^0} \approx 5.28\,\text{GeV}$, $m_{\Upsilon(4S)} \approx 10.58\,\text{GeV}$ [12, pp. 59, 85]). Thus,

$B\overline{B}$ meson pairs are the primary decay products (> 96%, [12, p. 85]). Those decays are interesting in terms of CP violation as discussed in section 3.2.3.

In general, as summarised in Ref. [32, pp. 20-21], Belle II addresses flavour and non-flavour physics topics. These include the search for connections of the SM to Dark Matter, which may help to discover Dark Matter particles, gauge bosons or symmetries. Belle II data will contribute to the improvement of the accuracy of, for example, the elements of the CKM matrix and the angles of the unitarity triangle. The study of quarkonia and quarkonia-like states will also benefit from Belle II data.

3.2.1 Quarkonia

Quarkonia generally refers to systems made of heavy quark-antiquark pairs of the same flavour, thus either to $c\bar{c}$, the charmonia, or to $b\bar{b}$, the bottomonia. With a lifetime of just $\sim 10^{-25}$ s, the t-quark decays before a $t\bar{t}$ system can be formed [12, p. 817]. The time for that would be in the order of $\sim 10^{-23}$ s according to *Production and decay properties of ultra-heavy quarks* [36].

A comprehensive list of quarkonia can be found in *Review of Particle Physics* [12]. Illustrations of the quarkonia states are shown in figures 3.1 (charmonia) and 3.2 (bottomonia). They differ in quantum numbers such as total angular momentum (J), parity (P), charge-conjugation (C) and mass.

The three lightest quarks u, d and s can form bound $q\bar{q}$ systems ($q = \{u, d, s\}$), too. However, due to the low mass of the light quarks, systems made of those are rather mixture states (see e.g. Ref. [12]).

Quarkonia and quarkonia-like states are subject of research. The latter often refers to states that share similarities with quarkonia but do not fulfil the expectations for quarkonia in certain aspects, such as mass, electric charge or decay modes. Some examples will be shown in the following.

Neutral Charmonium-like State X(3872)

In 2003, Belle reported an *Observation of a Narrow Charmoniumlike State in Exclusive* $B^{\pm} \to K^{\pm}\pi^{+}\pi^{-}J/\psi$ *Decays* [39]. The authors found a electric neutral multi-quark state close to the $D\overline{D}^{*}$ threshold (see figure 3.1).

The authors analysed the following decay in 152×10^6 $B\overline{B}$ events:

$$B^{+} \to K^{+} \underbrace{\pi^{+}\pi^{-}J/\psi}_{X(3872)}$$

A mass of 3872.0±0.6 (stat)±0.5 (syst) MeV was determined by the authors, hence the name $X(3872)$. In more recent Ref. [12] the particle is also referred to as $\chi_{c1}(3872)$. Its mass according to Ref. [12, p. 1911], is 3871.65 ± 0.06 MeV. Its quantum numbers were determined to be 1^{++} by LHCb in 2013 in *Determination of the* $X(3872)$ *Meson Quantum Numbers* [40] where the following decay was analysed:

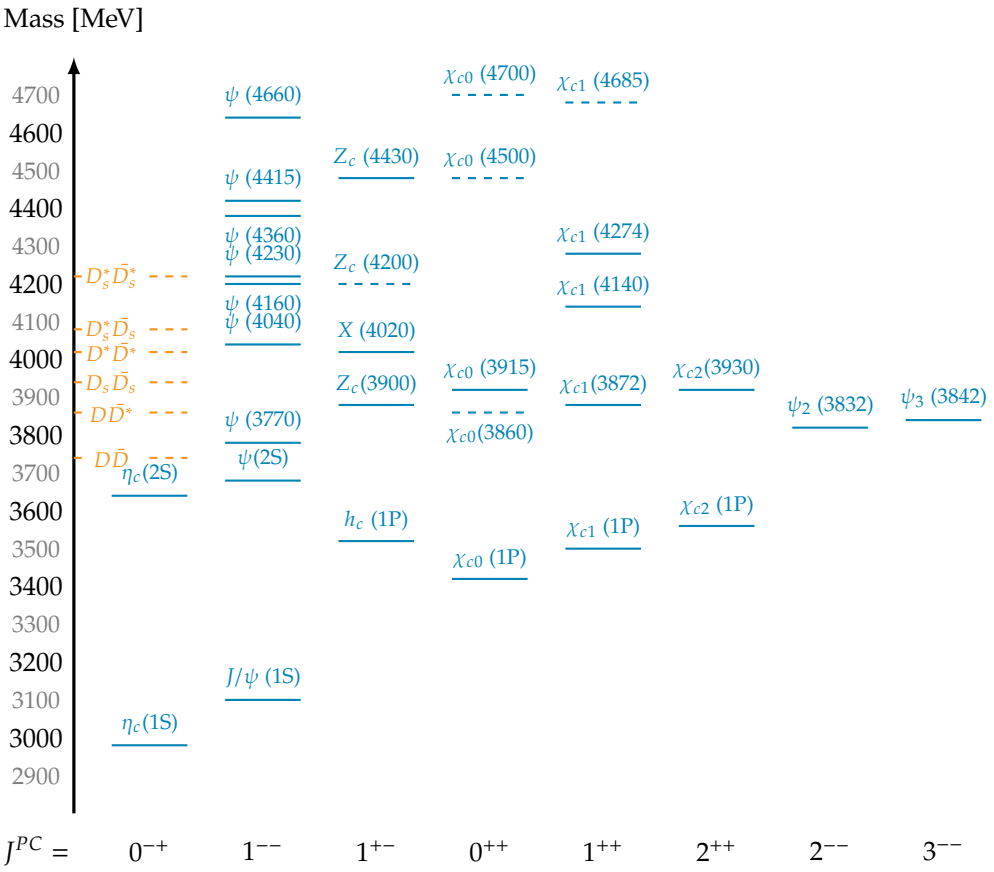

Figure 3.1: Charmonium spectrum. Adapted from *The charmonium system* [37], original figure by Particle Data Group licensed under CC BY-NC 4.0. Dotted lines for particles indicate that confirmation is needed; the dotted lines on the left side indicate particle decay thresholds [12, p. 1818].

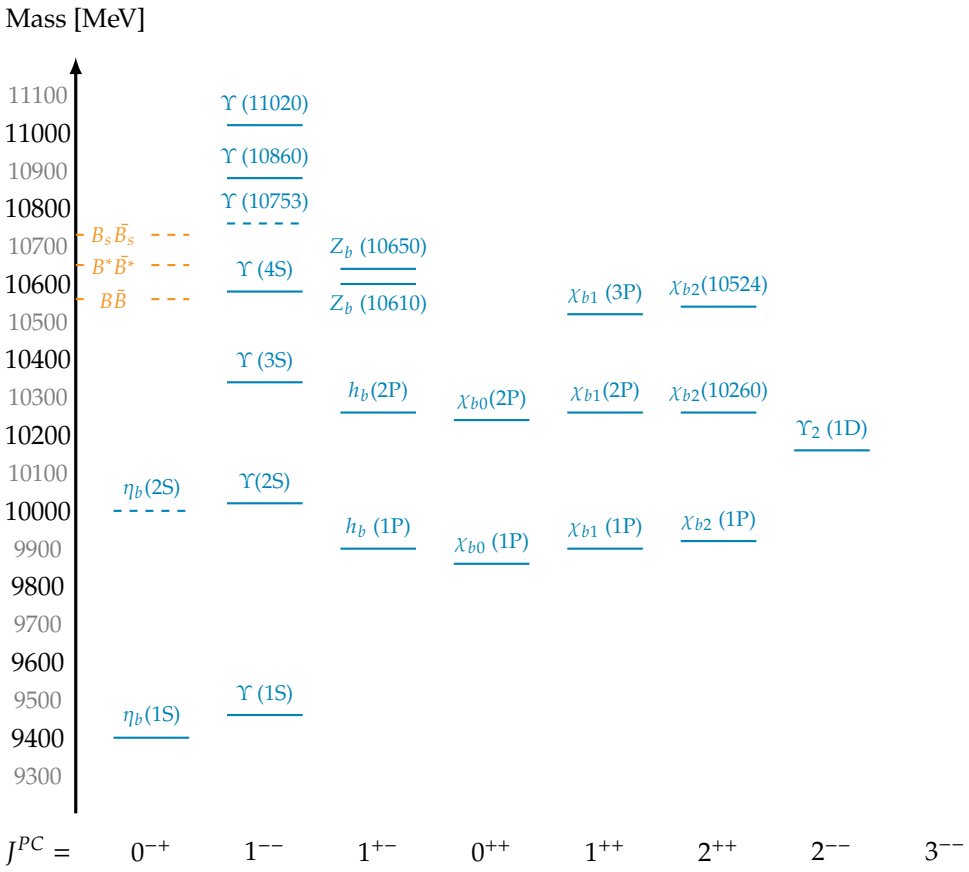

Figure 3.2: Bottomonium spectrum. Adapted from *The bottomonium system* [38], original figure by Particle Data Group licensed under CC BY-NC 4.0. Dotted lines for particles indicate that confirmation is needed; the dotted lines on the left side indicate particle decay thresholds [12, p. 1940].

$$
\begin{aligned}
B^+ &\to X(3872)K^+ \\
X(3872) &\to \pi^+\pi^- J/\psi \\
J/\psi &\to \mu^+\mu^-
\end{aligned}
$$

Discovering the $X(3872)$ was an important step forward in studying the nature of mesons with more than two constituent quarks. The $X(3872)$ might be a di-quark molecule, a tetraquark state or a charmonium-molecule [40, p. 222001-4].

Charged Charmonium-like State Z(4430)

Unlike $X(3872)$, $Z(4430)^\pm$ is a charmonium-like state, carrying a non-zero charge. The particle was reported by Belle in 2007 in *Observation of a Resonancelike Structure in the $\pi^{+-}\psi'$ Mass Distribution in Exclusive $B \to K\pi^{+-}\psi'$ Decays* [41].

The $Z(4430)^\pm$ was discovered in the following decay:

$$
\begin{aligned}
B &\to K \underbrace{\pi^\pm \psi'}_{Z(4430)^\pm} \\
\psi' &\to J/\psi\ \pi^+\pi^- \\
\psi' &\to \ell^+\ell^- (\ell = e \text{ or } \ell = \mu) \\
J/\psi &\to \ell^+\ell^-
\end{aligned}
$$

Its mass according to Ref. [12, p. 81] is 4478^{+15}_{-18} MeV. Its quantum numbers 1^+ were reported by Belle in 2013 in *Experimental constraints on the spin and parity of the $Z(4430)^+$* [42] and shortly after, in 2014, LHCb confirmed the resonant character of the $Z(4430)^-$ in *Observation of the Resonant Character of the $Z(4430)^-$ State* [43] where they presented Argand diagram analyses of $B^0 \to \psi'\pi^- K^+$.

Due to its electric charge its constituent quarks might be $(\overline{c}c\overline{u}d)$ [43, p. 222002-1].

3.2.2 Penguin Diagrams

Feynman diagrams are commonly used by particle physicists as a pictorial representation of physics interactions between particles including particle decays like the ones described in the last section. Those diagrams were introduced by Richard P. Feynman in publication *Space-Time Approach to Quantum Electrodynamics* [44] (1949) according to Ref. [45].

This section provides an overview of Feynman diagrams[1], focusing more on penguin processes and diagrams. Ref. *Penguin Decays of B Mesons* [47] (1998) provides

[1] The Feynman diagrams shown here were created using the TikZ-Feynman package [46].

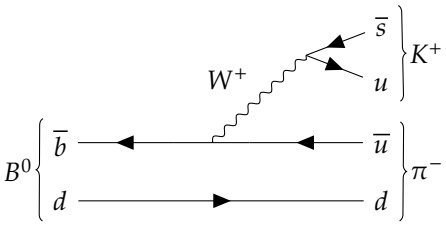

(A) $B^0 \to K^+\pi^-$: Example of a Feynman diagram for tree-level processes

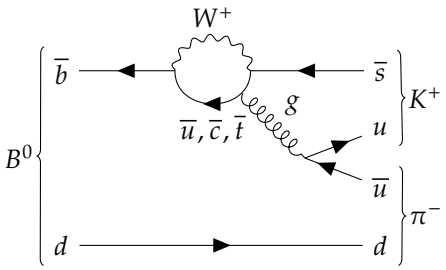

(B) $B^0 \to K^+\pi^-$: Example of a Feynman diagram for penguin processes

FIGURE 3.3: Two Feynman diagrams for the decay $B^0 \to K^+\pi^-$.

more details about the history of penguin diagrams and more examples for Feynman diagrams than this thesis.

Besides the penguin diagrams mentioned above, there are also tree-level Feynman diagrams. To compare the tree-level and penguin diagrams, figure 3.3 shows the decay $B^0 \to K^+\pi^-$ for both diagram types. The tree-level diagram in figure 3.3a is comparatively simple: a B^0 decays into a K^+ and a π^-. The decay takes place under the influence of the weak force which is mediated via a virtual W^+. The penguin decay in figure 3.3b introduces a loop which can include $\overline{u}$, $\overline{c}$ and $\overline{t}$ quarks to describe the flavour changing neutral current process b ($-1/3$ e) $\to$ s ($-1/3$ e). Thus, additional elements of the CKM matrix are involved which adds to the complexity of the decay, even though the final state is the same as in the tree-level process. Both particle decay modes have to be considered in particle physics analyses.

Corresponding diagrams can be made for charged B mesons as well. This was done by Belle, for example, when they reported a *Difference in direct charge-parity violation between charged and neutral B meson decays* [48]. In the reference one can find similar but more comprehensive Feynman diagrams as the ones presented in this section. Other diagrams relevant in particular for Belle II can also be found in Ref. [32].

As stated in Ref. [32, p. 254] $b \to sq\overline{q}$ transitions with light quarks ($q = \{u, d, s\}$) are potentially a valuable source for new physics because those transitions are penguin-process dominated and thus might be more sensitive to new physics processes than the tree-level dominated $b \to sc\overline{c}$ transitions.

The penguin diagram mentioned above was a gluonic process. Radiative and electroweak decays are also interesting since these decays are expected to be sensitive for new physics [32, p. 192]. Analyses of decays like $B \to \tau\overline{\nu}_\tau$ already showed devi-

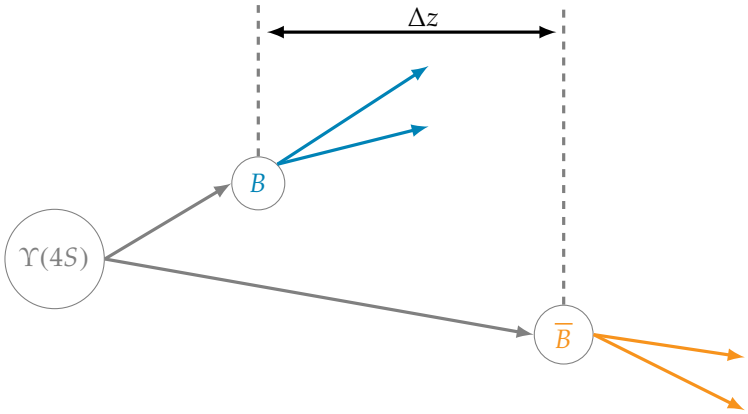

Figure 3.4: Illustration of Δz in B / $\overline{B}$ decays which can be measured due to a Lorentz boost in z direction.

ating results for $|V_{ub}|$ in 2006, for example [32, pp. 19-20]. A better understanding about such decays and the involved processes is expected to become available with Belle II data [32, p. 192].

3.2.3 CP Violation in neutral B Systems

Neutral B mesons mix with their antiparticles due to weak interaction ($B^0 \leftrightarrow \overline{B^0}$) similar to the neutral Kaons. This makes neutral B mesons also interesting for studying CP symmetry violating processes. One can distinguish the two mass eigenstates, B^0_H and B^0_L, which have a mass difference Δm_d in the order of 10^{-10} MeV [12, p. 59].

In 2001, the Belle collaboration reported an *Observation of Large CP Violation in the Neutral B Meson System* [49]. This was the result of an investigation of more than 30 million $B\overline{B}$ pairs and their decays. One of these B mesons with certain flavour (B^0 or $\overline{B^0}$) decays at time t_{tag} to final state f_{tag} while the other B meson, the one with opposite flavour, decays to final state f_{CP} at time t_{CP}.

The authors of Ref. [49] investigated CP eigenstates in $B \to (c\overline{c})K^0$ decays. They determined the flavour q of the B mesons ($q = +1$ for B^0, $q = -1$ for $\overline{B^0}$), the corresponding CP eigenvalues ξ_f, and the time difference $\Delta t = t_{CP} - t_{tag}$. The latter one can be calculated using the distance $\Delta z = z_{CP} - z_{tag}$ between the decay vertices of the neutral B mesons [49]:

$$\Delta t \simeq \frac{\Delta z}{c\beta\gamma} \tag{3.1}$$

Thus, for determination of Δt one has to know Δz as illustrated in figure 3.4. The more accurate the Δz, the more accurate the resulting Δt.

After determination of ξ_f, q and Δt, the authors found an asymmetry in the Δt distribution for events with $\xi_f q = +1$ and $\xi_f q = -1$ and therefore could illustrate CP violation in B meson decays.

In general, CP violating processes may show deviations from SM expectations due to new physics. Therefore, the study of CP violating processes as well as the improvement of the precision of the angles of the unitarity triangle are some goals of Belle II .

3.2.4 Unitarity Triangle Angles and CP Violation

The angles of the unitarity triangle might not add up to 180° taking only SM processes into account because of new physics phenomena. For this reason, it is of great interest to accurately determine the angles.

CP violating processes and the angles of the unitarity triangle are related topics. The current values for the angles can be found e.g. in *Averages of b-hadron, c-hadron, and τ-lepton properties as of 2021* [50] or on official website of *CKMfitter Group* [51].

In section 3.2.3, the Belle publication *Observation of Large CP Violation in the Neutral B Meson System* [49] was mentioned in the context of CP asymmetries in neutral B meson decays. The authors also investigated the unitarity triangle angle ϕ_1 or rather $\sin 2\phi_1$.

Angle ϕ_1

As shown in Ref. [12, pp. 264-265] one can determine angle ϕ_1 via the time-dependent asymmetry of B decays to a final state f:

$$A(t) = \frac{\Gamma(\overline{B^0}(t) \to f) - \Gamma(B^0(t) \to f)}{\Gamma(\overline{B^0}(t) \to f) + \Gamma(B^0(t) \to f)} \tag{3.2}$$

$$= S_f \sin(\Delta m_d t) - C_f \cos(\Delta m_d t) \tag{3.3}$$

where S_f and C_f depend on the amplitudes of the B^0 ($\mathcal{A}$) and $\overline{B^0}$ ($\overline{\mathcal{A}}$).

$$S_f = \frac{2\mathrm{Im}\lambda_f}{1 + |\lambda_f|^2}, \tag{3.4}$$

$$C_f = \frac{1 - |\lambda_f|^2}{1 + |\lambda_f|^2}, \tag{3.5}$$

$$\lambda_f = \frac{V_{tb}^* V_{td}}{V_{tb} V_{td}^*} \frac{\overline{\mathcal{A}}_f}{\mathcal{A}_f} = \frac{q}{p} \frac{\overline{\mathcal{A}}_f}{\mathcal{A}_f}. \tag{3.6}$$

Transitions like the ones examined in Ref. [49] ($b \to c\bar{c}s$) enable to set $S_f = -\xi_f \sin 2\phi_1$[2] and $C_f = 0$ [12, p. 264] simplifying the asymmetry to

$$A(t) = -\xi_f \sin(2\phi_1) \sin(\Delta m_d t). \tag{3.7}$$

The analysis of the decay of $B\overline{B}$ pairs done by the authors of Ref. [49] showed that $\sin 2\phi_1 \neq 0$.

The angle ϕ_1 is the one measured with the highest precision to date but increasing this precision even further by analyses of $b \to c\bar{c}s$ transitions is one way which can also lead to new physics discoveries [32, pp. 247-248].

Operating mainly at the $\Upsilon(4S)$ resonance with $B\overline{B}$ mesons as primary decay products (> 96% [12, p. 85]), Belle II is well suited for enhancing the precision of ϕ_1 and thus, Belle II data will help to significantly reduce the uncertainties here [32, pp. 245-247, 295].

The current average value of ϕ_1 is $(22.2 \pm 0.7)°$ [50, p. 052008-5].

Angle ϕ_2

Angle ϕ_2 can be determined via isospin analyses of decays such as $B \to \rho\rho$, $B \to \pi\pi$ and $B \to \rho\pi$, thus, $b \to u\overline{u}d$ transitions [12, p. 265]. However, a similar approximation as done for ϕ_1 ($S_f = -\xi_f \sin 2\phi_1$ and $C_f = 0$) cannot be made. The reason for this is, that both, the neutral-current penguin contributions from $b \to d(u\overline{u})$ and the charged-current tree contributions from $b \to u(\overline{u}d)$ to the decay amplitudes have to be taken into account [12, pp. 946-947].

One decay of interest for the analyses would be $B \to \pi^+\pi^-$. For final state $f = \pi^+\pi^-$, $S_{\pi^+\pi^-}$ can be written as

$$S_{\pi^+\pi^-} = \sqrt{1 - C^2_{\pi^+\pi^-}} \sin(2\alpha - 2\Delta\alpha) \tag{3.8}$$

with $\alpha = \phi_2$ and $\Delta\alpha$ as contribution from penguin processes [12, p. 947].

The current world average value for ϕ_2 according to Ref. [50, p. 052008-5] is $(85.2^{+4.8}_{-4.3})°$. Belle II data is expected to help to significantly reduce the uncertainty to just about 0.6° considering $B \to \pi\pi$ and $B \to \rho\rho$ decays [32, p. 246].

Angle ϕ_3

Angle ϕ_3 can be determined via the ratio of CKM-suppressed and -favoured amplitudes of $B \to DK$ decays (with D being a superposition of D^0 and $\overline{D^0}$) [32, pp. 296-298]. Those decays are special in that sense that no penguin contributions have

[2] In Ref. [12, p. 264] η_f denotes the CP eigenvalue instead of ξ_f.

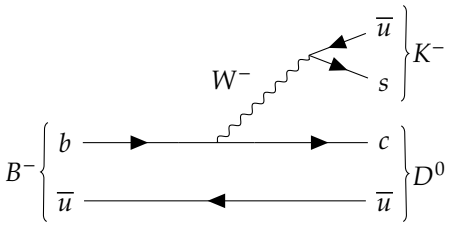

(A) CKM-favoured decay $B^- \to D^0 K^-$ to determine ϕ_3.

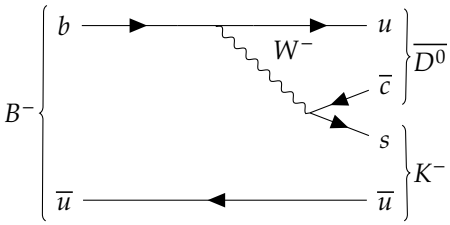

(B) CKM-suppressed decay $B^- \to \overline{D^0} K^-$ to determine ϕ_3.

FIGURE 3.5: Favoured and suppressed decays of $B^- \to DK^-$ (D either D^0 or $\overline{D^0}$) ($|V_{ub}| < |V_{cb}|$) to determine ϕ_3.

to be considered which makes them quite clean [32, p. 297]. The amplitude ratio of the suppressed $B^- \to \overline{D^0} K^-$ and the favoured $B^- \to D^0 K^-$ can be written as

$$\frac{A(B^- \to \overline{D^0} K^-)}{A(B^- \to D^0 K^-)} = r_B e^{i(\delta_B - \phi_3)} \tag{3.9}$$

where r_B represents the ratio of magnitudes and δ_B the strong phase difference [32, p. 297]. The corresponding tree-level Feynman diagrams are shown in figure 3.5.

The current world average for ϕ_3 is $(66.2^{+3.4}_{-3.6})^\circ$ [50, p. 052008-5]. Belle II aims for a 1°-level precision for ϕ_3 [32, p. 299].

3.3 SuperKEKB Collider

The SuperKEKB collider is the successor of KEKB, the asymmetric electron-positron collider used for Belle. KEKB was in operation from 1998 to 2010 [2]. It was operated at centre-of-mass energies close to the $\Upsilon(4S)$ resonance, using asymmetric beam energies of $E_- = 8\,\text{GeV}$ (e^- beam) and $E_+ = 3.5\,\text{GeV}$ (e^+ beam) [2]. Thus, the main product of beam collisions were the same as for SuperKEKB: $B\overline{B}$ pairs.

The publication *Achievements of KEKB* [2] lists several milestones. One of those has been achieved by the continuous optimisations of KEKB. This enabled the collider to reach a maximum peak luminosity of $\mathcal{L} = 2.108 \times 10^{34}\,\text{cm}^{-2}\text{s}^{-1}$ in June 2009. Besides exceeding its design luminosity of $\mathcal{L} = 1.0 \times 10^{34}\,\text{cm}^{-2}\text{s}^{-1}$, KEKB also set the world

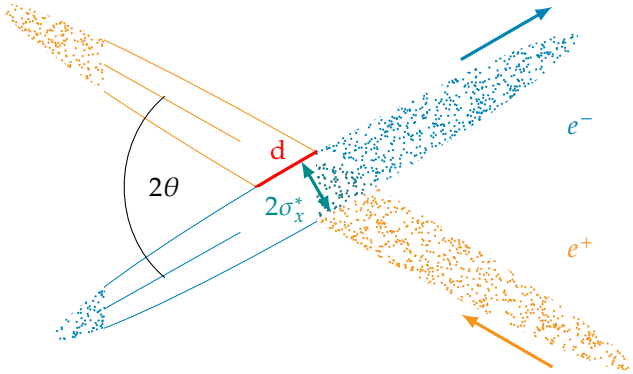

FIGURE 3.6: Illustration of colliding e^- and e^+ bunches. The bunches collide with half crossing angle $\theta = 41.5\,\text{mrad}$, horizontal (shown in figure) / vertical beam sizes $\sigma_x^* = 10.7\,\mu\text{m}$ / $\sigma_y^* = 62\,\text{nm}$ (e^-) and $\sigma_x^* = 10.1\,\mu\text{m}$ / $\sigma_y^* = 48\,\text{nm}$ (e^+). The beam currents $I_+ = 3.60\,\text{A}$ (e^+) and $I_- = 2.60\,\text{A}$ (e^-) are more than twice the currents used in the KEKB collider. Each of the 2,500 bunches with lengths of 5-6 mm are made of 9.04×10^{10} positrons and 6.53×10^{10} electrons. The properties mentioned up to this point were taken from Ref. [35]. d denotes the overlap region and can also be written as σ_x^*/Θ as an approximation [3, pp. 19-22].

record at the time. In the end, KEKB achieved a total integrated luminosity of $1.041\,\text{ab}^{-1}$ [2].

Comprehensive information on the SuperKEKB collider can be found in Ref. [35], from which the following information is taken unless otherwise stated.

The beam energies in the SuperKEKB collider differ slightly from those used in KEKB. The energies for the electron beam and positron beam are $E_- = 7\,\text{GeV}$ and $E_+ = 4\,\text{GeV}$, respectively. The energy adjustments have been made i.a. to improve Touschek beam life time of the positron beam and to reduce the horizontal emittance of the electron beam. This also lead to a reduced Lorentz boost of 0.28 [3, p. 139]. Thus, Δz between B meson vertices (see figure 3.4) is reduced as well but that is expected to be compensated with the vertex resolution performance of the Vertex Detector (VXD) [3, p. 139]. The two parts of the VXD are discussed in sections 3.4.1 and 3.5.

SuperKEKB uses a novel nanobeam collision scheme which is illustrated in figure 3.6. The nanobeam collision scheme enables a design luminosity of $\mathcal{L} = 8 \times 10^{35}\,\text{cm}^{-2}\text{s}^{-1}$ and an expected total integrated luminosity of $50\,\text{ab}^{-1}$ [35]. SuperKEKB has already set the world record for the highest luminosity several times: for example in December 2021 with $\mathcal{L} = 3.81 \times 10^{34}\,\text{cm}^{-2}\text{s}^{-1}$ (see *KEK website* [52]) and in June 2022 with $\mathcal{L} = 4.7 \times 10^{34}\,\text{cm}^{-2}\text{s}^{-1}$ (see *Belle II website* [53]). A comparison of luminosities of various experiments with the design luminosity of Belle II is shown in figure 3.7. Equation 3.10 [35] shows how the luminosity can be calculated.

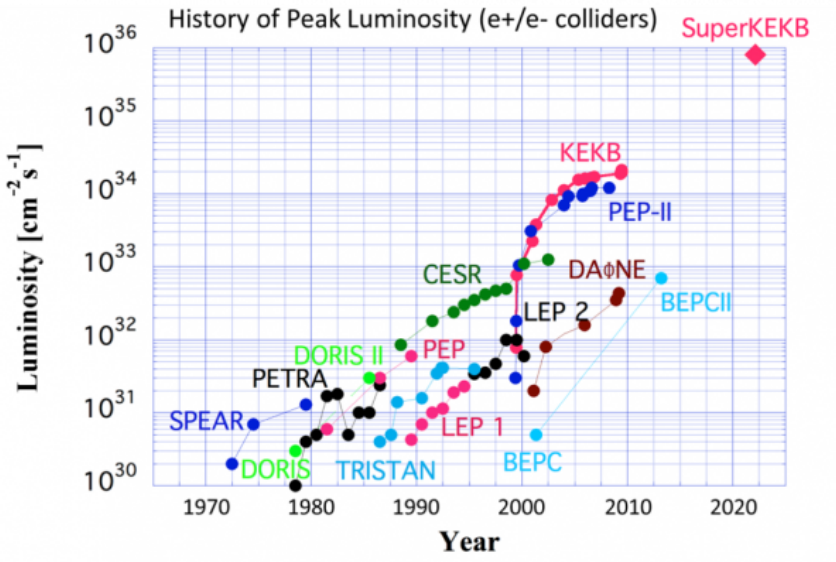

Figure 3.7: SuperKEKB's luminosity in comparison with other experiments, including KEKB. © KEK [54]

$$\mathcal{L} = \frac{\gamma_{\pm}}{2er_e}\left(1 + \frac{\sigma_y^*}{\sigma_x^*}\right)\left(\frac{I_{\pm}\epsilon_{y_{\pm}}}{\beta_y^*}\right)\left(\frac{R_L}{R_{\epsilon_y}}\right) \tag{3.10}$$

$\gamma_{\pm}$	Lorentz factors (± indicating either electron (-) or positron (+))
r_e	classical electron radius
σ_x^*, σ_y^*	beam sizes at the interaction point
β_y^*	beta function at the interaction point
$I_{\pm}$	beam current (± indicating either electron (-) or positron (+))
$\epsilon_{y_{\pm}}$	beam-beam tune shift parameter (± indicating either electron (-) or positron (+))
R_L, R_{ϵ_y}	correction factors

A schematic overview of SuperKEKB is shown in figure 3.8 on the facing page. The electron / positron beams are injected by a 600-m linear accelerator. The beams then enter the collider rings, both with a circumference of 3,016 m. In the interaction region, the nanobeam collision scheme is realized by the final-focus superconducting magnet system (QCS) which focus the beams to achieve the design luminosity of SuperKEKB. Figuratively speaking, the beam bunches are squeezed at the interaction point by the QCS magnets. The data from the particle collisions is collected by the Belle II detector, which will be discussed below.

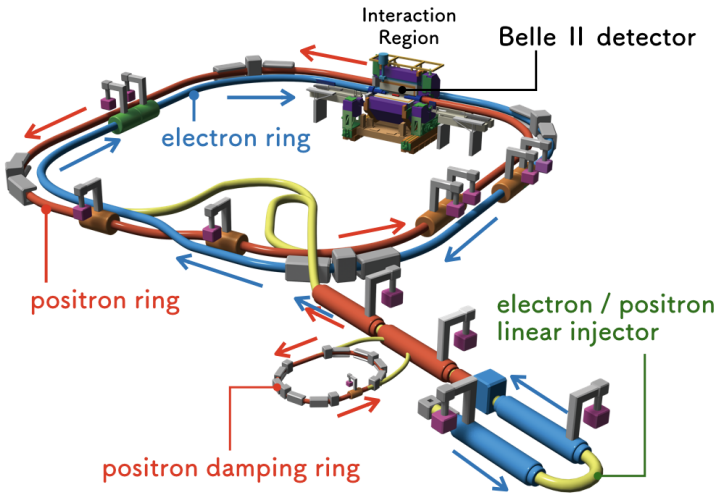

Figure 3.8: The SuperKEKB collider and the Belle II detector at KEK in Tsukuba, Japan. © KEK [55]

3.4 Belle II Detector

The Belle II detector consists of several subdetectors as shown in figure 3.9. Figure 3.9a illustrates the size of the complete detector while figure 3.9b is a close-up of the detector components which are closest to the IP: the VXD which is consisting of the PXD (red) and the Silicon Vertex Detector (SVD) (yellow).

The Belle II subdetectors have been upgraded in parallel with the KEKB collider since the end of Belle operation. The following sections are intended to give a brief overview of each system. For more detailed information, the reader is referred to the comprehensive *Belle II Technical Design Report* [3] or to the references used in the sections below.

The barrel-like design around the IP is common to most Belle II subdetectors. They are enclosed by end caps which contain subdetector elements as well. Hereinafter, the direction *forward* and *backward*, respectively, indicates either a direction in beam boost direction (direction of the electron beam) or a direction in opposite direction (direction of the positron beam) with respect to the IP of the collider.

The Belle II detector operates with a maximum trigger rate of 30 kHz [32, pp. 38-40]. Its commissioning phases are described e.g. in *The Belle II Physics Book* [32, pp. 40-41, 461-462]. In Phase I the first beam revolutions in the collider were started but without the Belle II detector nor the QCS.

A major milestone for Belle II in Phase II was reached on the night of the 25th to the 26th of April 2018 (Japan Standard Time). That night, the very first electron-positron collisions were successfully realised[3].

[3] I was lucky to witness this special moment at KEK, as I was operating the PXD in the control room of Belle II that night.

At the time of writing this thesis, the Belle II subdetectors are being maintained and optimised. According to DESY Confluence page [56] a long shutdown period started in 2022. This shutdown is expected to last 15 months.

3.4.1 Silicon Vertex Detector (SVD)

The SVD is situated closely to the IP with only one subdetector, the PXD, being closer. The SVD enables precision detection of tracks close to the IP as part of the VXD. Four layers of double-sided silicon microstrip detectors (DSSDs) with radii between 38 mm and 140 mm are arranged in a barrel-like shape around the IP between the PXD and the Central Drift Chamber (CDC). The detector covers an polar-angular acceptance of $17° < \theta < 150°$. In forward direction, the three outer detector layers are slanted between 11.9° and 21.1° to optimise the material budget used while maintaining the detector performance.

The readout has been optimised to meet requirements such as radiation tolerance and fast readout. The SVD data is forwarded to the Belle II DAQ using the unified high-speed belle2link protocol (see e.g. *Belle2Link: a Global data Readout and Transmission for Belle II Experiment at KEK* [59] or Ref. [3, pp. 388-392] for further information about belle2link).

The SVD properties stated above are taken from paper *Belle II Silicon Vertex Detector* [60] where the reader can find more information about the SVD as well as several depictions of the hardware.

SVD data is also used by the DATCON for determination of Regions of Interest on the PXD layers [61]. The Regions of Interest will be further described in section 3.5.2 on page 33.

3.4.2 Central Drift Chamber (CDC)

Starting from the innermost subdetectors, the CDC is the third Belle II subdetector. The cylindrical wire chamber has a diameter of 2.2 m and, following the barrel-like arrangements of the other subdetectors, it surrounds the VXD.

Its main purpose is tracking and identification of charged tracks, determination of their momenta and provision of trigger signals. In comparison with the CDC used in Belle detector, the number of sense wires has been increased from 8,400 to 14,336. The cylinders are made of CFRP while the end plates are made of aluminium. Since multiple scattering has to be considered, the CDC was built as low material detector. The expected higher beam background is taken into account by reduced sizes of the inner CDC azimuthal cells. A low-Z (i.e. few protons) gas mixture is used in the chamber. The CDC data is forwarded to the Belle II DAQ system via Rocket I/O link.

The above information and more details about the CDC as well as the properties can be found in reference *Central Drift Chamber for Belle II* [62].

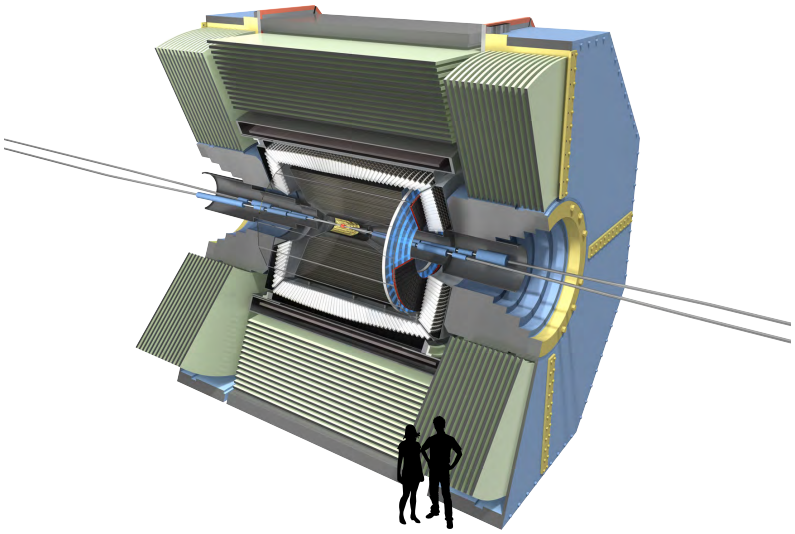

(A) Schematic inside-view of the Belle II Detector. © Belle II / KEK [57]

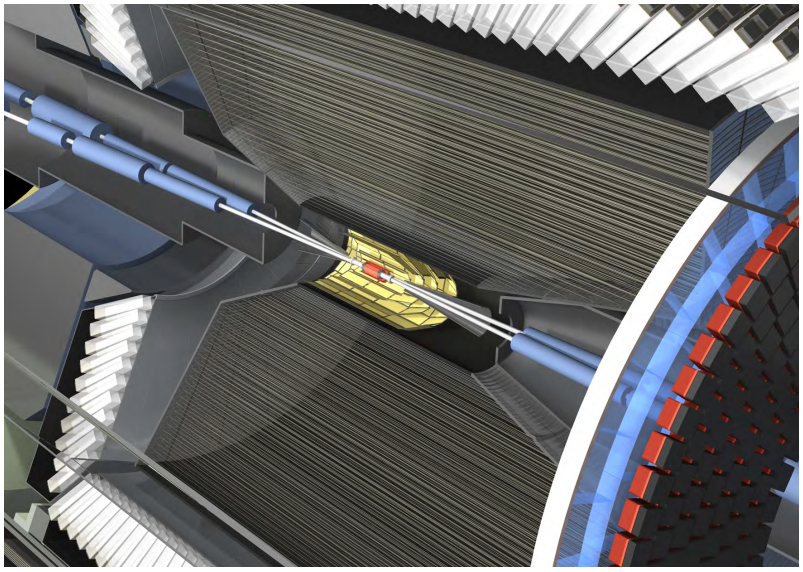

(B) Close-up of the innermost detectors: the PXD (red) and the SVD (yellow). © Belle II / KEK [58]

FIGURE 3.9: The Belle II Detector.

3.4.3 Particle identification

Time of Propagation Counter (TOP)

The quartz bars of the Time-Of-Propagation counter (TOP) are situated between the Electromagnetic Calorimeter (ECL) and the CDC. The subdetector was designed for the identification of incident charged hadrons. These produce Cherenkov photons which are reflected multiple times in the quartz bars of the TOP. Each quartz bar has a focusing spherical mirror at one end and a prism at the other. The former reflects the photons but it also reduces chromatic dispersion. On each prism, two rows of 16 photomultiplier tubes with a total of 512 channels collect the Cherenkov photons. There are 8,192 photomultiplier tube channels in the whole TOP.

The detector measures the time of propagation of the Cherenkov photons. A reconstruction algorithm determines the type of the particle. It also uses information from the CDC about the point of impact and the momentum of the particle.

The analogue signal sampling, the data digitization, the readout as well as the transmission of data to the Belle II data acquisition involve i.a. a custom-designed waveform sampling Application Specific Integrated Circuit (ASIC) and Xilinx Zynq-7000 systems on a chip. The TOP is designed to meet the requirements of the average global trigger rate of 30 kHz and data transfer of up to 120 MB/s.

The mentioned information about the TOP was taken from *Front-end electronic readout system for the Belle II imagining Time-of-Propagation detector* [63] were more details about the TOP properties and performance can be found.

Aerogel Ring-Imaging Cherenkov Detector (ARICH)

The Aerogel Ring-Imaging Cherenkov Detector (ARICH) is another component of Belle II particle identification subdetectors. It is placed in the endcap (forward direction) of the Belle II detector and therefore does not have the usual barrel-like shape of most of the other subdetectors. Incident particles create Cherenkov photons in a silica aerogel radiator which then are detected in a photon detector where the Cherenkov cones from the incident particles are collected as ring images. The ring diameters depend on the types of the particles, thus there are different ring images for kaons and pions.

The mass m of incident charged particles with momenta p and Cherenkov angle θ_c can be calculated with

$$m = \frac{p}{c}\sqrt{n^2 \cos^2 \theta_c - 1}$$

where n is the refractive index of the aerogel which is in the range of ~ 1.04 to 1.05.

The photon detector was designed to provide the necessary position resolution to distinguish kaons and pions. The photon detector is placed at a distance of about 200 mm from the aerogel radiator. The whole system was built considering the limited space in Belle II detector and with the goal for optimal photon resolution and detection.

The information provided here and more comprehensive insight into the ARICH properties can be found in reference *Particle identification performance of the prototype aerogel RICH counter for the Belle II experiment* [64].

3.4.4 Electromagnetic Calorimeter (ECL)

The ECL, situated outside the TOP and ARICH, follows the barrel-like design of most of the Belle II subdetectors but also has endcap sections similar to the ARICH. The barrel section has an inner radius of 1.25 m and a length of 3 m. It is composed of 6,624 CsI(TI) crystals, each in form of truncated pyramids with an average cross section size of $6 \times 6\,\mathrm{cm}^2$ and length of 30 cm. 2,112 CsI crystals in total are used in the endcaps. The ECL covers a polar angle region of 12.4° to 155.1°. For Belle II, the focus of the ECL upgrade was on improving the calorimeter electronics while maintaining high photon energy resolution, using the same crystals as in the Belle experiment.

The information about the ECL was taken from reference *Electromagnetic calorimeter of the Belle II detector* [65] where more details about the readout and the hardware can be found.

3.4.5 K_L^0 and μ Detector (KLM)

The K_L^0 and μ Detector (KLM) is the outermost subdetector of Belle II and is situated outside of the Belle II solenoid. It is divided into two Endcap KLMs (EKLMs) and one Barrel KLM (BKLM). Both parts consist of 14 iron plates and 14 (endcaps) or 15 detector layers (barrel). In Belle experiment glass electrode resitive plate chambers (RPCs) were used for the KLM. However, the much higher background in Belle II has a huge impact on the RPC efficiency, especially for the endcaps. Therefore, RPCs are used only for the barrel part while scintillators are used for the endcaps.

Track extrapolations from CDC are used to determine whether a particle detected by the KLM is either a hadron or a muon. Reconstructed neutral ECL clusters and corresponding clusters in KLM, as well as track reconstruction based on these clusters and charged particle vetos, are used to determine K_L.

The above information is taken from the *Belle II Technical Design Report* [3, pp. 313-319].

3.5 Pixel Detector (PXD)

The Pixel Detector is the innermost subdetector of the Belle II detector. A comprehensive description of the PXD can be found in the *Belle II Technical Design Report* [3, pp. 76-138].

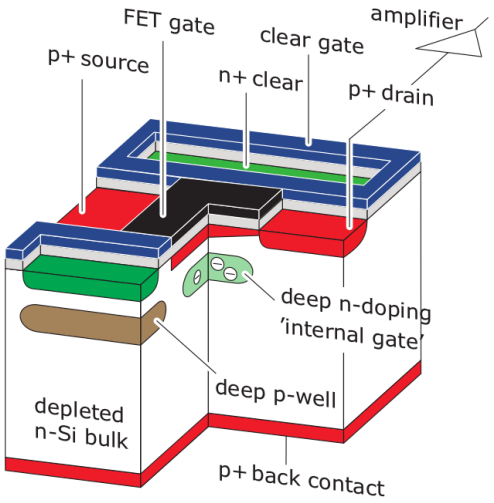

Figure 3.10: Technical drawing of a DEPFET pixel as shown in *Belle II Technical Design Report* [3, p. 79].

The sensitive area of the PXD is based on the Depleted Field Effect Transistor (DEPFET) detector concept. The operation principle of a DEPFET pixel as discussed in Ref. [3, pp. 79-83] is shown in figure 3.10. As stated in Ref. [3, p. 79] the operation principle is as follows: a DEPFET pixel is made of a silicon bulk ("n-Si bulk") and an integrated p-channel metal-oxide-semiconductor field-effect transistor (MOSFET) or junction field effect transistor (JFET). Fully depletion of the silicon bulk can be achieved by applying high negative voltage to the "p^+ back contact". A potential minimum – the "internal gate" – collects the electrons from electron-hole pairs created by incident particles in the silicon bulk. The internal gate can be cleared by applying a positive voltage to the "n^+ clear". However, as long as the internal gate is not cleared, the electrons can modulate the channel current, which can be read out non-destructively.

The Belle II PXD consists of 40 modules, also called half-ladders (HLs) [3, pp. 78,92]. Each HL has 250 columns × 768 rows = 192,000 pixels [66]. The sensitive lengths of the HLs enable to cover the angular range from $17° < \theta < 150°$ [3, p. 78] (like the SVD as discussed in section 3.4.1 on page 26).

Schematic drawings of the PXD HLs are shown in figure 3.11. A single HL consists of the sensitive area made of DEPFET pixels and components for data acquisition. A full ladder is made of two glued HLs as shown in figure 3.11b. The complete PXD consists of 20 ladders in total. Those are arranged in two layers around the IP as illustrated in figure 3.11c. The layers have radii of 14 mm (inner layer) and 22 mm (outer layer) [3, p. 78].

Each pixel on a HL has its own unique row and column coordinates. The HLs of both PXD layers have in common that the 256 rows closest to the IP are smaller than the other 512 rows. The number of pixels is the same for the inner and outer PXD layers. However, the pixel sizes of the inner and outer layers are different.

Pixel Sizes	256×250 Pixels (close to IP)	512×250 Pixels
Inner Layer	55×50 µm	60×50 µm
Outer Layer	70×50 µm	85×50 µm

Table 3.1: Pixel sizes of the PXD modules as stated in Ref. [66].

Therefore, the HLs of the outer layer provide a larger sensitive area. In the column direction, all pixels, regardless of their proximity to the IP and PXD layers, have the same size of 50 µm. An overview of the pixel sizes according to Ref. [66] (2021) is given in table 3.1. However, the pixel sizes and numbers on HLs have also been communicated Belle II internally (for example in the conference contribution [67] (2016) by C. Marinas and K. Nakamura).

The PXD can be tested with a few or even a single HL. This made it possible to carry out the tests described in chapter 5, in which only up to four HLs were used.

3.5.1 PXD Data Acquisition

A part of the PXD DAQ hardware is located on the PXD modules. The readout ASICs outside the sensitive PXD area are shown in figures 3.11a, 3.11b and 3.11c. The readout is performed in a rolling-shutter mode by three different types of ASICs [3, pp. 77-78]. A comprehensive discussion about those can be found in Ref. [3, pp. 79-89] while only a brief overview of that reference is given below.

One type of the readout ASICs are the SWITCHERs. In figure 3.11a the SWITCHERs are located below the sensitive area. They are used to select the rows to be read and to clear the internal gate. This is done for four rows in parallel [3, p. 84]. When selected, the pixel currents are processed by the Drain Current Digitizers (DCDs) (right of the sensitive area in figure 3.11a) which are connected to the pixels via the drain lines [3, p. 84]. The data is then forwarded the Data Handling Processors (DHPs) (right of the DCDs in figure 3.11a) which buffer the data and perform a zero-suppression of the data [3, p. 88]. Further data processing takes place outside of the PXD modules. The receiver of the PXD data are the Data Handling Engines (DHEs) which are part of the DHH system.

Information about the DHH system (and results from a test campaign in 2014) can be found in *FPGA Based Data Read-Out System of the Belle 2 Pixel Detector* [68] which is used as reference in the following. It should be noted that since the publications of Ref. [3] (2010) and Ref. [68] (2014/2015) the names of certain components have been changed: the DHH Controller (DHHC) is now called the Data Handling Concentrator (DHC), the Data Handling Hybrid (DHH) is renamed to Data Handling Engine (DHE) while the name of the whole system is Data Handling Hub (DHH). In this thesis, the new names are used.

Each DHC and DHE is equipped with a Virtex-6 VLX130T FPGA and 4 GB of

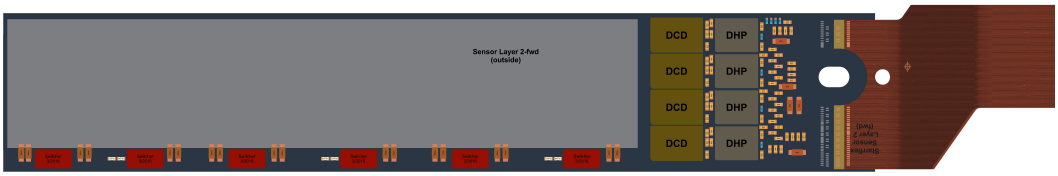

(A) A single PXD module with 768×250 pixels, also referred to as half-ladder. The readout electronics, consisting of DCDs and DHPs, are located on the right side of the module, outside the acceptance region of the Belle II detector. Below the pixels (grey area) six SWITCHERs (red) enable a row-wise read out of the pixels.

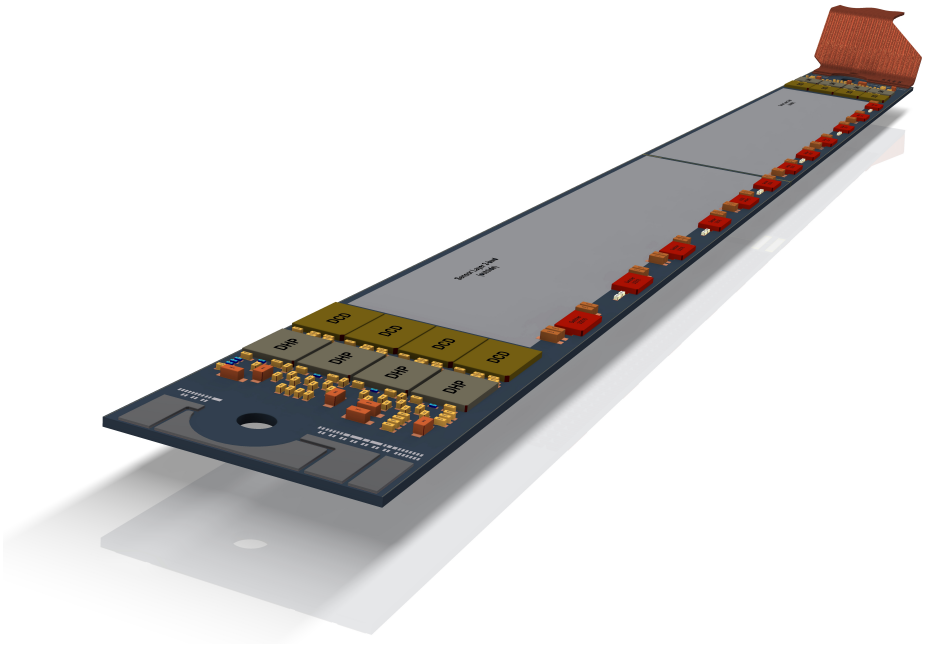

(B) Two PXD modules glued to one ladder. The readout electronics are placed outside the detectors acceptance region.

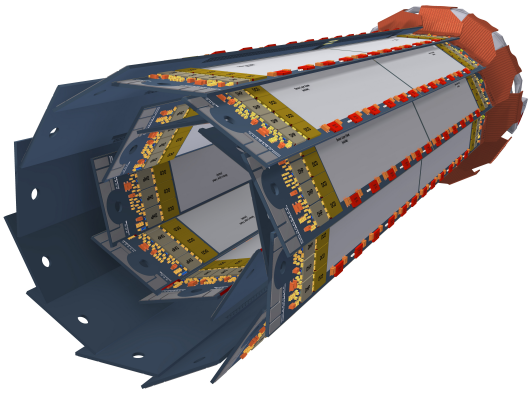

(C) Arrangement of the 20 ladders. The sensitive areas of the two layers are different in size. The inner layer is shorter than the outer layer.

FIGURE 3.11: PXD module(s). Courtesy of K. Ackermann.

memory for e.g. cluster reconstruction, sub-event building, and to provide an interface for slow control of the front-end ASICs.

A single DHE is connected to the four DHPs of one HL. Five DHEs each are connected to a single DHC. The data of each of the eight DHCs is forwarded to the ONSEN using 32 connections (4 connections per DHC) in total. The ONSEN is discussed in more detail in chapter 4. It performs a PXD data selection before the data is forwarded to the event-builder-2, where the data from the other subdetectors is collected as well. The data is then stored for physics analyses.

3.5.2 Regions of Interest on PXD Ladders

The Belle II detector collects data relevant for physics analyses as well as background events. Ref. [3, pp. 64-67] lists the beam-induced backgrounds relevant for the Belle II experiment. The higher luminosity, smaller beam and interaction point sizes of SuperKEKB compared to its predecessor come at the cost of more background events like Touschek scattering.

As mentioned in section 3.5.1, the DHH data is filtered before being sent to EB2. The idea is to keep only PXD data which is relevant for physics analyses and discard everything else. So only data collected from certain pixels are to be kept and data from other pixels can be discarded. This selection of data is performed by the ONSEN system which will be discussed in chapter 4. However, although the ONSEN carries out the data selection, the PXD data to be selected is calculated by two independent systems: the HLT and the DATCON.

The HLT is a computer farm which uses information from other subdetectors to perform real-time track extrapolation to the PXD HLs to determine the Regions of Interest on the sensitive area of the PXD [69]. The DATCON only uses information from the SVD for the RoI determination; instead of a computer farm, the DATCON employs FPGAs for this [61]. Only data from pixels covered by at least one of the RoIs are being kept and forwarded to EB2.

The shape of each RoI is rectangular by design. Therefore, only two pixel coordinates are necessary to describe a single RoI: the *start row* and *column*, and the *end row* and *column*. The assignment of the RoIs to the correct PXD HL is based on the DHE ID, the ID of the DHE that is connected to the HL in question. The DHE ID is part of the data format specifications for HLT, DATCON and DHH (see appendix A).

A simplified illustration of RoIs on PXD modules determined via track extrapolation and the track intersection through the modules is shown in figure 3.12.

Alternative shapes (for example elliptic RoIs) and an optional tracking including the PXD data as well were discussed in *Development of the Online Data Reduction System and Feasibility Studies of 6-Layer Tracking of the Belle II Pixel Detector*[4] [7, pp. 54-56].

[4]The "6-Layer" in the title refer to the six layers of the VXD: four SVD layers and two PXD layers.

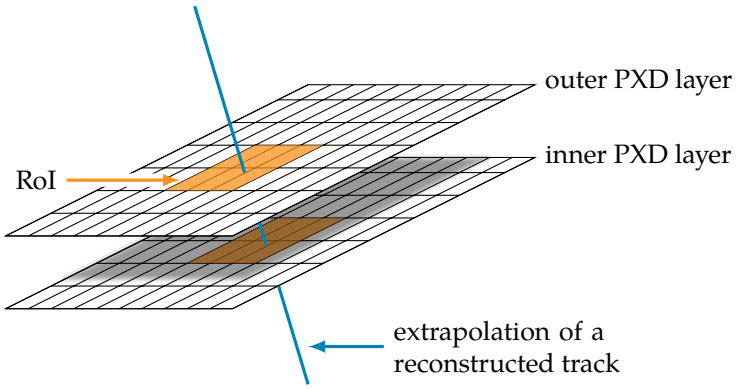

FIGURE 3.12: Illustration of RoIs on PXD modules determined by the extrapolation of a reconstructed track. For a better overview, only 2×70 pixels and one RoI per layer are shown. Any angle between the inner and outer layer modules is neglected. RoIs are calculated by the two independent systems HLT and DATCON.

Chapter 4

The ONSEN System

4.1 Overview

The PXD data rate is expected to be ~ 20 GB/s (assuming a PXD occupancy of 3%) which is about ten times the data rate expected from all other Belle II subdetectors combined [4]. Therefore, the HLT and the DATCON determine RoIs on the PXD layers, which are used for a data selection as mentioned in section 3.5.2.

The data selection itself is carried out by the Online Selection Nodes (ONSEN) system. Before sending the data to EB2, the ONSEN discards the PXD data that is not covered by any RoI. This method of data selection is expected to reduce the PXD data rate by a factor of 10 [5]. Another factor of 3 is expected to be achieved by rejecting complete events, thus, the total reduction factor is 30 [4]. The decision whether a event is kept is made by the HLT. This information is sent to the ONSEN in addition to the RoIs and some other data (e.g. trigger number, run number, ...). The HLT data format specification relevant for the ONSEN can be found in appendix A.

The Belle II research group at JLU has contributed to the development and testing of the hardware, firmware and software of the ONSEN system. Thus, the ONSEN has been the subject of several publications including *Development of FPGA-Based Algorithms for the Data Acquisition of the Belle II Pixel Detector* [6] (2015). Ref. [6] provides a comprehensive overview of the ONSEN system. Therefore, it was used as a reference during the work on this thesis, and most of the information about the ONSEN provided in this dissertation can be found there as well.

At the time of publication of Ref. [6] further firmware developments such as those discussed in section 4.5 were in progress. In addition, various ONSEN tests were still to be conducted in test campaigns and when the final ONSEN hardware was delivered and installed at KEK. Information about some of these tests can be found in chapters 5 (test campaigns at DESY) and 6 (tests at KEK).

4.2 ONSEN Hardware

The ONSEN consists of FPGA-based nodes which meet the Belle II requirements for processing data at high data rates. Originally developed as single nodes with five FPGAs each, it was later replaced by a modular five-nodes design, each equipped with one FPGA. A summary of hardware revisions can be found in Ref. [6, p. 70].

Regarding the hardware aspect two types of nodes can be distinguished: the nine Compute Node Carrier Boards (CNCBs), each equipped with a Xilinx Virtex-4 FPGA and the 33 Advance Mezzanine Cards (AMCs), each equipped with a Xilinx Virtex-5 FPGA. The specifications of these FPGAs can be found in *Virtex-4 Family Overview* [70] (Virtex-4 FX60) and *Virtex-5 Family Overview* [71] (Virtex-5 FX70T) which are the official product specifications from Xilinx.

The ONSEN AMCs receive and transmit data using two Small Form-factor Pluggable (SFP+) cages which enable data transmissions at up to 6.25 Gbps. The SFP+ cages can be used either with transceivers for Ethernet cables or for optical fibres. The latter ones are used at KEK for sending PXD data and RoI data to the ONSEN as well as for forwarding ONSEN-processed data to the EB2. In tests during development (see sections 4.5 and 4.6) or in test campaigns (see chapter 5), however, the ONSEN-processed data and the HLT data was mostly transmitted via Ethernet cables. This enabled to build setups where PCs could be used as substitutes for EB2 and HLT which were not available for all tests, especially not at JLU.

On each AMC, two 2 GB Random Access Memory (RAM) modules are available for data buffering and slow control[1], among others. One 2 GB RAM module is available on each CNCB. A non-volatile 64 MiB Flash memory is available on each AMC and CNCB to store a Linux operating system which is running on PowerPCs. A 4 MiB PROM (only on AMCs) enables to store bitstreams for FPGA programming after system power-up.

The ONSEN hardware is shown in figure 4.1. Each CNCB can be equipped with up to four AMCs as shown in figure 4.1a on the next page. Figure 4.1b shows the ONSEN power supply unit (PSU) and the rear transition module (RTM). The RTM is plugged into the CNCB and provides i.a. Ethernet and JTAG interfaces to the connected CNCB. This and more extensive information about the RTM, and the ONSEN hardware in general, can be found in Ref. [6, pp. 63-70].

During the development and testing of the ONSEN, several types of shelves were used. Some of those are shown in figure 4.2 on page 38: the shelf shown in figure 4.2a was used for first tests with ONSEN CNCBs. It was also used in the test beam campaign at DESY in 2016 which is discussed in chapter 5. Up to two CNCBs can be plugged into this shelf. The 14-slot-shelf shown in figure 4.2b was used for firmware tests at an advanced stage of development in Gießen as well as for tests performed at DESY in 2017. It is similar to the one used for the ONSEN at KEK.

The final version of the ONSEN was produced in 2015. The hardware was tested for technical functionality by the entire ONSEN development team at JLU. Various tests were conducted to verify that the hardware works properly. These included tests of the connections, the RAM and the Flash memory, among others. The hardware that passed the tests was sent to KEK mid-2017 to be installed on site as part of the PXD data acquisition. For documentation purposes, the ONSEN hardware has been entered into a database at the Institut für Hochenergiephysik (HEPHY) (restricted access: [72]) to track its location and current setup; for example, which AMC is connected to which CNCB.

[1] Information about the EPICS-based slow control can be found in Ref. [6, pp. 81-83], for example.

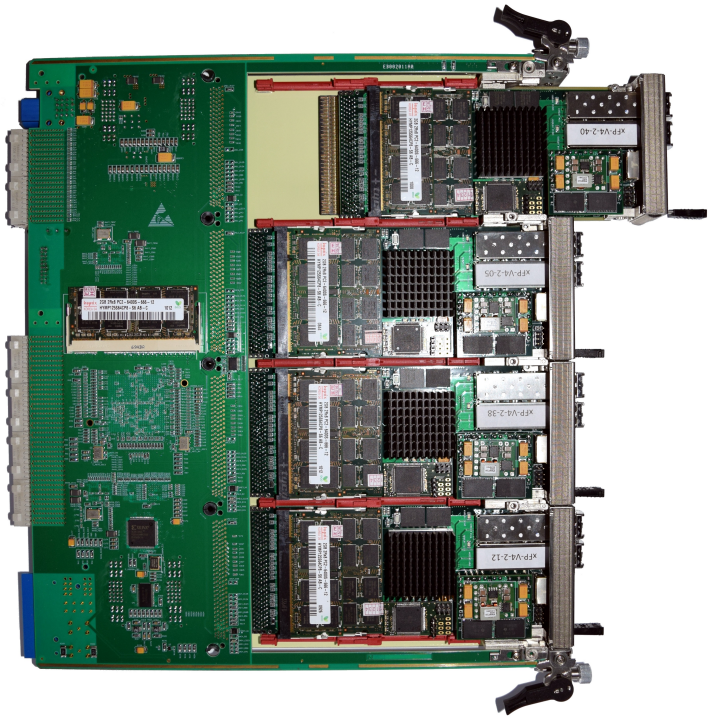

(A) ONSEN CNCB and four AMCs. The PSU is situated on the backside (not visible on photo). [a]

[a] Original photo (w/o removed background) was already used by Belle II members from JLU for talks and posters like my Deutsche Physikalische Gesellschaft (DPG) meeting contribution *Tests of final hardware revision of the Belle II PXD data reduction system* [73], among others.

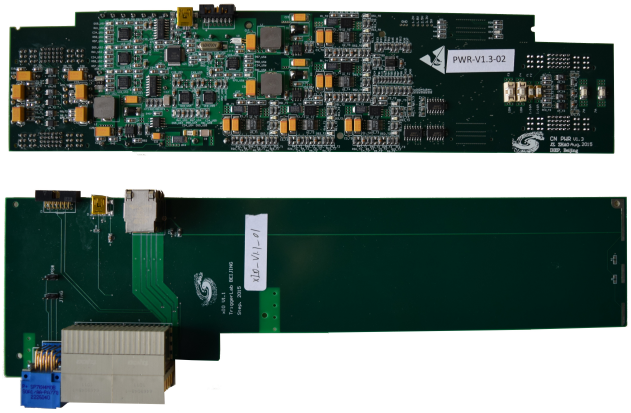

(B) ONSEN PSU and RTM.

FIGURE 4.1: ONSEN hardware used for Belle II . The hardware was developed at the IHEP, Beijing

(A) ATCA shelf with two slots and two ONSEN CNCBs plugged into. Each carrier board was equipped with just one AMC. This reduced setup already enables to perform tests with Merger and Selector firmwares. The setup was used for first tests with CNCBs as well as for tests performed at DESY in 2016. [a]

[a] Original photo (w/o removed background) was already used by Belle II members from JLU for talks and posters like my DPG meeting contribution *Test Runs of a Belle II PXD Prototype Readout System* [74], among others.

(B) ATCA shelf with two ONSEN CNCBs. This shelf was used for most tests carried out in Gießen but also for tests at DESY in 2017. Photo courtesy of T. Geßler.

FIGURE 4.2: Shelves used for ONSEN.

4.3 Pocket-ONSEN

The final hardware version of the ONSEN enabled the use of the Low Voltage Differential Signaling (LVDS) links between CNCBs and AMCs which are needed for the RoI distribution on the CNCBs (see section 4.5). In versions from May 2014 and earlier, the links were not usable, so the focus of firmware development at that time was on other parts of the ONSEN [6, pp. 70,73].

In many cases, firmware developments could be tested in setups without CNCBs, making AMC-only setups a viable option. ONSEN setups consisting only of AMCs are referred to as *Pocket-ONSEN* [6, pp. 73-74]. The Pocket-ONSEN made it possible to test the basic functionality of the ONSEN even without usable LVDS links or CNCBs. For example, Pocket-ONSEN setups were used for first tests of the main feature, the selection of PXD data based on RoIs. Another feature which was tested with a Pocket-ONSEN-like setup is discussed in section 4.5.2.

Pocket-ONSEN setups are limited by the number of AMC slots of the shelves used. At the time of this work, µTCA shelves with space for up to four AMCs were used in most setups.

During the test campaigns at DESY which are discussed in chapter 5, the Pocket-ONSEN served as a backup solution. It was also used in parallel with the global testbeam runs (runs including PXD and SVD) for tests with scaled-down DHH or DATCON setups.

The Pocket-ONSEN was also used for first tests at KEK. The setup used in late-2015 is shown in figure 4.3 on the next page.

The development on the firmware for Pocket-ONSEN was stopped in ~ 2016 when the final hardware versions became available. However, a Pocket-ONSEN could be set up at any time but might require minor firmware adjustments.

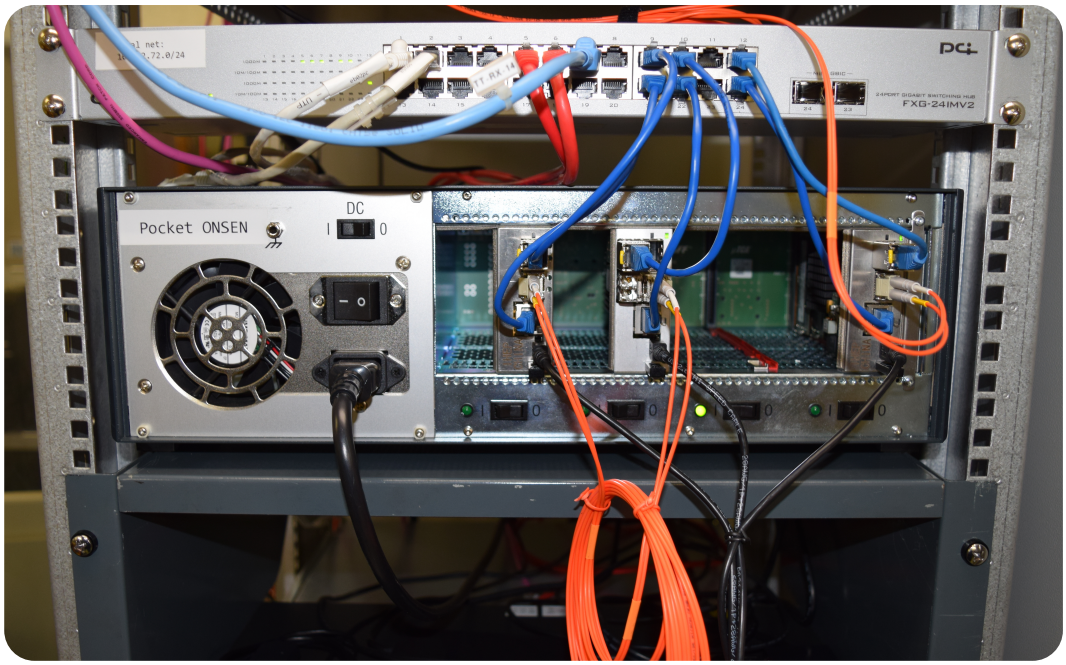

FIGURE 4.3: The Pocket-ONSEN as used at KEK in late 2015 / early 2016. Three AMCs are plugged into a μTCA shelf which provides connections between the cards.

4.4 ONSEN Firmware

4.4.1 Overview

The ONSEN firmwares for the AMCs and CNCBs were developed since ~ 2010 in a collaborative effort by the Belle II group at the JLU. The main purpose of the ONSEN, applying the RoI selection on the PXD data, is discussed in particular in *Development of the Online Data Reduction System and Feasibility Studies of 6-Layer Tracking for the Belle II Pixel Detector* [7].

The *Pixel Filter* Intellectual Property (IP) core significantly reduces the PXD data rates by discarding background data which is not relevant for further analysis. Other firmware components handle data receiving, storing and forwarding, among others. For Multi Gigabit Transceiver (MGT) and LVDS connections dedicated Aurora IP cores are used. SiTCP IP cores are used for Ethernet connections to HLT and EB2.

The SiTCP and MGT-Aurora IP cores implemented in ONSEN are described in thesis *Development of FPGA-Based Algorithms for the Data Acquisition of the Belle II Pixel Detector* [6, pp. 86-88, 129-144]. More information about SiTCP in general can be found in official manual [75] and website [76]. More information about the 8bit/10bit encoding of the Xilinx Aurora protocol which is used in ONSEN can be found in *Aurora 8B/10B Protocol Specification* [77]. For firmware development, we used Xilinx PlanAhead which included tools for the creation of IP cores and

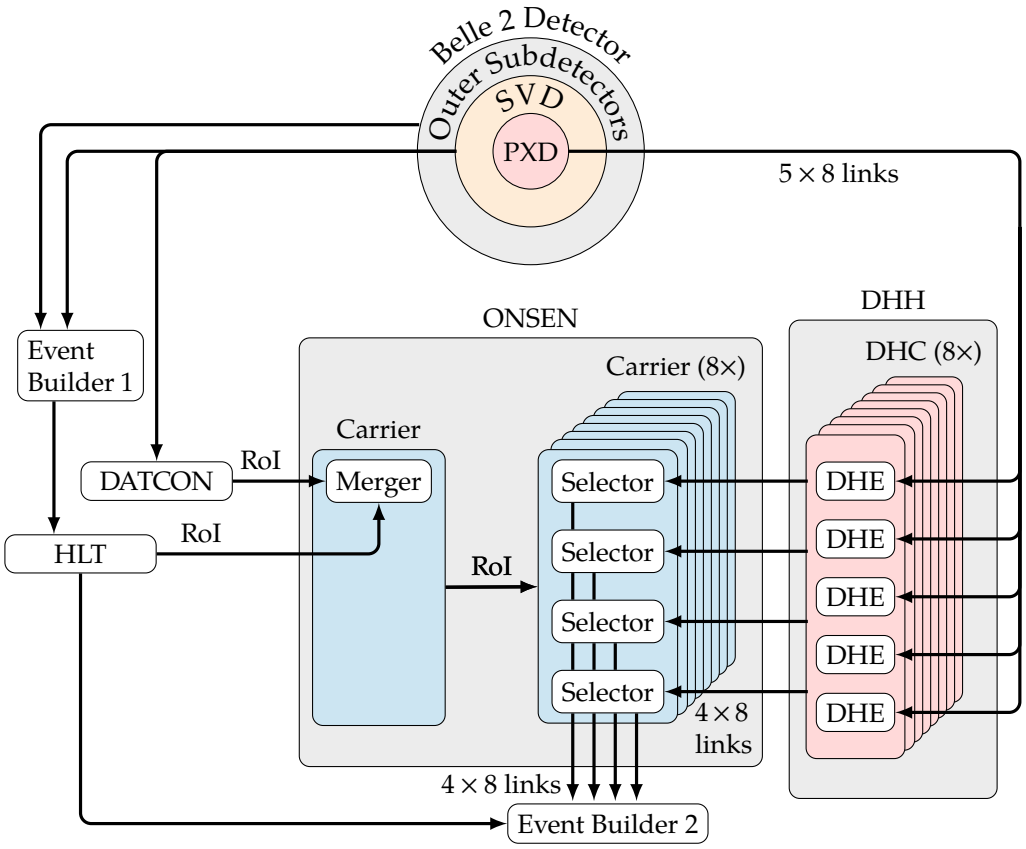

Figure 4.4: Simplified scheme of ONSEN in final Belle II setup. The ONSEN hardware consists of nine CNCBs and 33 AMCs in total. Four AMCs each are plugged into eight CNCBs in total to serve as Selectors. A single Merger AMC is plugged into a ninth CNCB. The Merger receives RoIs from the HLT and the DATCON systems. The PXD data is preprocessed and forwarded by the DHH system. The DHH consists of 40 DHEs and eight DHCs which multiplex the 40 PXD connections to just 32 connections to the ONSEN. The ONSEN discards any PXD data outside the RoIs and sends the selected data to the EB2.

tools for firmware upload to the FPGAs, among others; see manual [78] for more information. The Xilinx ChipScope logic analyzer (see documentation [79] for more information) was used during development to analyse and debug the firmware.

Two types of firmware are running on the FPGAs of the ONSEN. Thus, one can distinguish between the Merger and the Selector firmware running on either AMCs or CNCBs. The Merger firmware is used for receiving and processing of RoIs while the Selector firmware handles receiving and processing of PXD data. The Merger firmware is used on a single AMC and CNCB, respectively. The Selector firmware is running on the other 32 ONSEN AMCs and 8 CNCBs. A simplified overview of ONSEN connections to other systems of Belle II DAQ and the corresponding data flow is shown in figure 4.4.

The work on this dissertation aimed to complement the firmware by adding features

like the RoI distribution on the ONSEN CNCBs (see section 4.5) and the handling of faulty and rejected events (section 4.6). Contributions presented in this work are implemented in ONSEN firmware running at KEK or are at least available in ONSEN firmware repositories for later usage.

In the following sections, several IP cores are mentioned. The npi_write, npi_read and belle2_format_handler_ll IP cores, among others, are discussed in more detail in Ref. [6]. The Pixel Filter (pixel_filter_ll IP core) is discussed in thesis [7] where the name "RoI Selection Core" is used. Other IP cores like ptr_lut_write are described in Belle II ONSEN group internal documentations. Most of the cores provide LocalLink interfaces which are used for data transmission between the IP cores [6, p. 79]. A detailed documentation of the LocalLink interface specifications can be found in Ref. [80].

Note that in this thesis, the terms trigger number and event number have the same meaning and are used interchangeably. Note further that some data format specifications relevant for the ONSEN are discussed in appendix A.

4.4.2 Merger

The ONSEN Merger AMC receives the RoIs from HLT and DATCON (see section 3.5.2). The former is a mandatory input for the ONSEN while the latter is an optional input. Since the DATCON RoIs are processed on FPGAs and not on a computer farm like the HLT RoIs [61], the DATCON RoIs for a given trigger number are expected to be sent to the ONSEN before the corresponding HLT RoIs. Therefore, the DATCON RoIs must be buffered by the Merger until the HLT RoIs for the same trigger number are received.

A simplified overview of the data flow and the firmware components running on the Merger AMC is shown in figure 4.5. RoIs received by the Merger are passed to the Parsers (roi_parser in belle2_format_handler_ll IP core). The Parsers i.a. verify the Cyclic Redundancy Check (CRC) checksum in the data and extract the trigger number. DATCON RoIs are written to RAM (Memory) by the Data Writer (npi_write_ll IP core) until the corresponding HLT RoIs become available. The combination of memory address and trigger number as well as additional information (e.g. information if an error was found in data) is stored in a look-up table (LUT) (ptr_lut_write / ptr_lut_read IP cores).

When HLT RoIs for a given trigger number become available to the Merger, then the corresponding DATCON RoIs are read from memory by the Data Reader (npi_read_ll IP core). The data from HLT also contains information on whether the PXD data for the entire event should be discarded.

If no corresponding DATCON data is available at all at the time the HLT RoIs are received by the Merger, then dummy data will be added to the data stream instead (see appendix A). The introduction of dummy data ensures that the Belle II data format specification is met, even if not all (optional) data is available to the ONSEN.

Data from both RoI sources are merged by the RoI Merger (roi_merger_ll IP core).

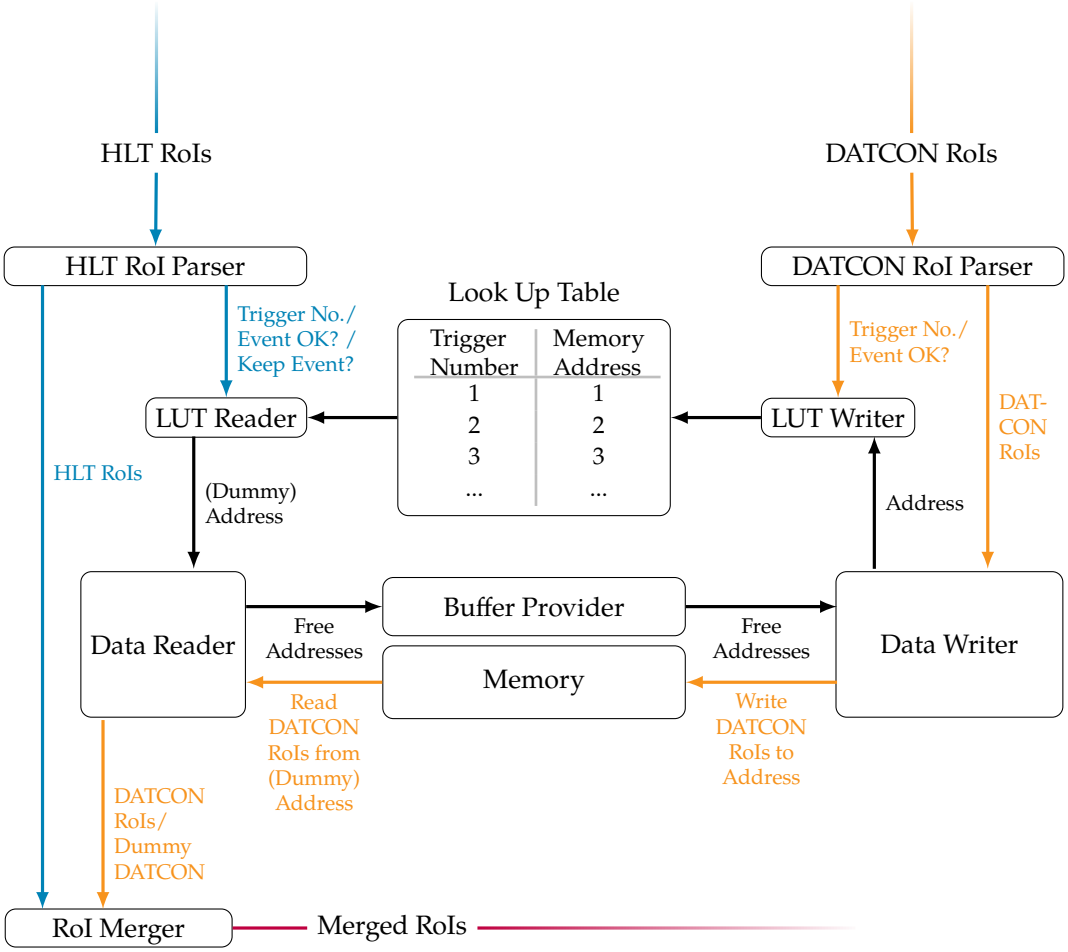

Figure 4.5: Simplified overview of the data flow in ONSEN Merger.

The merged RoIs are then distributed to the ONSEN Selectors as described in section 4.5. The RoIs read out from the Merger will not be kept any longer in RAM and the memory becomes available for new data. Exception: if the data contains errors like incorrect CRC. In this case, the data may remain in memory for debugging purposes. The development of an option to automatically clear the memory was part of this work and is discussed in section 4.6.3.

4.4.3 Selector

The ONSEN Selector AMCs are the receiver of the RoIs from the Merger and of the PXD data forwarded by the DHH system. Like the DATCON RoIs are expected to be sent to the Merger before the corresponding HLT RoIs, the PXD data is expected to be available to the Selectors before the merged RoIs from the Merger.

The simplified Selector AMC data flow shown in figure 4.6 is similar to the one of the Merger. Instead of DATCON RoIs, the Selectors receive PXD data from the DHH system. The data is passed to the Parser (pxd_parser in belle2_format_handler_ll

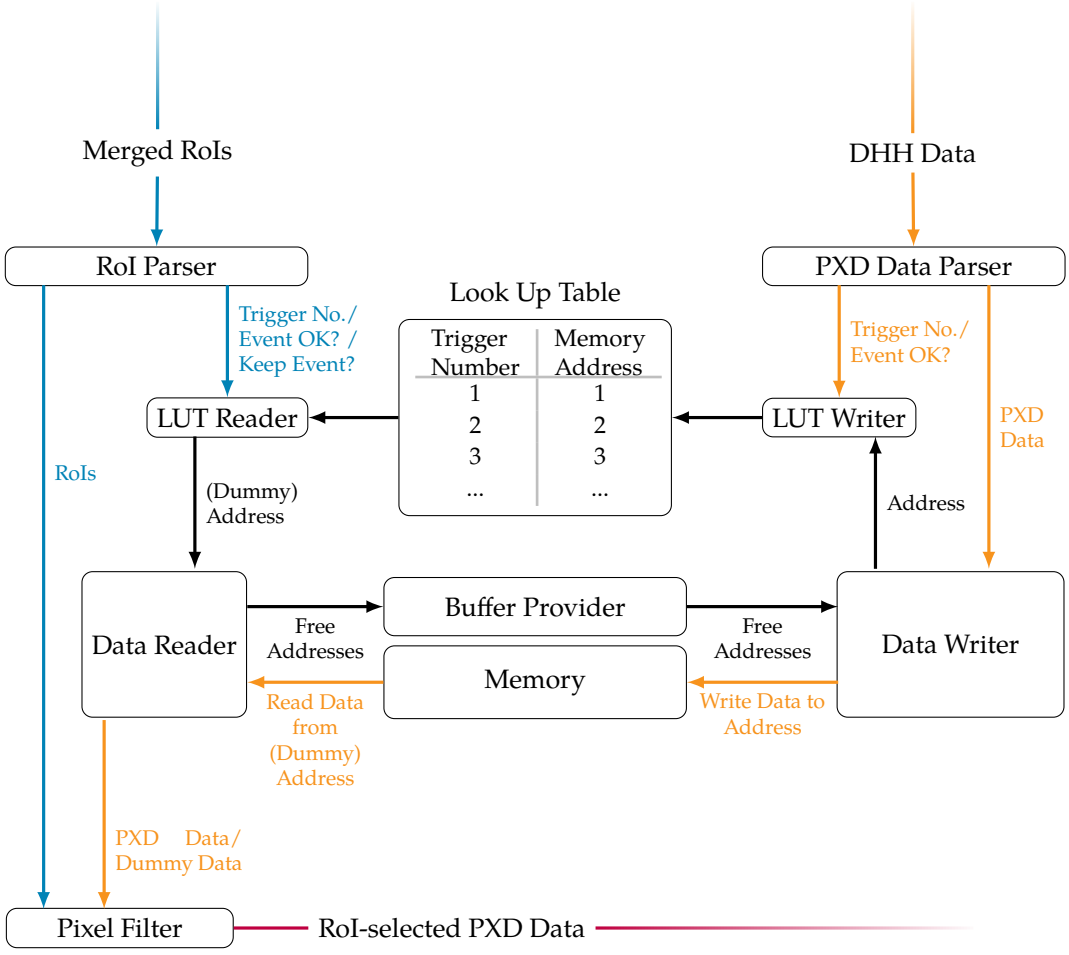

Figure 4.6: Simplified overview of the data flow in ONSEN Selector.

IP core) and is written to memory until the corresponding RoIs are received. As soon as RoIs have become available, the data is read out of memory and further processed.

The main feature of the Selector is to filter the PXD data based on the RoIs (pixel_filter IP core) before sending it to EB2. Even so, the data from the DHH is not a mandatory input for the ONSEN. If the Selectors receive RoIs for a trigger number for which no corresponding PXD (DHH) data is available, then dummy data is sent instead (see appendix A). Therefore any data sent from ONSEN to EB2 comply with the Belle II data format specification and contains (dummy) DATCON and / or (dummy) DHH data as well as additional data like information about the data size (see the Index frame in appendix A) and optionally the merged RoIs from the Merger.

From a technical point of view, the only mandatory data input for ONSEN are the HLT RoIs. As soon as ONSEN receives data from the HLT, the data is processed and sent to EB2, regardless of whether ONSEN has received DHH or DATCON data before or not.

4.5 RoI Distribution on Carrier Boards

4.5.1 Overview

The implementation of a RoI distribution on the ONSEN CNCBs was part of this work. The RoI distribution basically consists of three components: the *RoI Fork*, the *Trigger / Event Number Selection* and the *DHE Selection*. All three components will be described in the next sections. Before that, a prototype RoI distribution using only Pocket-ONSEN(-like) setups is discussed.

It should be noted that the development of the RoI distribution on CNCBs was still in progress at the time of the tests at DESY discussed in chapter 5. In tests without the RoI distribution, every RoI was sent to every available ONSEN Selector by default.

The RoI distribution on CNCBs was tested at JLU and at KEK. The tests at KEK are discussed in chapter 6. Information about the slave registers of the IP core used for operation, monitoring and tests are listed in appendix C.1.

4.5.2 Prototype: RoI Distribution on AMCs

The prototype version of the RoI distribution running only on AMCs was tested in 2014 as part of my master thesis [81]. By that time the final hardware version was not yet delivered to JLU. Available CNCBs were not suitable for intended firmware development and testing due to hardware issues. For example, the LVDS links between AMCs and CNCBs were not usable at that time [6, p. 73] as mentioned above. In addition, the firmware for the Selector AMC was distributed to two AMCs: one AMC for PXD data selection based on RoIs and another AMC to serve as "sender"[2]. The sender was used to add the Index frame (see appendix A.2) to the processed data. As of now, data selection as well as the sender functionality are running on the same Selector AMC firmware, making any additional sender AMC redundant.

Pocket-ONSEN(-like) setups were used for development and tests of the firmware. I set up a test system using up to two µTCA shelves in parallel. One for Merger and Selectors, another one for the now redundant senders. The AMCs of the two shelves were connected via optical fibres. The RoIs from the Merger were sent to the Selectors via the backplane of the µTCA shelf. The distribution of RoIs with specific trigger numbers was based on a LUT with 64 entries in total. In this setup, all Selectors received HLT RoIs for all DHE IDs. A prototype DHE ID filter was implemented in the Selector AMC firmware making it possible to select RoIs for up to five different DHE IDs.

The collaborative development, testing and optimisation of the ONSEN firmware continued in the years following my master's thesis. The implementation of a RoI distribution on the CNCBs of the final hardware version based on trigger number

[2] In my master thesis I also used the term "outsender".

and DHE ID is part of this thesis. The RoI distribution on AMCs, without the use of CNCBs, is not part of the final Belle II setup.

4.5.3 RoI Fork

On firmware level, the data flow of the RoI data can be controlled via the *RoI Fork*. The RoI Fork is an adapted version of the Fork (*ll_fork* IP core) which was used in a test campaign at DESY (see section 5.3) and the follow-up tests at JLU (see section 5.5) in 2017, among others.

The RoI Fork is implemented in the CNCB firmware of the Merger and the Selectors. On the Merger CNCB, the ONSEN operator can select the RoI-receiving Selector CNCBs in a Control System Studio (CSS) user interface[3]. This comes with several advantages: for example, one can choose not to send any RoI to one or more Selector CNCBs. This can be necessary, if several CNCBs are used for different tests in parallel. In the Belle II Phase II tests at KEK, for example, we excluded CNCBs that were not needed due to low data rates resulting from a reduced PXD and DHH setup. At that time, the data could be processed using only a reduced ONSEN setup. The settings can be adjusted at any time, e.g. between two Belle II physics runs.

As mentioned above, the RoI Fork is used on Merger and Selector CNCBs. Figure 4.7 on the facing page illustrates the RoI data flow from the Merger CNCB to the Selector CNCBs. In this figure, all RoIs are sent to all Selector CNCBs for further processing.

Figure 4.8 on page 48 shows the RoI Fork as used in the Selector CNCB firmware. Only up to four AMCs can be plugged into a single CNCB. Therefore, the user can only select up to four AMCs, depending on the availability of the hardware.

4.5.4 Trigger / Event Number Selection

Each Selector AMC receives only data with certain trigger numbers from the DHH system in final data acquisition setup due to load balancing between DHH and ONSEN. The Selector AMCs plugged into the same Selector CNCB are expected to receive data for the same trigger numbers. Since there are up to eight Selector CNCBs in total, the trigger number selection is designed to send RoIs to up to eight Selector CNCBs based on the three least significant bits (LSBs) of the trigger number (value range `000` = 0_{10} to 111 = 7_{10}).

The ONSEN operator can change the settings using a CSS user interface as illustrated in figure 4.9. The most reasonable setting depends on the DHH-ONSEN connections.

As part of this work, a test of the trigger number selection, also referred to as event number selection, was performed at KEK (see chapter 6). The selection was based on predefined test patterns.

[3]More information about CSS can be found on the official website [82]

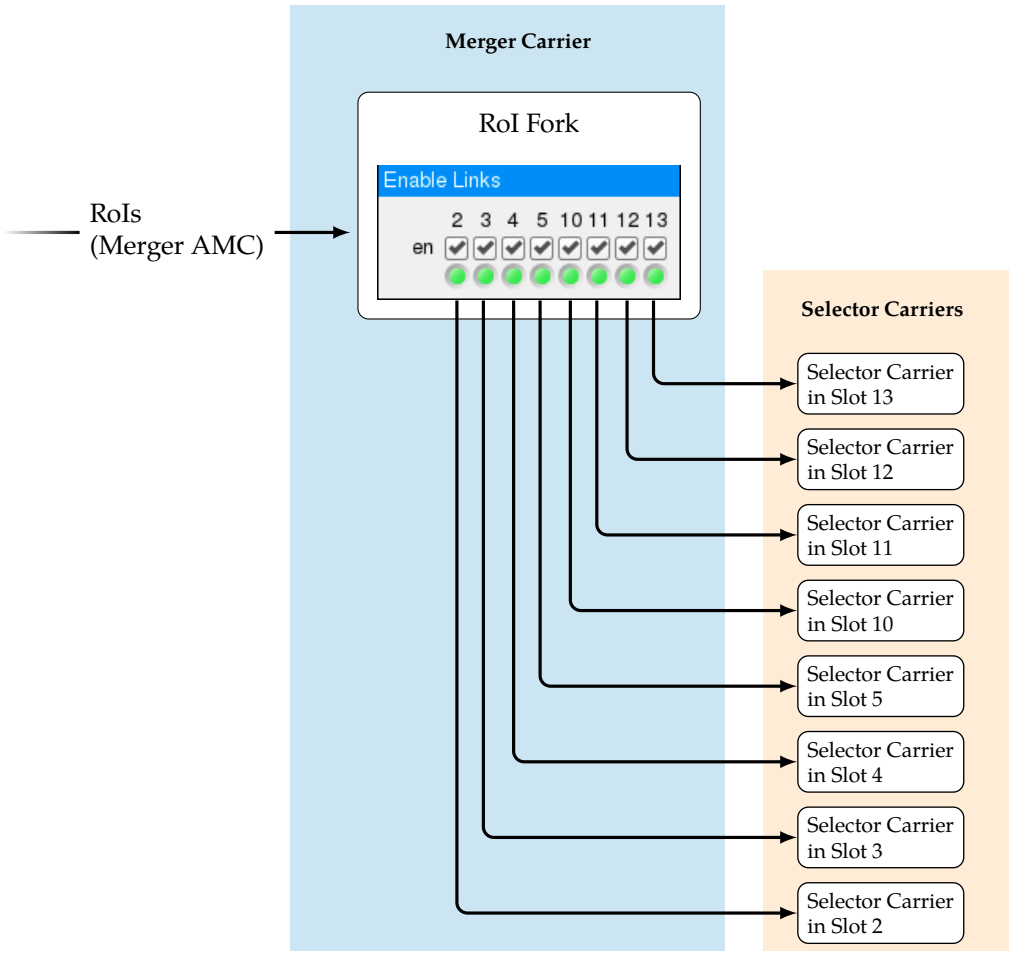

FIGURE 4.7: RoI Fork as used on the Merger CNCB. Received RoIs are forwarded to the eight Selector CNCBs based on the settings in the "Enable Links" box of a CSS user interface. The box is the representation of bits set in a slave register (see appendix C.1). The green light indicates that the link was enabled successfully. Here, all RoIs are sent to each Selector CNCB plugged into the slots of an ATCA shelf.

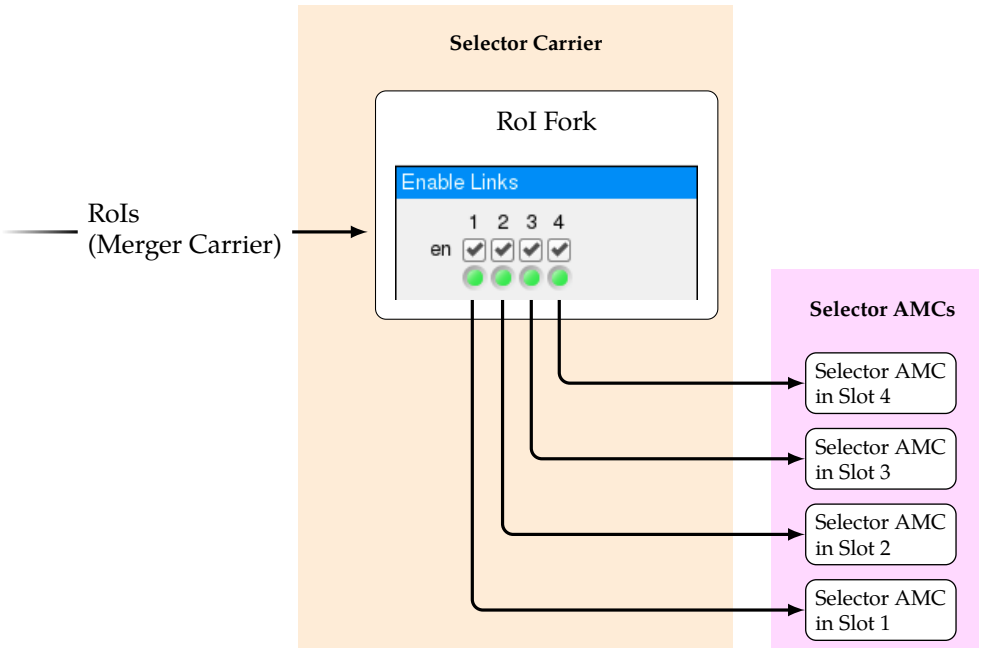

Figure 4.8: RoI Fork as used on the Selector CNCBs. Here, all RoIs from the Merger CNCB are sent to each Selector AMC available in the Selector CNCB. Up to four AMCs can be plugged into each CNCB. Therefore, only up to four links can be enabled in the CSS user interface. The green light indicates that the link to the AMC was enabled successfully.

4.5.5 DHE Selection

The DHE selection principle is similar to the trigger number selection. The DHE selection is performed on the Selector CNCBs after the trigger number selection on the Merger CNCB. Like the trigger number selection, it can be configured via a CSS interface as shown in figure 4.10.

The trigger number selection affects all RoI data (RoIs, checksums, etc.) for a given trigger number. The DHE selection affects only the RoIs. Since each Selector AMC receives data from one DHC and thus from up to five DHEs, only RoIs for those DHEs are needed.

The DHE ID is defined by six bits, thus, up to 64 different IDs are possible. As there are only 40 HLs in total, only 40 DHE IDs are actually needed. Even so, undefined IDs can be selected in the DHE Selection as well. One of these IDs was used for the tests described in chapter 6. The IDs used by the DHH are printed in black in figure 4.10 and undefined IDs are printed in grey.

4.5.6 RoI Distribution

The last sections introduced the three components of the RoI distribution which was developed as part of this thesis. The RoIs with certain trigger numbers and DHE IDs

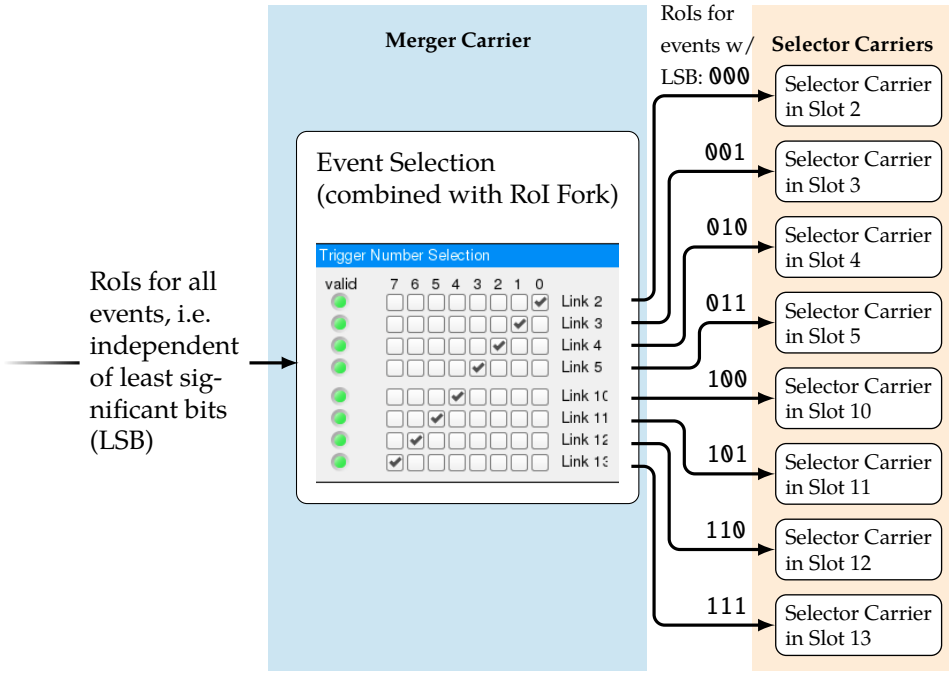

FIGURE 4.9: RoI trigger number selection as used on the Merger CNCB. While the Fork enables the links to the Selector CNCBs, the trigger number selection defines which RoIs must be sent to which Selector CNCB. The trigger number selection is based on the three LSBs of the trigger number. In this example each Selector CNCB receives 1/8 of all events.

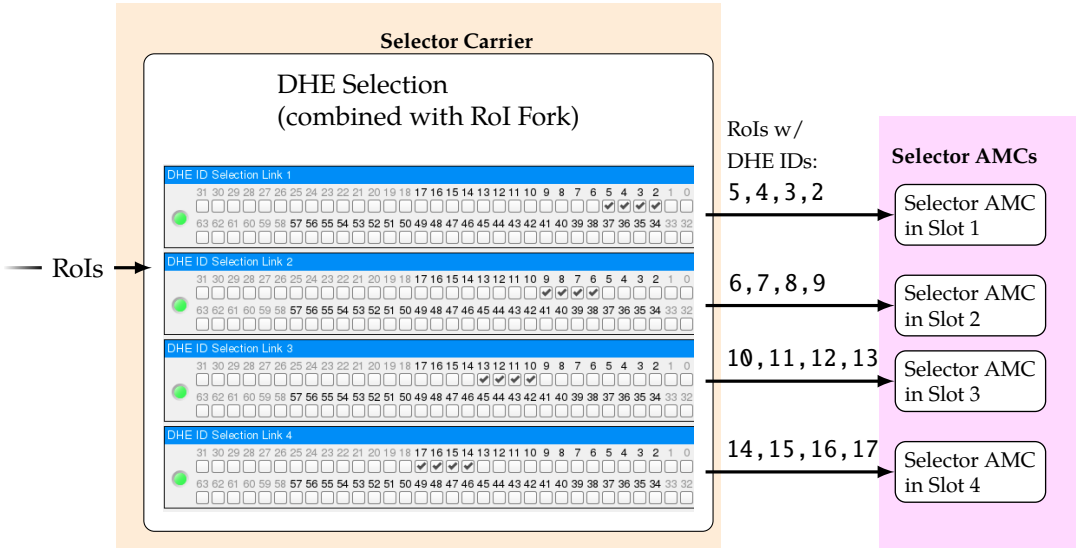

FIGURE 4.10: DHE selection as used on the Selector CNCBs. Received RoIs are forwarded to the Selector AMCs depending on the selected DHE IDs. Up to 40 DHEs are available but the DHE ID is made of six bits making up to 64 different IDs possible. This is taken into account in the DHE Selection user interface.

are selected either on the Merger CNCB or on the Selector CNCBs. Both selections are part of the very same IP core. Thus, one could combine the trigger number and DHE selection e.g. in the Merger CNCB and send only RoIs with certain trigger numbers and DHEs IDs to the Selector CNCBs. However, this would make the CSS user interface unnecessarily complicated. Therefore, the Merger and Selector user interfaces were designed to display either the trigger number selection or the DHE selection.

The user interfaces for Merger CNCB and Selector CNCBs, as used at the time of the tests discussed in chapter 6, are shown in figure 4.11 on the facing page. There is a green status-light below each check-box ("Enable Links") / left of the check-boxes (trigger number and DHE selections) to indicate whether the selected link is correctly activated. If there is no green light for a check-box, no data will be transmitted to the corresponding receiver.

If a link could not be enabled successfully, there are several possible reasons. A simple reason could be that the settings were changed during a Belle II physics run. ONSEN settings can only be changed properly when the system is not running, i.e. no physics run is being performed. Link problems can also be caused by (faulty) firmware updates, network problems or hardware failures.

All parts of the RoI distribution are shown at once in figure 4.12 on page 52. As mentioned above, the user must first select the Selector CNCBs that are to receive RoIs (RoI Fork). After that, the user can select the relevant trigger numbers for each of these Selector CNCBs (Trigger Number Selection). The user can then select the DHE IDs to sent only RoIs for the corresponding HL to certain Selector AMCs (DHE Selection).

Whatever the settings, the user must always ensure that each Selector AMC receives the RoIs for the connected DHC / DHEs. Incorrect settings might result in unintended loss of data. If there is any change of the DHH-ONSEN connections needed, one can easily adjust the RoI distribution settings to take that into account.

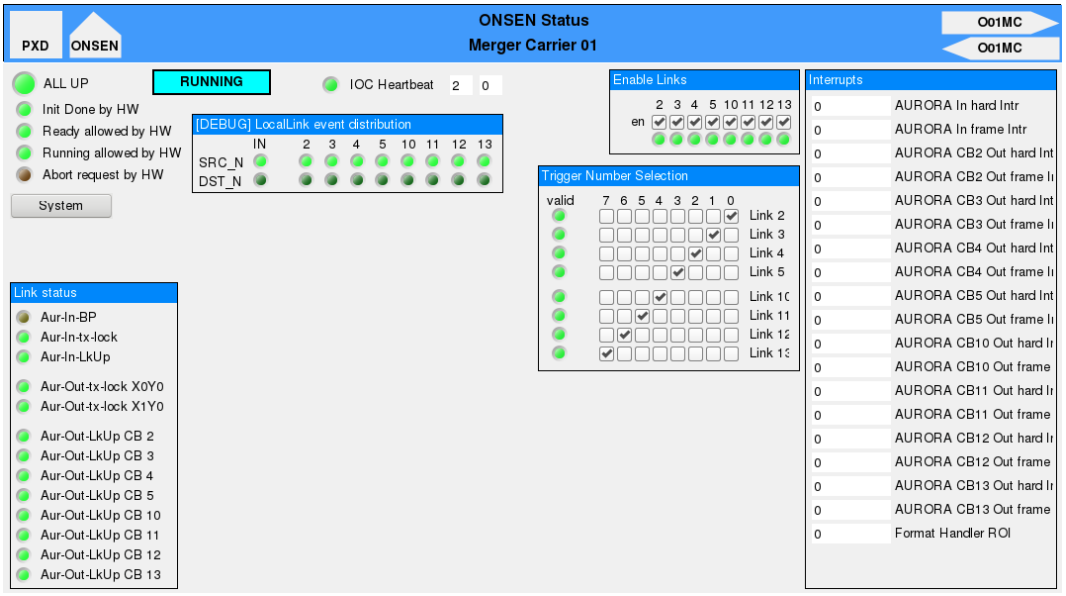

(A) CSS user interface of the ONSEN Merger CNCB. The check-boxes on the top right control the links to the Selector CNCBs (RoI Fork). The check-boxes below control the trigger number selection.

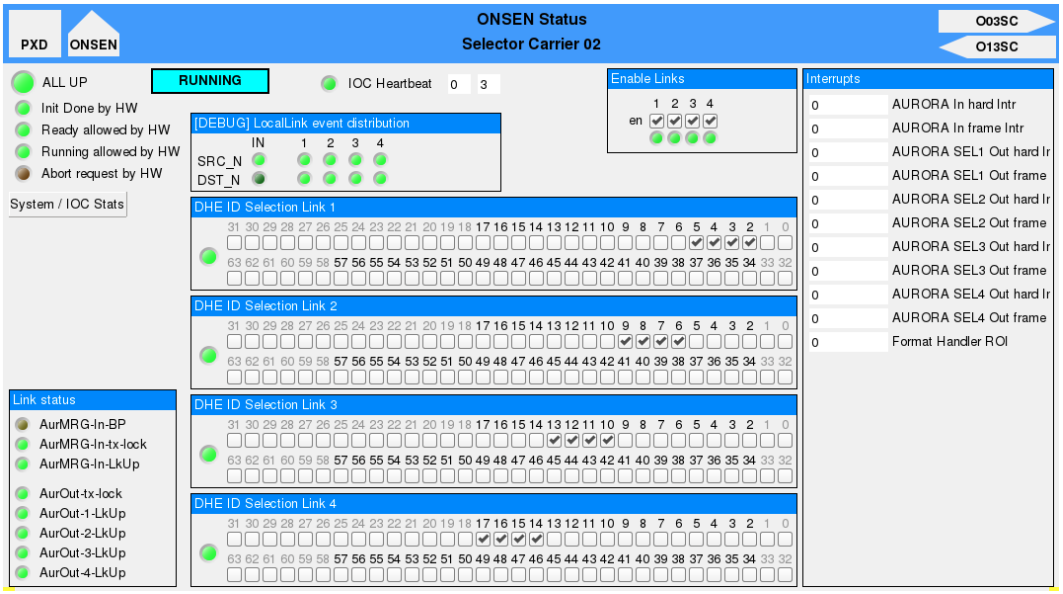

(B) CSS user interface of the ONSEN Selector CNCB. The check-boxes on the top right control the links to the Selector AMCs (RoI Fork). The check-boxes below control the DHE selection.

FIGURE 4.11: CSS interfaces of the ONSEN CNCBs as used at the time of tests at KEK (see chapter 6). The RoI distribution settings can be changed by using the check-boxes.

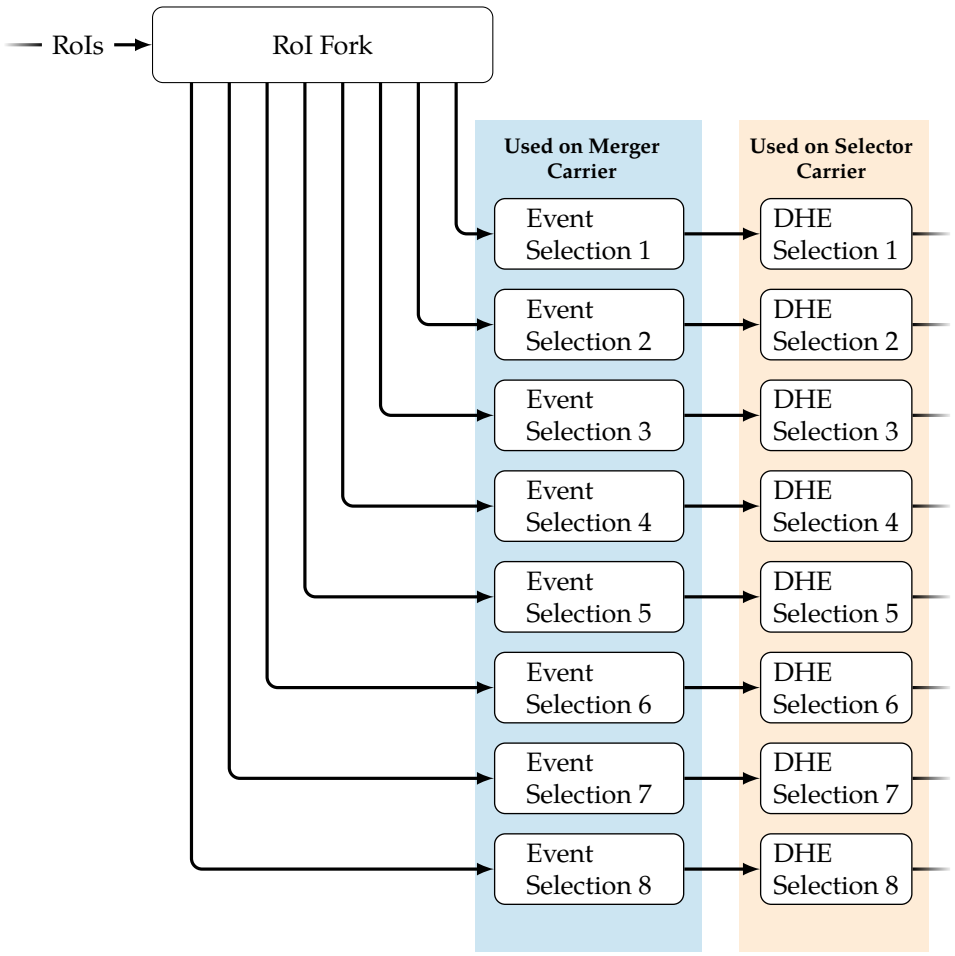

Figure 4.12: RoI distribution in ONSEN. RoIs are forwarded to up to eight Selector CNCBs / four Selector AMCs based on the RoI Fork settings. Two selections are made after that: the trigger number selection on the Merger CNCB and the DHE selection on the Selector CNCBs.

4.6 Other Firmware Adaptations

4.6.1 Overview

At the time of writing, the ONSEN firmware was being optimised and tested by several developers in parallel. The ONSEN software and firmware developments are available in a Git repository used by the ONSEN developers at JLU. The repository includes data generators, firmware and software of the ONSEN IP cores as well as firmware components for specific purposes such as CRC calculations, among others.

The firmware adaptations for the ONSEN discussed below were developed as part of this thesis. There are other firmware adaptations made by other developers which are only mentioned without further details. In chapter 5, for example, test campaigns are discussed which revealed errors in the ONSEN data processing e.g. when unexpected data is delivered to the system. Therefore, for some time, the focus shifted to development and testing to make the ONSEN more reliable in such situations. Some of the observed issues and test scenarios are discussed in sections 5.4 and 5.5. However, the details of the firmware changes are not covered in this thesis.

The RoI distribution was tested at KEK. For these tests, the IP core *IP Writer* was developed. The core as well as the tests are discussed in chapter 6.

Note that the HLT, DATCON and DHH were not available at JLU at the time of firmware development covered in this thesis. As a workaround, all test-relevant data that was used during development was emulated on PCs using dedicated C++ programs.

4.6.2 Handling of HLT-rejected Events in ONSEN

The RoI data from the HLT contains several bits ("flags") which trigger actions in the ONSEN data processing. As mentioned in section 4.4.2, the HLT data also contains information on whether the PXD data for a trigger number should be discarded completely. This information is conveyed by the "Accept"-bit, highlighted in figure 4.13 which shows the HLT data format specification relevant for the ONSEN.

When PXD data or rather DHH data, was completely discarded based on the Accept-bit, then the ONSEN did not send any data to EB2. At the same time, the EB2 received data from the HLT for all trigger numbers. It was not immediately clear whether it was expected that the ONSEN-processed PXD data would be missing or not. Therefore, as part of this work, the RoI Parser (roi_parser) and the LUT Reader (ptr_lut_read) were adapted.

Instead of sending nothing when the PXD data is rejected by the HLT, the ONSEN firmware was adapted to send the dummy data that is also sent if no DHH data is available for the RoIs. Thus, ONSEN data for every trigger number is forwarded to

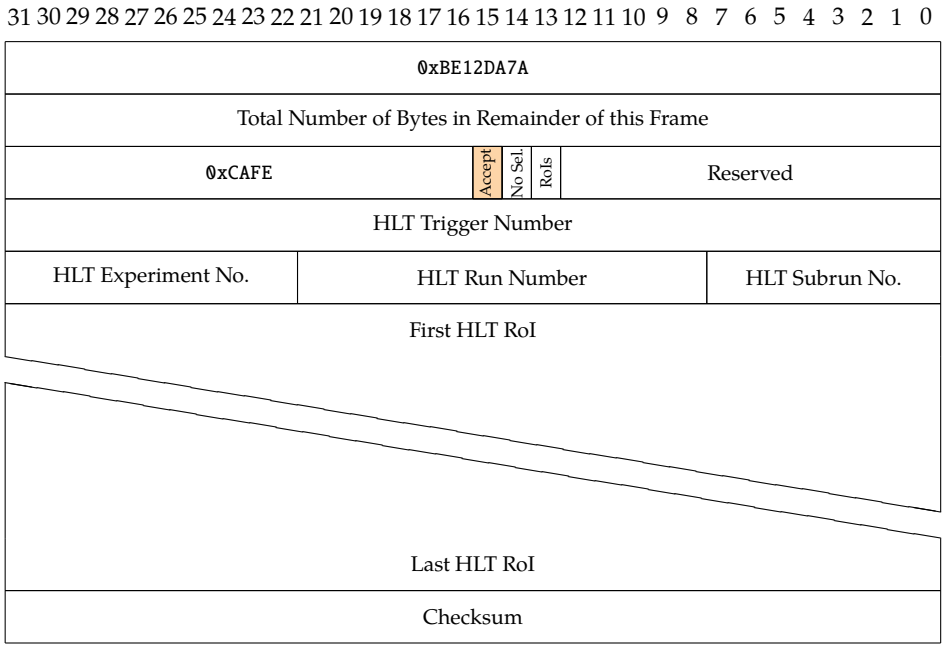

Figure 4.13: HLT data format relevant for the ONSEN. The "Accept"-bit indicates whether the PXD data for a trigger number should be discarded. Other bits (flags) can disable the selection based on RoIs ("No Sel."-bit) or enable the RoIs from the Merger to be added to the data stream sent to EB2 ("RoIs"-bit). Data format adapted from Ref. [6, p. 167]; an additional `0xBE12DA7A` was introduced after the reference was published.

EB2 and any unintentional loss of ONSEN-processed events can be easily detected without having to analyse whether the event was rejected by the HLT.

The ONSEN data frames which are sent to EB2 when the data for a given trigger number has been completely discarded are shown in figure 4.14. The content of these frames is discussed in more detail in the appendix A.

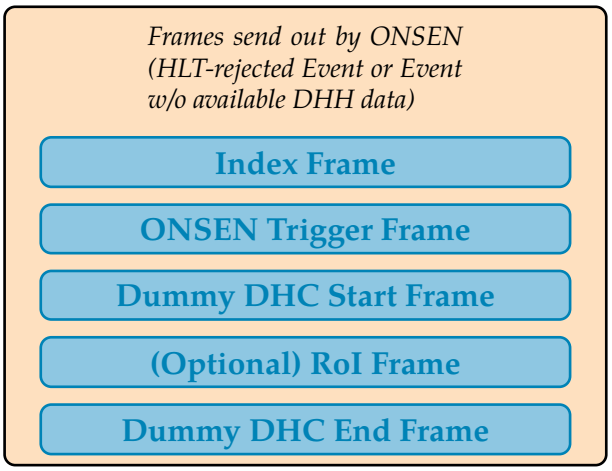

Figure 4.14: Data frames sent by ONSEN Selectors to EB2 when the event has been rejected by the HLT. The DHH data (if present) is replaced by dummy frames. The same frames are sent by ONSEN if no DHH data is available for HLT RoIs for a given trigger number.

4.6.3 Clearing ONSEN RAM from invalid Data

DATCON data and PXD data are buffered in the RAM of the Merger and Selector AMCs, respectively, until the corresponding HLT RoIs are available. Once the data has been successfully processed, it is forwarded to EB2. The data is then no longer needed in ONSEN and the buffers are used for new data.

During the development of the ONSEN firmware, great efforts were made to ensure the reliability of the system. Thus, if the processed data was invalid for any reason (e.g. indicated by a incorrect CRC checksum), the data was kept in buffers for analysis and debugging. The data was also kept if DATCON or DHH data for a given trigger number (with valid data) was sent to ONSEN more than once before the corresponding HLT RoIs have become available. The trigger number is taken into account when buffering data as indicated in figures 4.5 and 4.6. So if there is data for the very same trigger number more than once, this might indicate incorrect data processing in or before ONSEN.

Depending on the frequency of the occurrence of invalid or overwritten data, the RAM fills up more or less quickly and the memory space available for other data becomes less. In the worst case scenario, the memory must be cleared manually by rebooting the ONSEN system. To avoid this situation, the ONSEN firmware and software, respectively, in particular those for the Data Reader (npi_read_ll) and

the LUT Writer (ptr_lut_write), were adapted to clear the RAM from any invalid or overwritten data. The data is no longer kept for analysis and no RAM is wasted. Invalid and overwritten events are still counted in ONSEN monitoring, thus such errors won't be missed by the ONSEN operator.

4.7 Selector Data Sizes and Rates

4.7.1 Comparison of the Selector Input and Output Data Sizes

The following section aims to illustrate the changes of data sizes before and after the selection of PXD data in ONSEN. An overview of the data formats discussed in this thesis can be found in appendix A. More comprehensive information can be found in Ref. [6, pp. 163-172] or in (internal) Belle II documentations.

The ONSEN selects PXD data based on RoIs and HLT rejection of complete events to significantly reduce the expected PXD data rate of $\sim$ 20 GB/s. However, the ONSEN does not just remove data, it also adds certain data frames. Depending on the size of the PXD data, the data sent by the ONSEN to the EB2 may be larger than the DHH data received by the ONSEN. Of course, this is more of an edge case that is not expected in normal Belle II operation. The sizes of the frames added by the ONSEN are listed in table 4.1.

The relevant DHH data frame sizes for this estimation are listed in table 4.2 for a single ONSEN Selector. A setup where each Selector receives data from five DHEs (and five HLs) is assumed for the calculation. There are data frames of constant size which contain various informations like the trigger number and the CRC checksums. Other data frames vary in size depending on the number of PXD hits. Furthermore, the number of DHP frames is not limited to one per DHP and trigger number. For simplicity, just one frame per DHP is taken into account for the following.

The constant size of DHH data per trigger number and Selector is 20 Byte (1×DHC Start) +80 Byte (5× DHE Start) +240 Byte (4×5 DHP frames (without PXD data))

Size of ONSEN introduced Frames	
Index Frame	8 Byte + 4 Byte × number of frames
Trigger Frame	32 Byte
RoI Frame	12 Byte + 8 Byte × number of RoIs

Table 4.1: Size of the data frames added by the ONSEN. The Index frame contains information about the number of frames and the size of each frame. There is no fix number of frames for each trigger number, thus, the size of the Index frame is not constant. The Trigger frame contains information from the RoI sources (HLT and DATCON). Its size is always 32 Byte. The optional RoI frame contains all RoIs for a given trigger number. The RoI frame will not be considered in the estimations.

Size of DHH Frames	
DHC Start	20 Byte
DHE Start	80 Byte (=16 Byte/DHE × 5 DHE)
DHP	12 Byte/DHP × 5 DHE × 4 DHP/DHE + hits in PXD (2-4 Byte/hit)
DHE End	80 Byte (=16 Byte/DHE × 5 DHE)
DHC End	16 Byte

Table 4.2: Size of DHH frames for a single Selector AMC per event. Each ONSEN Selector is expected to receive data from one DHC and up to five DHEs. For the estimation, four DHP frames per DHE are taken into account.

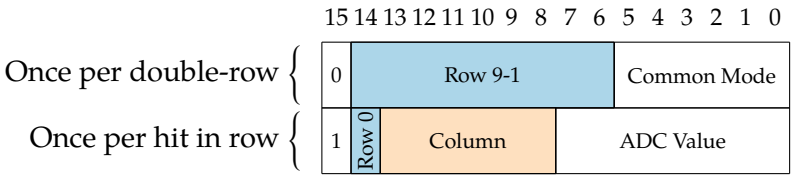

Figure 4.15: Pixel coordinates (highlighted) as sent to ONSEN. The least significant bit of the pixel row is in a different 2-byte word than the other bits of the pixel row. Thus, the pixel column and the LSB of the pixel row are needed for each hit, while the other pixel row bits are needed only once per double-row. Adapted from Ref. [6, p. 164]

+80 Byte (5× DHE End) +16 Byte (1×DHC End) = 436 Byte.

The data size of a single pixel hit depends on its location on the PXD module. As shown in figure 4.15, the first 2 Byte of the pixel coordinate are only needed once per double-row because the least significant bit of the row coordinate is in a different 2-byte word where the pixel column coordinate can also be found. Therefore the first 2 Byte can be omitted for pixel hits in the same (double-) row. So either 2 Byte or 4 Byte are needed to describe the pixel coordinates. In the following, an average data size of 3 Byte per hit is assumed to keep the estimation simple.

Assuming a constant number of frames sent by DHH (without PXD hits) for each trigger number, the data size of the resulting ONSEN Index frame can be calculated: 8 Byte + 4 Byte × 33 = 140 Byte. Since the size of the ONSEN Trigger frame is also constant (32 Byte), 172 Byte must be considered in addition to the constant DHH data. Thus, there is a constant data size of 172 Byte + 436 Byte = 608 Byte sent by the ONSEN Selector AMC for a given trigger number. The optional RoI frames are not included in this estimation.

The rejection of PXD data based on RoIs only makes sense when a "break-even point"[4] in terms of the number of hits on the PXD modules is reached. For simplicity, differences in data sizes depending on the type of the rejection (HLT-rejection of complete events or selection of PXD data based on RoIs) are ignored. In this

[4] Actually a term used in economics; it indicates e.g. how many units of a product have to be sold to make profit.

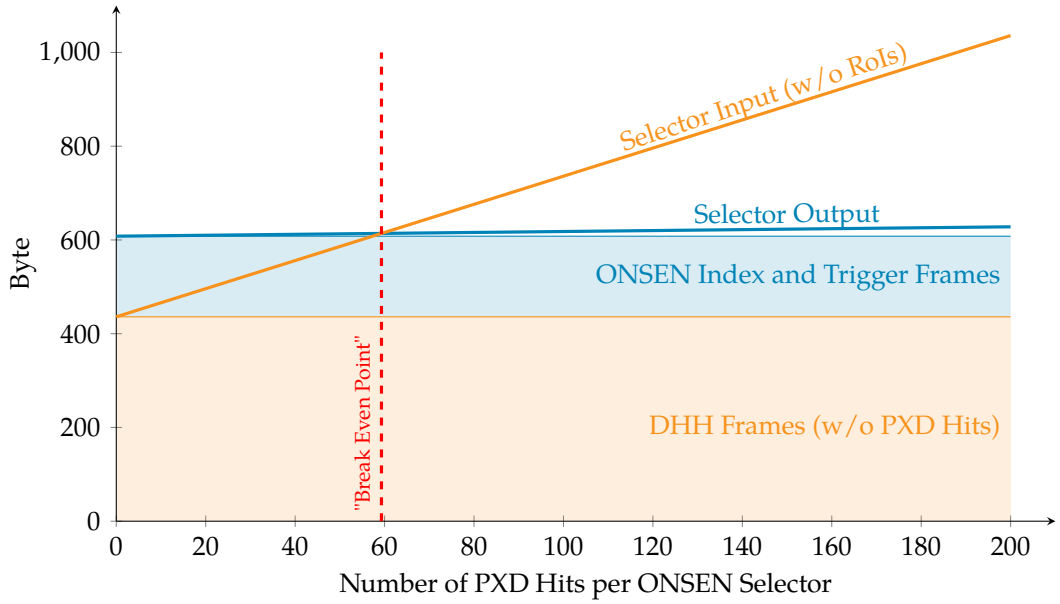

Figure 4.16: ONSEN input and output data sizes. A size of 3 Byte has been considered for each pixel. For simplicity, a PXD data rate reduction factor of 30 is assumed to be achieved by data selection based on RoIs. The HLT-rejection of complete events was not taken into account.

estimation, it is assumed that the expected reduction factor of 30 is achieved using only RoI-based data selection.

With the aforementioned data size estimates, the data selection based on RoIs is useful once there are at least $\sim$ 60 pixel hits in the DHH data for each Selector. Figure 4.16 illustrates the calculation described for a single Selector.

4.7.2 Selector Input and Output Data Rates

In Belle II operation, the expected maximum PXD occupancy of 3% is equal to

$$0.03 \times 192{,}000\,\text{pixels/DHE} \times 5\,\text{DHE/DHC} = 28{,}800\,\text{pixels/DHC}.$$

There are a total of eight DHCs, so 3% PXD occupancy equals

$$8\,\text{DHC} \times 28{,}800\,\text{pixels/DHC} = 230{,}400\,\text{pixels}$$

which is also the maximum number of pixels expected on average as input data for the Selectors. This is equivalent to 5,760 pixels per PXD half-ladder.

Using the data size estimates above, a trigger rate of 30 kHz and taking eight DHCs into account, gives a data rate of

$$(8\,\text{DHC} \times 436\,\text{Byte/DHC} + 3\,\text{Byte/pixel} \times 230{,}400\,\text{pixel}) \times 30\,\text{kHz} \approx 20.8\,\text{GB/s}.$$

The data is distributed to 32 Selector AMCs. Therefore, the input data rate for each Selector AMC is ~ 650 MB/s. Assuming a reduction factor of 30, the output data rate of each Selector AMC is ~ 22 MB/s and the total ONSEN output data rate is only

$$20.8\,\text{GB/s} \times \frac{1}{30} \approx 700\,\text{MB/s}.$$

Note that for this calculation a rough assumption of an average data size of 3 Byte for each pixel hit has been made. So the actual output data rate of the Selectors is expected to be less than in this estimate. Similar calculations in Ref. [6, pp. 53-55] and Ref. [83, p. 66] assumed 2.5 Byte on average for each pixel hit. In total a data size of ~ 17.3 GB/s for a PXD occupancy of 3% at the maximum trigger rate of 30 kHz was estimated in these references.

4.8 Test Setups at JLU

The test setups at JLU were lacking the HLT, the DATCON, the DHH and the EB2. For testing of the ONSEN system, the RoI data from HLT and DATCON, and the DHH data was emulated using dedicated C++ programs.

The HLT-RoIs were sent via Ethernet cables to the ONSEN Merger AMC using PCs. The emulated DATCON and DHH data was sent via Ethernet cables to AMCs to convert the SiTCP input to an optical (Aurora) output, which was then sent via optical fibres to the ONSEN. So for each DATCON and DHH emulation an additional AMC was required. The ONSEN-processed data was sent via Ethernet cables to a PC.

Only the test setups at DESY or at KEK provided all ONSEN-relevant systems and enabled to identify ONSEN problems in an environment similar to the one used for the Belle II experiment.

Chapter 5

ONSEN Tests at DESY

5.1 Overview

At the time of this work, two VXD test beam campaigns were carried out at DESY (Hamburg, Germany) in 2016 and 2017. The campaigns were carried out with scaled-down DAQ systems (incl. HLT, DATCON, DHH and EB2) and provided a valuable opportunity to identify unexpected behaviour at hardware and firmware level in a setup similar to the one used at KEK for the Belle II experiment.

A number of $\sim 100 \times 10^6$ events (2016) and $\sim 300 \times 10^6$ events (2017) were collected in several hundred runs and analysed after the respective campaigns[1]. The stored data from both campaigns has a total size of several terabytes. The data was analysed by several institutes / members of the Belle II collaboration.

Information about runs performed at DESY can be found in the Belle II Elog [84] (restricted to Belle II members). The Elog also contains details of runs taken at KEK.

5.2 DESY Test Beam Facility

The DESY II test beam facility [85] provides a comprehensive overview of the DESY test beam facility and used as reference in this section.

The DESY provides three independent test beam areas: TB21, TB22 and TB24. An electron or positron beam with momenta in the range of $1\,\mathrm{GeV}/c$ to $6\,\mathrm{GeV}/c$ can be used in each of them.

In the DESY II synchrotron, electrons or positrons circulate with energies up to $E_{max} = 6.3\,\mathrm{GeV}$ in normal operation. For the test beam areas, there is no direct extraction of the DESY II beams. The beams for the test areas are generated via multiple conversion processes. Carbon fibres in the DESY II beam line are used to generate bremsstrahlung photons. The photons hit a target where electron-positron pairs are generated. Several targets are available for this purpose. These are made of either aluminium or copper in various sizes.

The PCMAG, a superconducting solenoid which was provided by KEK, enables the use of magnetic fields of up to 1.25 T at the DESY test beam area [85].

[1] These numbers include only events from a subset of runs taken at DESY for which I determined the number of events using the Belle II Analysis and Software Framework (BASF2). Thus the numbers presented here do not represent the total number of events collected.

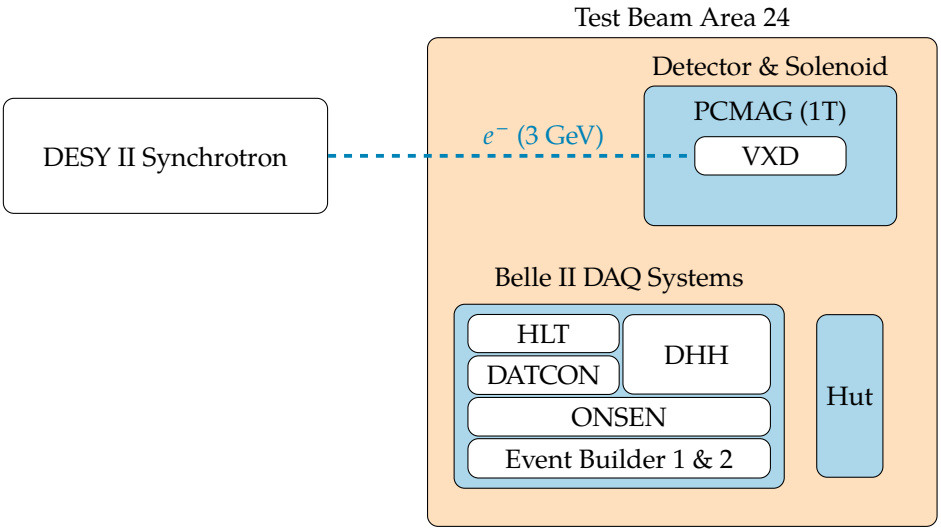

Figure 5.1: Schematic overview of the DESY test beam setup. Belle II test campaigns were performed in test beam area 24 (TB24). The beam energy and the magnetic field are based on run 243 (2017) which is discussed later in this thesis. Scaled-down VXD and DAQ systems were used. The testers monitored and operated the test runs from a nearby hut in the test beam area.

5.3 Test Setups

The Belle II tests were carried out in test beam area TB24(/1) where electron beams with energies of up to 5 GeV (2017) were used. The setup included a scaled-down VXD composed of up to four PXD half-ladders, four SVD layers, and a scaled-down DAQ system setup. The tests were operated and monitored from a nearby hut.

Figure 5.1 shows in a simplified way the setup used for the Belle II tests at DESY. The values for the beam energy and magnetic field are based on the settings used for a run which is discussed in section 5.6 and listed in Belle II Elog [84, run 243] (2017). In this run, data was collected with a trigger rate of 1.3 kHz and an electron beam with an energy of 3 GeV. The PCMAG solenoid provided a magnetic field of 1 T. No collimator was used.

The tests were carried out with up to four PXD half-ladders. Two modules used in the tests are shown in figure 5.2.

The PXD and SVD modules, and their arrangement as used in tests at DESY are shown in figure 5.3, an adapted screenshot of the event display used for monitoring. In addition, two RoIs calculated by the HLT are shown; one RoI for each PXD module in a single event. Further discussion of RoIs in both PXD layers follows in section 5.6.3.

In pre-2016 test beam campaigns, Pocket-ONSEN(-like) setups were used. Results of those ONSEN tests at DESY, are discussed in theses [7, pp. 69-80] and [6, pp. 98-108], among others.

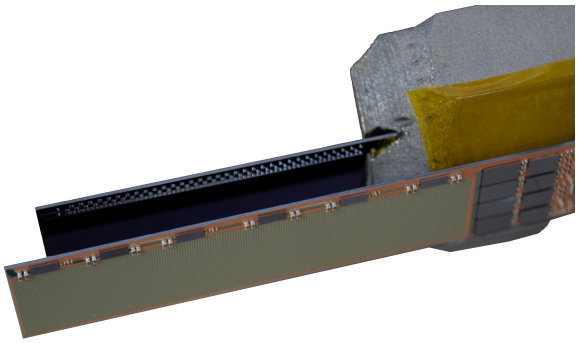

Figure 5.2: Photo of the PXD modules (half-ladders) used for tests with electron beam at DESY. The size of the sensitive area of the outer layer module, which is shown more prominent on this photo, is $6.144 \times 1.25\,\mathrm{cm}^2$.

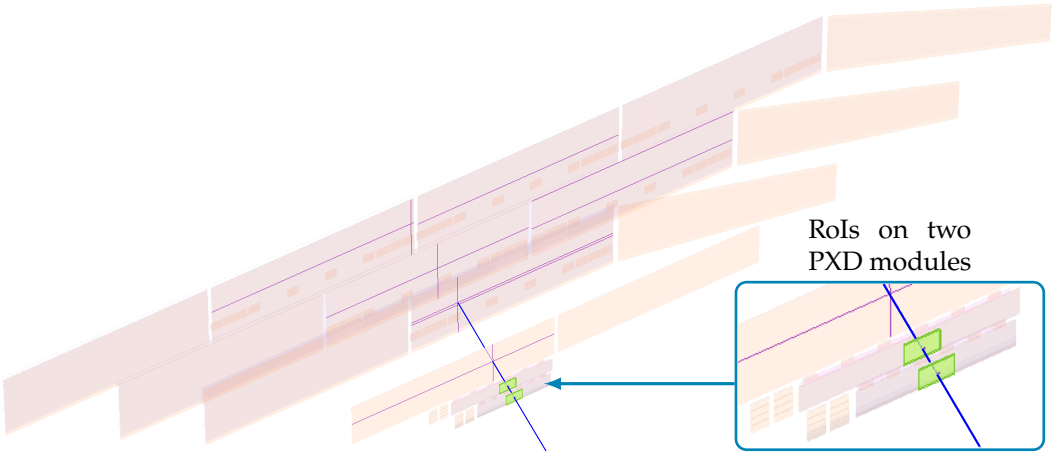

Figure 5.3: Two PXD and four SVD layers as used in tests at DESY. A RoI (green) for each PXD module was calculated based on a reconstructed track (blue). The picture was adapted from a screenshot of the event display which was used at the time of the tests.

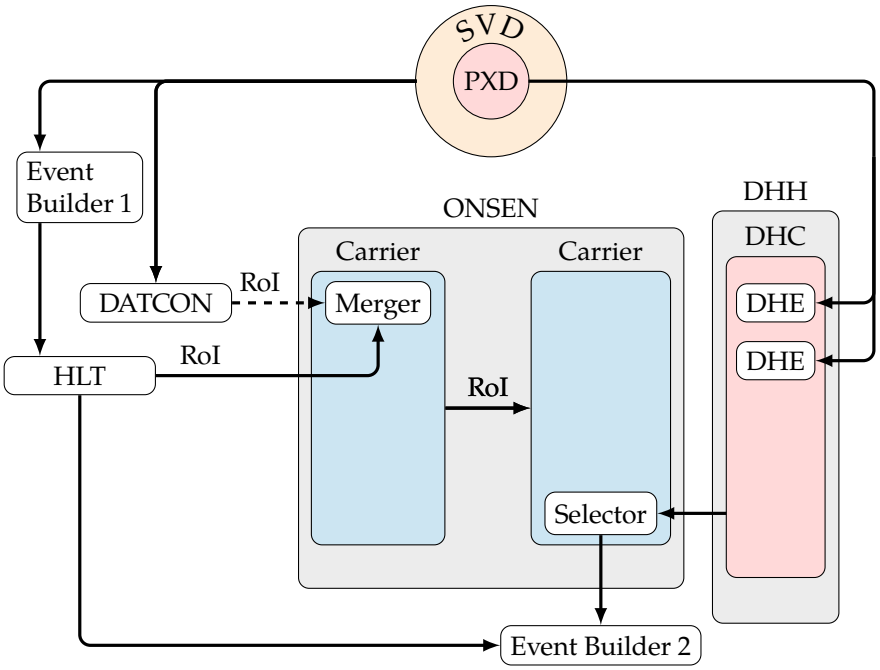

Figure 5.4: Setup at DESY in 2016. One Selector AMC received data from a DHC with two connected DHEs. The Merger received RoIs from the HLT. The DATCON was not used as RoI source in most of the runs.

In 2016 test campaign, a reduced ONSEN setup consisting of two CNCBs (Merger and Selector CNCB) and two AMCs (one Merger and one Selector) was used. The ONSEN CNCBs were plugged into a 2-slot-ATCA shelf (see figure 4.2a on page 38). The test setup is illustrated in figure 5.4. The ONSEN received PXD data from one DHC with two connected DHEs in most of the runs. The HLT was the main RoI source for the ONSEN; the DATCON was connected to the ONSEN in just a few runs. Data from the ONSEN was sent to the event-builder-2.

The 2017 setup shown in figure 5.5 differs slightly from the 2016 setup. The number of available PXD modules was increased to up to four PXD half-ladders. At that time, a second DHC and two additional DHEs were used for the readout of the PXD HLs. However, not all hardware was available in all test runs. The data discussed later in this chapter, was collected with only two PXD HLs. The 2-slot-ATCA shelf used for the ONSEN in 2016, was replaced in 2017 by a 14-slot ATCA shelf with a full-mesh backplane (see figure 4.2b on page 38). An equivalent shelf is used in the final KEK setup.

In 2017, the DHH data was not sent directly to the two Selector AMCs. Instead, the data was redirected to other AMCs, hereinafter referred to as *Fork* cards, which were plugged into the Merger CNCB. The Forks forwarded the DHH data to the Selectors and also to a local PC where the data was stored for debugging. This allowed to analyse unexpected behaviour that might be caused by incoming data. The DHH data was not stored in each run as this would have meant storing a significant amount of data on an ordinary PC. Therefore, the AMCs that acted as Forks were loaded with either the Fork-firmware or a firmware that simply forwarded the data

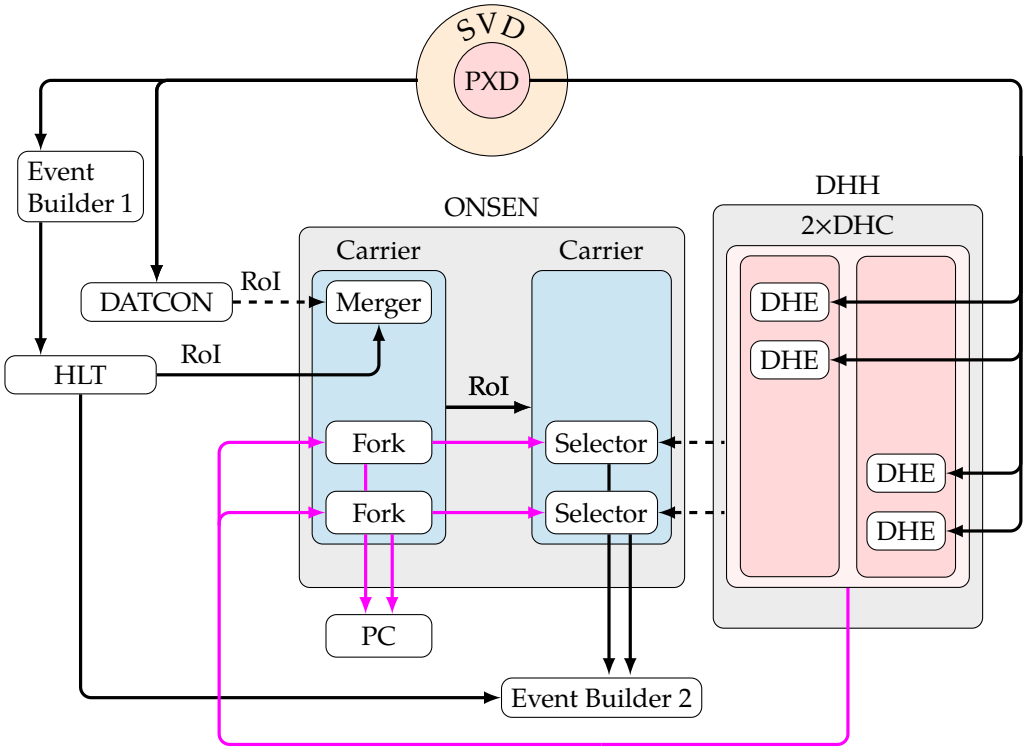

Figure 5.5: Setup at DESY in 2017. Data of DHH system with up to four DHEs (one for each of the four PXD half-ladders), was redirected to Fork cards which forwarded the incoming data to the Selector AMCs and, in some runs, to a PC for an optional analysis. As a side effect, comparison of DHH data and ONSEN-processed data was possible. This is done in section 5.6 for test data collected in a test setup including two DHEs. The DATCON was not included in most of the test runs.

from DHH to ONSEN.

In both test beam campaigns, the ONSEN AMCs were plugged into ONSEN CNCBs. μTCA shelves were available to serve as backup solution if the CNCBs hardware failed for any reasons. In worst case scenario, the tests would have been continued using a Pocket-ONSEN setup.

5.4 Observations in Tests at DESY

The following focuses on the ONSEN and discusses some of the most troubling issues found in the tests. This thesis does not cover all the observations made during the test campaigns. Besides the results presented here, additional results and lessons learned from the test campaigns were discussed Belle II internally e.g. at regular Belle II General Meetings (B2GMs) or at conferences (see Ref. [67], for example). Some other test setups and results can be found in publications like Ref. [86] and Ref. [87].

5.4.1 Temperature Dependency of Links

Although the ONSEN had been tested numerous times at the JLU before the test beam campaigns at DESY in 2016 and 2017, the tests at DESY showed surprising behaviour of the ONSEN data processing.

The focus of the tests at JLU was on the general functionality as well as the development of new features. However, the ONSEN hardware was located in the JLU laboratory of the II. Physics Institute where the environmental conditions were quite stable. The ONSEN was therefore tested under certain constant conditions at JLU. As a result, ONSEN internal settings and adjustments that ensured proper data processing and link stability etc., were unintentionally dependent on the environmental conditions – or, to be more precisely – on the temperature of the laboratory. For the test beam campaigns, however, the hardware was transported to DESY where the environmental conditions were different.

During the test runs at DESY (2016), we noticed that the data flow in ONSEN was not stable. This resulted in data corruption and in a loss of complete events. To rule out hardware defects, we tried different combinations of the Merger and Selector hardware for retesting and further investigation. We also started to focus on the firmware, especially on the Aurora IP cores used in ONSEN for handling LVDS links between AMCs and CNCBs.

As the firmware had worked without such errors at JLU we assumed that the new environment might have an effect on the ONSEN data processing. To investigate the issue further, we adjusted the fan speed of the shelf and thus the temperature of the AMCs and CNCBs, and covered empty AMC slots in the shelf to optimise airflow. At the same time, we analysed the stability of data flow using the Xilinx Chipscope logic analyzer. With this setup and some exploratory testing, we were able to trace the problem down to the clock-delay-settings of the Aurora IP core used

in the CNCBs. We found that there was an unexpected temperature dependency: the LVDS links became unstable when the CNCB temperature exceeded 58°C.

We tested different clock-delay-settings of the Aurora core using Chipscope. We kept the clock-delay that worked reliably in tests at DESY. However, this was only a hotfix introduced to ensure stable data flow in the test campaign. After the test campaign, the Aurora link setting was changed to automatically adjust the clock-delay after each restart of the ONSEN.

5.4.2 Undefined States

In addition to dependencies on environmental conditions, undefined (invalid) data input could cause ONSEN errors at the time of the test beam campaigns. From a technical point of view, the ONSEN was designed to process data with well defined specifications. In tests performed at JLU, the emulated data complied with the official data format specification.

During test campaigns at DESY, especially in 2017, the ONSEN data processing often got stuck or corrupted shortly after the start of a test run. In the first case the ONSEN did not read and process any more data, resulting in an interrupted data flow between the PXD and the EB2. In other cases, we found that the trigger numbers in the ONSEN-processed data were inconsistent. The errors could not be reproduced in every test run. In several test runs the ONSEN data processing was working for several hours without any issues.

In 2017, however, such errors occurred too frequently, making analysis of the received data unavoidable. The Fork cards were used for this purpose. The DHH data was redirected to the Forks where it was sent to the Selectors and to a PC where it was stored for analysis. This enabled to carry out further investigation in a convenient way, and even retesting using the same data.

We found that, especially in consecutive runs, the ONSEN did not process the data correctly. Further analysis showed that ONSEN was receiving data fragments from previous test runs before the actual start of a test run. In most cases, this led to incorrect data processing in ONSEN, which made a full restart of the ONSEN firmware ("cold-start") necessary. Unfortunately, this took several minutes and in some cases had to be done twice. This led to follow-up tests, which are discussed in section 5.5.

5.4.3 Changed Mapping of PXD Pixels

In 2016, a new version of PXD half-ladders was used. It came with a different pixel mapping than the previous version, which affected the ONSEN interpretation of the pixel coordinates in the DHH data. We became aware of the changed mapping at the time of the test campaign, thus, the ONSEN firmware had not yet been adapted to take the changed mapping into account at that point in time.

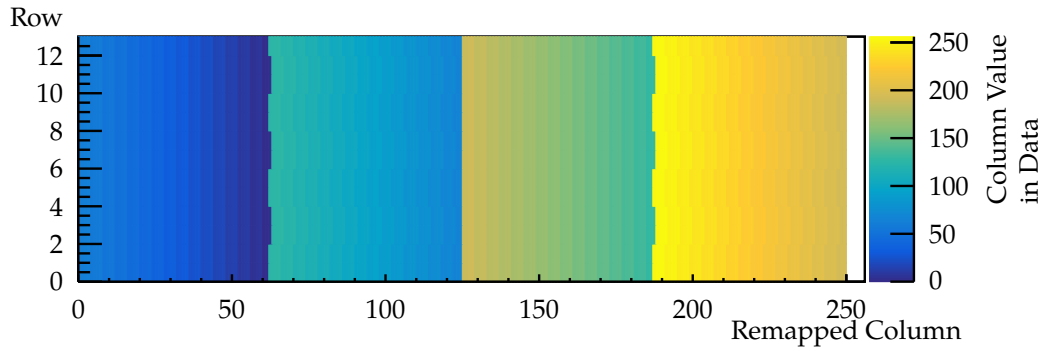

FIGURE 5.6: Illustration of mapping changes for one PXD half-ladder. From ONSEN point of view, the changed mapping was one of the most important changes discovered in DESY test campaign in 2016. Data loss due to the changed mapping could be avoided by choosing RoI sizes accordingly.[a]

[a]The changed mapping was also discussed in Belle II meetings (with similar representations of mapping changes). For example in workshop contribution *Mysterious Mapping Mess* [88, p. 9] by F. Lütticke

For the test campaign in 2017, the ONSEN firmware (pixel_filter IP core) was adapted to take the changed mapping into account for the PXD data selection based on RoIs. This solution required the actual remapping to be done offline with the BASF2.

The mapping changes are shown in figure 5.6. For this illustration, emulated DHH data for a 100% PXD occupancy was remapped using BASF2. The "Row" and "Remapped Column" represent the remapped pixel coordinates while the colour gradient in "Column Value in Data" shows the pixel column coordinates before the remapping. There are four sections visible, one for each of the four DHPs which are part of a PXD half-ladder. In each DHP-section, the coordinates are shifted. At the DHP borders, the mapping of the coordinates is more complicated.

The mapping for inner forward, inner backward, outer forward and outer backward modules is different. There is also a "flip" in the row direction to consider. The effects of incorrect mapping are shown in figure 5.7 on the facing page. 100% occupancy on a single PXD half-ladder was emulated in 100,000 events. 546,845 RoIs have been emulated so that the RoI-selected data resembles the Belle II logo when correctly mapped. The ONSEN-processed data was then unpacked using BASF2 with and without correct mapping.

At the time of the tests in 2016, data loss due to the mapping issue could be avoided by skipping the RoI-selection of PXD data in ONSEN, or by setting sizes of the RoI in column direction such that no data loss could occur due to the changed mapping.

The (internal) Belle II note [89] lists the official numbering scheme for PXD and SVD. The reference contains the information, how the PXD pixels can be addressed and transformed to natural coordinates.

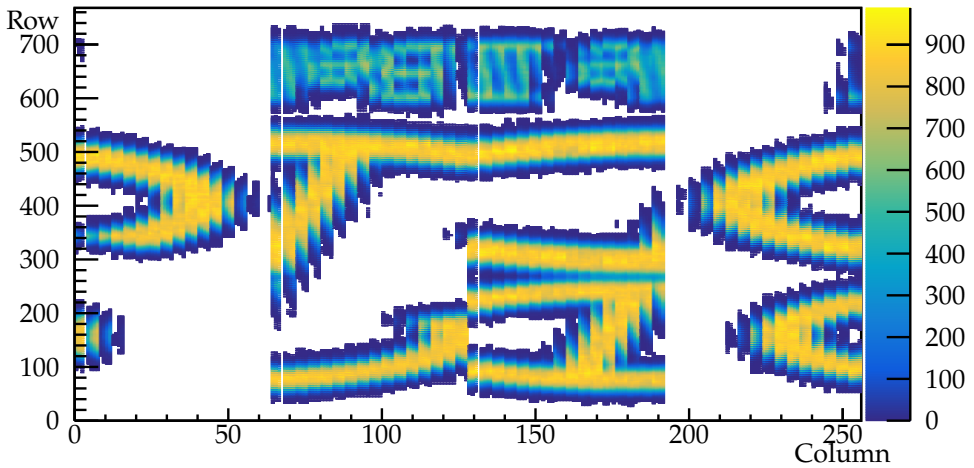

(A) Data with incorrect mapping.

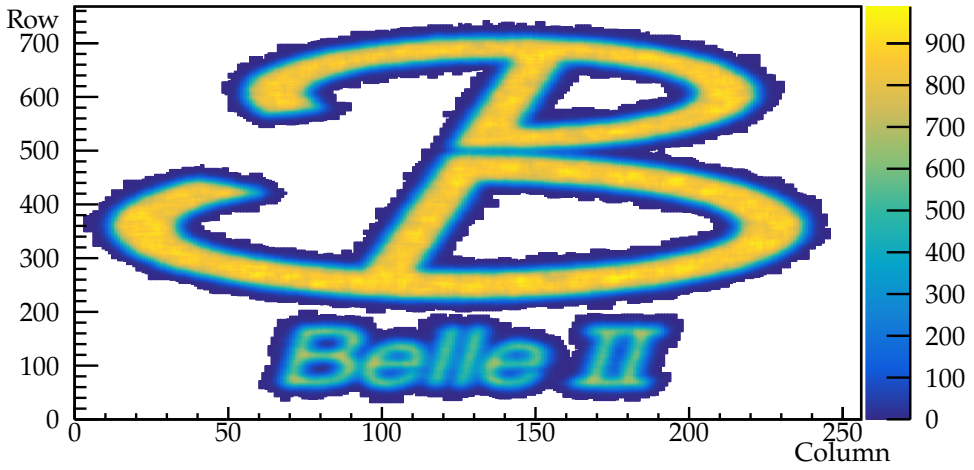

(B) Data with correct mapping.

FIGURE 5.7: Comparison of data w/ and w/o correct mapping. 100,000 emulated uniform distributed PXD data events and 546,845 emulated RoIs in total were used as data set. The RoI-selected PXD data of all events resemble the logo of the Belle II collaboration if the correct mapping has been applied. The gradient indicates the number of RoI-selected data on the PXD module.

5.4.4 Trigger Number Mismatch in Data

Some data collected in test beam campaigns had inconsistent trigger numbers in the ONSEN-processed data. Different types of mismatches were observed. Some originated in the DHH (e.g. mismatch of DHC and DHE trigger numbers), some in the ONSEN system (e.g. mismatch between HLT and DHH trigger numbers).

The conditions that lead to inconsistent trigger numbers were not fully understood at the time of the test beam campaigns. However, this error was not observed in tests conducted prior to the test beam campaigns. Therefore, after the DESY test beam campaigns, extensive tests were carried out at JLU to find conditions leading to trigger number mismatches and other incorrect data processing in the ONSEN system. These tests are discussed in the following.

5.5 Follow-up Tests at JLU

We learned a lot from the test beam campaigns, which showed the need for such testing to find unexpected or unintended side effects that were not considered at the time of development. It's unlikely that testing at JLU alone would have revealed a dependency on environmental conditions such as temperature.

At time of the test beam campaigns, the ONSEN-processed data was collected by the EB2 and stored in sroot files. The data in these files were used for further testing of the ONSEN shortly after the 2016 test campaign. The ONSEN relevant data (i.e. DHH and HLT RoIs) was extracted and formatted such that the data could act as data input for the ONSEN again. The data was used in tests which were conducted in close cooperation between the ONSEN developers.

Since the data from the test beam campaign was used, we expected to be able to reproduce the observed errors which may have been caused by specific data constellations not covered by the ONSEN firmware. Unfortunately, this approach did not yield any new relevant findings to prevent the errors observed in 2017.

In 2017 test beam campaign, invalid data received by the ONSEN system caused errors with high severity. These included incorrect merging of HLT and DHH data (trigger number mismatches), and unexpected interruptions in data processing (back pressure, lost links) requiring a complete restart of the ONSEN system.

Therefore, after the test beam campaign, the focus of the tests was on the behaviour of the ONSEN when receiving corrupted/fragmented data. An exploratory testing approach was followed for these tests. The data from DHH, HLT and DATCON was emulated and the ONSEN-processed data was analysed using dedicated C++ programs (see appendix B) for test-specific data checks.

In addition, tests were conducted to analyse the behaviour of the ONSEN when the data corruption occurs while the ONSEN is receiving data. In these tests, the data input links were manipulated using a modified version of the Fork firmware. The modified Fork was used to introduce errors in several test scenarios. For these tests, the data was sent from PC to the "Link Manipulation" AMCs using Ethernet cables.

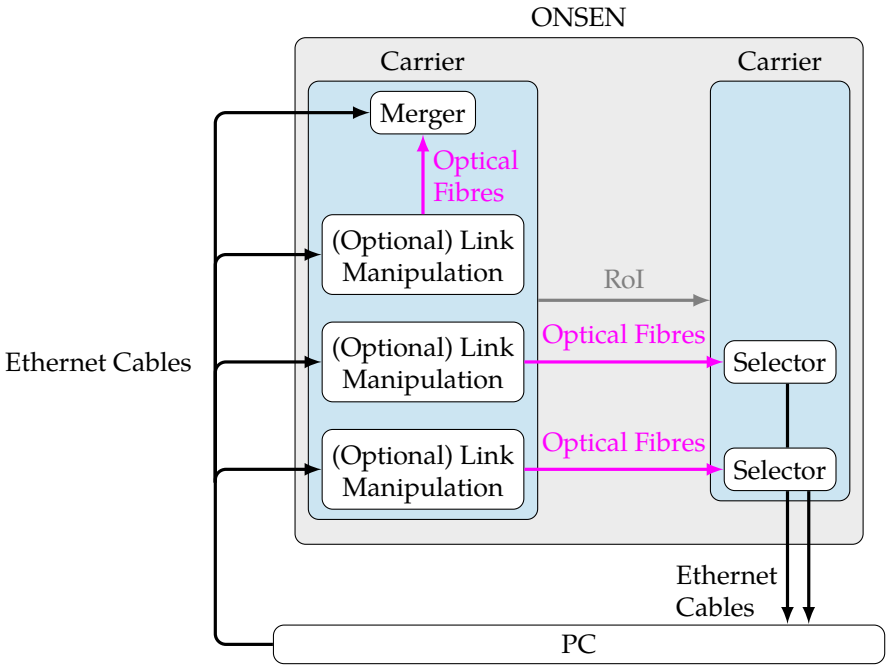

Figure 5.8: Setup at JLU (Gießen) for follow-up tests after the DESY test campaign (2017). The Fork firmware was adapted to corrupt the links in specific tests; in other tests corrupted data was sent from a PC and just forwarded to the ONSEN. Emulated DATCON and DHH data was transmitted via optical fibres (Aurora), emulated HLT data and ONSEN-processed data was transmitted via Ethernet cables (TCP). The test setup was also discussed e.g. in meeting contributions [90] and [91].

The data was then sent to the Merger and Selector AMCs using optical fibres. We analysed the ONSEN-processed data and also used the Chipscope logic analyzer for analysis of the data flow in ONSEN. A schematic overview of the test setup is shown in figure 5.8.

The results of the test scenarios listed below were discussed and evaluated by the ONSEN developers: no unexpected behaviour or severe ONSEN data processing errors with high priority were found. However, invalid data inputs can cause back pressure in ONSEN, leading to a stop of data flow. In this case, the affected hardware can be soft-reset using the ONSEN user interface for monitoring and controlling. The user interface as used at the time of the follow-up tests is shown in figure 5.9.

Missing Data

- Missing first four bytes of DHC Start frame
- Missing HLT magic word (see section A.3)

Redundant Data

- Send DHE Start frame at least twice
- Send HLT data for specific event twice
- Send HLT header twice

Figure 5.9: User interface for monitoring and operation of the ONSEN at the time of the follow-up tests of the test campaign in 2017. Here, the user interface for a single Selector is shown. It is a slightly modified version of the user interface shown in Ref. [6, p. 82].

Unusual Data

- Send invalid RoI coordinates
- Send DHH data not in expected ascending DHE ID order
- Send many RoIs (up to 70)
- Send many frames in a single event (up to 100)

Link Manipulation

- Improper start of DHC data stream
- Improper end of DHC data stream
- Improper LocalLink "Source Ready" control signal

Other Corruption

- Inconsistent run numbers in HLT and DHC frames
- Send DHC End frame before DHC Start frame
- Incorrect CRC checksum in DHC Start frame / DATCON RoIs

Additional three conditions were found to cause errors with high severity in the ONSEN system. These issues are listed in table 5.1. The investigated conditions were also presented in Belle II meetings, for example in the B2GM contribution [90] and in DEPFET conference contribution [91].

As a result of the experience gained from the test beam campaign and the follow-up tests, the ONSEN firmware was adapted by the ONSEN developers so that the severe errors observed no longer occur in the scenarios described. In addition, several data checks have been implemented in the ONSEN firmware to prevent invalid or inconsistent data input.

Investigated Conditions with serious Impact on ONSEN Data Processing	
Condition	**Observations**
Incorrect CRC checksum in HLT data	The Merger discarded the corrupted data and some of the data for the next trigger number. The Merger blocked any further incoming RoIs. When the Selector buffers were filled completely, the (emulated) DHH system could not send any further data to the ONSEN. A restart of the ONSEN system was necessary.
Incomplete DHH data	ONSEN-internal buffer management did not end the data for an event properly when the DHH data was not complete for any reason. The data of the next event was merged with the incomplete data and then processed as a single event. In total, two events were corrupted. There was no further impact on the ONSEN system. No restart of the system was needed for further processing of HLT / PXD data.
DHC Start frame received twice	A redundant second DHC Start frame was not discarded by the ONSEN. This lead to a trigger number mismatch in ONSEN-processed data: HLT data with a given trigger number was merged with DHH data for another trigger number. For proper data processing, a restart of the system was required. A soft-reset did not solve the issue.

Table 5.1: Problematic conditions found in follow-up tests. These conditions caused incorrect ONSEN data processing. Therefore, the ONSEN developers at JLU have modified the firmware so that these conditions no longer have a negative effect on data reception and processing in ONSEN. The results were also presented in DEPFET conference contribution [91] and in B2GM 2017 [90], among others.

5.6 Analysis of the Data

5.6.1 Information about the Data Sample

The following is an analysis of a data sample of 5×10^6 events collected during the 2017 test beam campaign at DESY (run 243). This particular data sample was chosen because all 5×10^6 events were recorded in a single run. In most of the runs considered in this thesis, significantly fewer events were collected. In addition, the DHH data was forwarded by the Fork cards to a PC where it was stored for debugging purposes. The run was performed with an electron beam energy of 3 GeV, a magnetic field of 1 T, a trigger rate of 1.3 kHz, and without collimator. Two PXD HLs were used, one for each PXD layer.

The information about the run can be found in Belle II Elog entry for run 243 performed on 26th of February 2017 [84, run 243] (restricted to Belle II members). The selected data was classified as good in the Elog.

The sroot files recorded by the EB2 were prepared for further analysis ("unpacked") using BASF2. The resulting root-files[2] were used for the plots which will be shown below.

5.6.2 Comparison of Data before and after ONSEN Processing

The DHH data which was stored on a PC enabled comparison of the number of pixels in the DHH and the ONSEN-processed data. Each pixel has a coordinate on the PXD half-ladder that can be described as a row-column combination (see figure 4.15). In the following, the column entries in the data are used to determine the number of pixel coordinates and thus, the number of pixel hits in the data.

The comparison of the number of pixel hits before and after RoI-selection is shown in figure 5.10 on the next page. A total of 33,675,402 pixel hits were reduced by ONSEN to just 3,244,266 pixel hits. The reduction of pixels in the data corresponds to a reduction factor $^{33,675,402}/_{3,244,266} \approx 10.38$, which is in accordance with the expectation of a data reduction factor of 10 [5] (without event rejection). However, the reduction factor is highly dependent on the size of the RoIs. In the data analysed, the RoIs was up to 5 mm (100 columns) wide and up to 15 mm long (in row direction). If a different maximum size of RoIs had been used in the analysed test run, the reduction factor would also be different.

The complete ONSEN-processed data as written to storage is larger than the data input transmitted by the (scaled-down) DHH. This is a consequence of the test setup: there were only a few pixels on average in each event. Therefore, there were too few pixel hits to reach the "break-even point" discussed in section 4.7.

Figure 5.11 on page 76 shows a comparison of the ADC values of the investigated PXD data before and after RoI-selection in ONSEN. The ONSEN-processed data resemble a Landau-function as one would expect in test setups using an electron

[2] More information about ROOT can be found on the official website / publication [92]

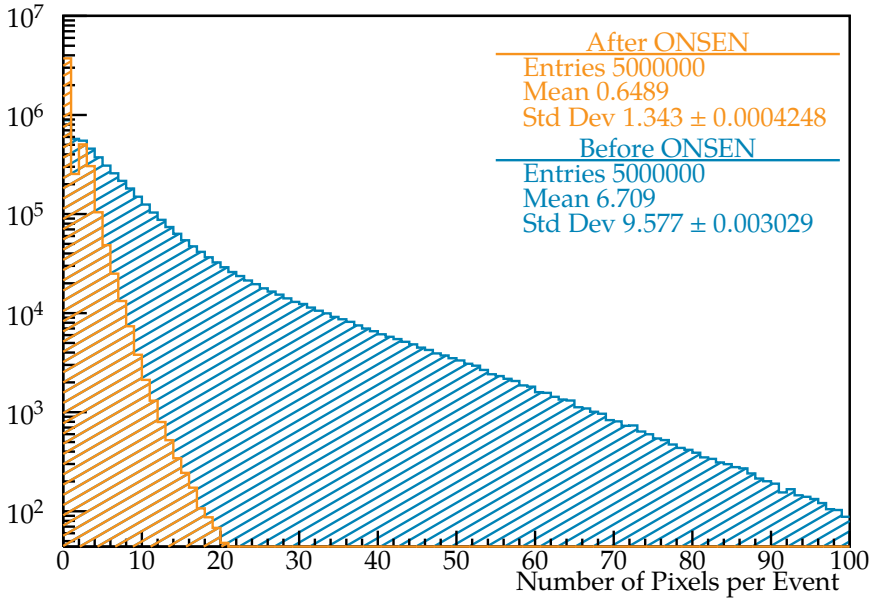

Figure 5.10: Comparison of the number of transmitted pixel coordinates per event from DHH system to ONSEN and from ONSEN to EB2. The plots show the results of a set of 5×10^6 events from the DESY test beam campaign in February 2017.

beam. Corresponding results from previous test campaigns can be found in Ref. [6, p. 101], for example.

5.6.3 Number of correlated RoIs on both Layers

A single RoI can cover an area on several PXD half-ladders. However, in the data from HLT and DATCON, each RoI is assigned to exactly one DHE and thus to one PXD HL. Therefore, a RoI covering an area on several modules, is split into two or more RoIs with different DHE IDs.

In tests at DESY, only a single half-ladder per layer was used in the run analysed in this thesis. When the RoIs covered the edge of the PXD module, it was not clear whether the RoI really ended there. Given this, only the RoIs located on only one PXD HL for sure were taken into account. RoIs with row coordinates equal to zero (the lowest possible row number) and / or 767 (the highest possible row number), and column coordinates equal to zero (the lowest possible column number) and / or 249 (the highest possible column number) were not included in the analysis.

The plots in 5.12 show the number of RoIs on each layer. Only events with at least one RoI on each PXD HL were included in this analysis, therefore, there are no entries for zero RoIs. In the data sample, 723,311 events contained at least one RoI on each PXD module. The maximum number of RoIs in the same event was found to be three for each of the two modules.

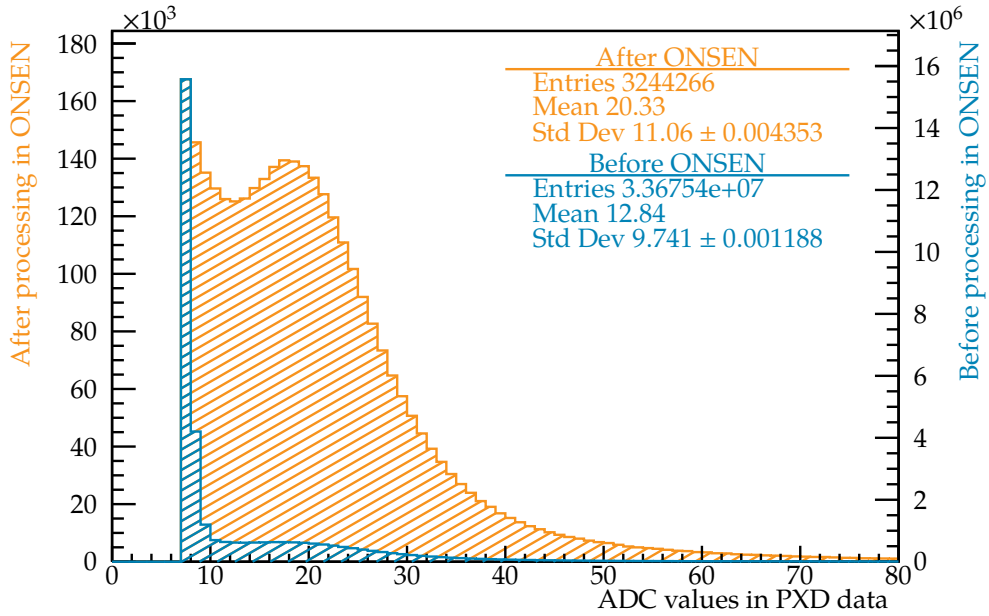

Figure 5.11: ADC values of the pixels. The values of the PXD data before and after data selection in ONSEN system are compared.[a].

[a] A similar ADC plot for comparison of data in- and outside RoIs was created by B. Spruck with data from 2016 test beam campaign. That result was discussed in Belle II meetings e.g. in slide 8 of meeting contribution *ONSEN System - Lesson from DESY testbeam 04/2016* [93]

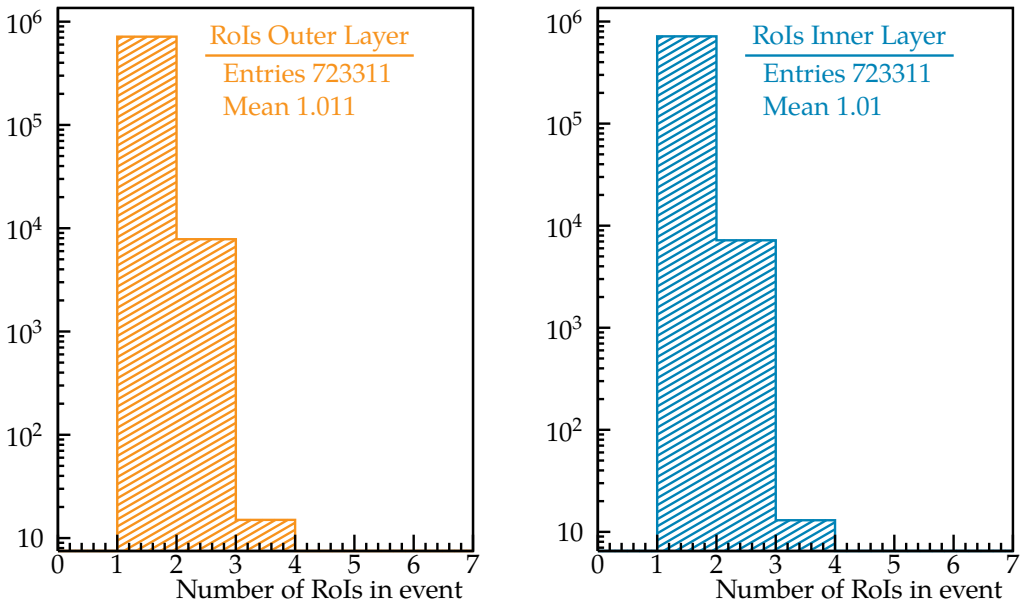

FIGURE 5.12: Total number of HLT-RoIs in the same event. 723,311 events meet the requirement of at least one RoI on each of the two PXD layers. Only RoIs with column / row coordinates unequal to zero, or 249 and 767, respectively, were included in the analysis.

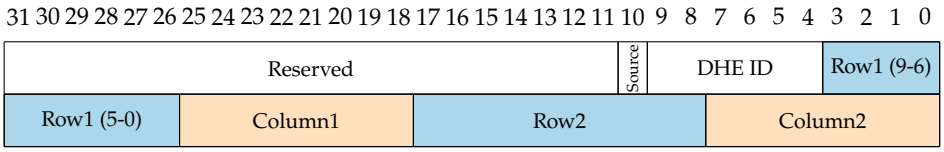

Figure 5.13: RoI coordinates (highlighted) as sent to ONSEN. The RoI data also contains information about the source system (HLT or DATCON) as well as the DHE ID. Data format adapted from Ref. [6, p. 167]

5.6.4 Correlation of Data on both PXD Layers

Given the number of RoIs discussed above, a correlation between the data of the inner and outer PXD layer was expected.

While the pixel coordinates describe single pixels on the sensitive area of the PXD HLs, there are two coordinates needed for the description of each RoI because they describe areas on the PXD modules. The coordinates of the RoIs are defined by the start row and end row (Row1 and Row2), and the start column and end column (Column1 and Column2). An excerpt from the RoI data format specification is shown in figure 5.13.

For the 2D-plots shown below, the centre between start and end coordinates of either the rows or the columns was calculated as shown in equation 5.1.

$$\text{Centre of RoI row (column)} = \frac{\text{Row1 (Column1)} + \text{Row2 (Column2)}}{2} \tag{5.1}$$

As described above, a single RoI can cover areas on several modules. The following does not include RoIs with start or end coordinates at the edges of the modules. Thus, RoIs possibly overlapping to neighbouring (possibly not available) modules were excluded.

In figure 5.14 on the next page the centres of the RoI column coordinates and the RoI row coordinates on the inner and outer layers of the PXD are shown in 2D-plots. Both plots show a correlation between the coordinates as expected. In the plots, the different pixel sizes of the PXD HLs as listed in table 3.1 on page 31 were taken into account.

The correlation between the RoI rows (figure 5.14b) appears to be shifted compared to the correlation between the RoI columns (figure 5.14a). This shift is caused by the different lengths of the sensitive areas of the PXD half-ladders. Although all PXD modules have the same width, the size of the pixels in row direction depends on the PXD layer and the proximity to the interaction point. Therefore, the modules in the inner PXD layer are shorter than the modules in the outer layer. The half-ladders of both layers are arranged such that the zero coordinates of the rows are shifted by $\sim 1.16\,\text{cm}$ (see figure 5.2 on page 63).

The plots in figure 5.15 on page 80 show the correlation between RoI-selected pixel coordinates. As expected, the plots look similar to the RoI equivalents. Again, the pixel sizes were taken into account.

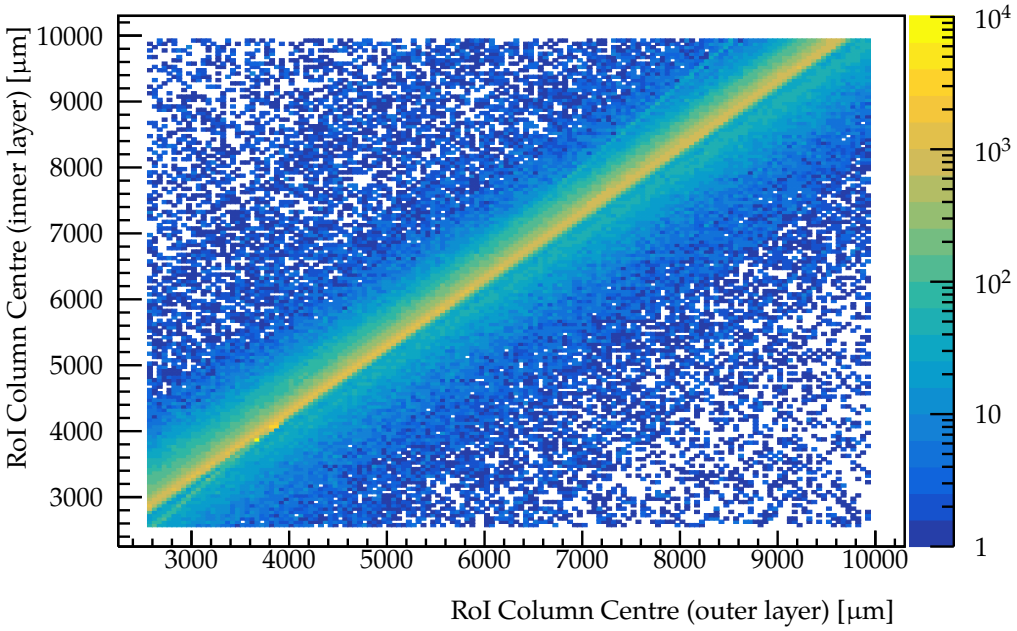

(A) Correlation between the RoI centres in column direction.

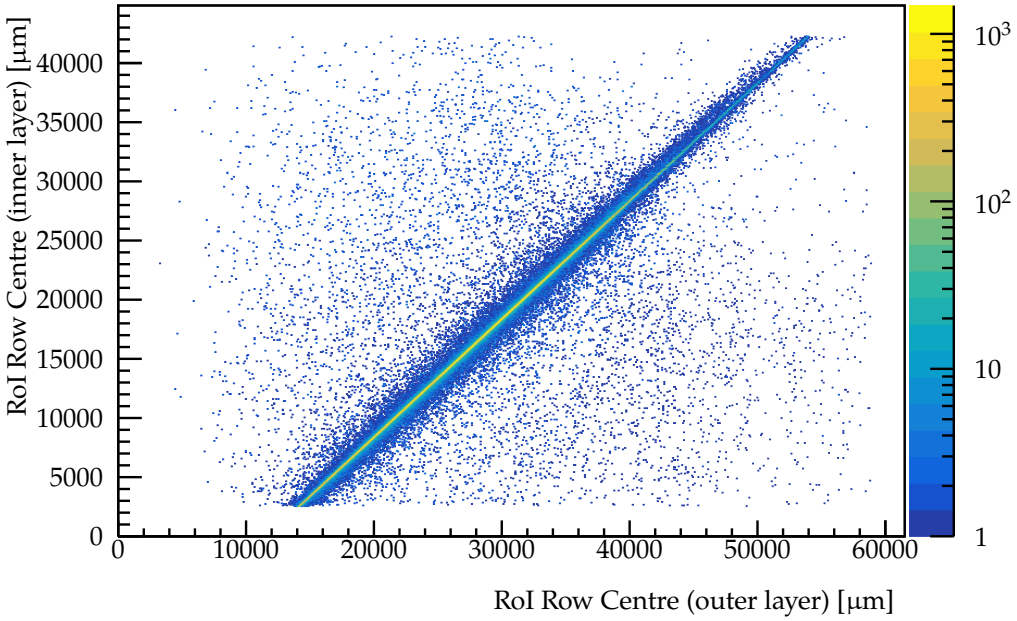

(B) Correlation between the RoI centres in row direction. The correlation is shifted due to the different sizes of the sensitive areas in row direction.

FIGURE 5.14: Correlation between the RoI centres on the two PXD layers. RoIs with coordinates on the edges of the module were excluded.

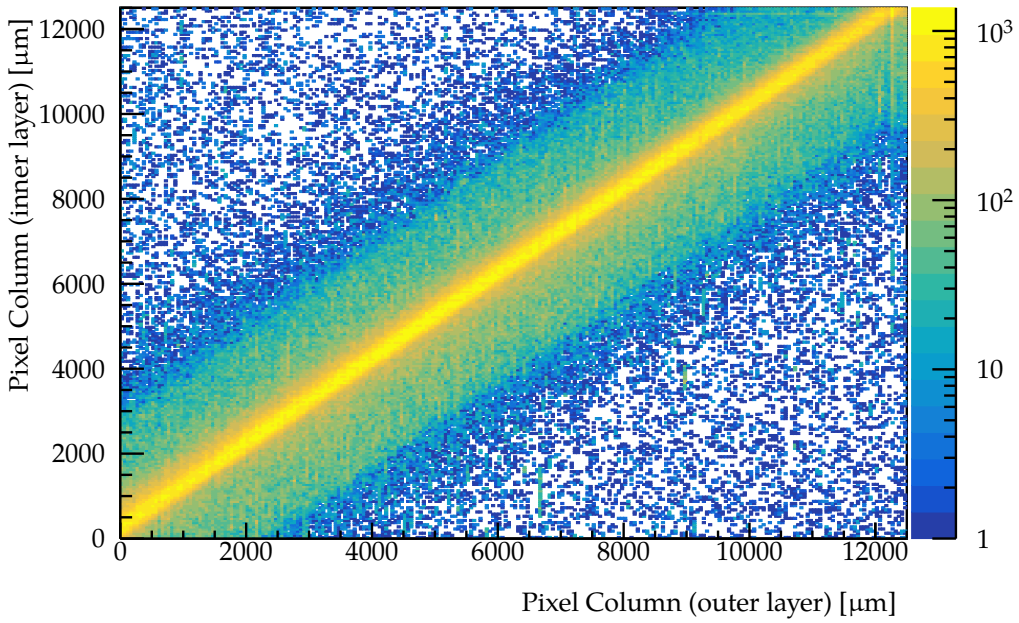

(A) Correlation between the RoI-selected pixel column coordinates.

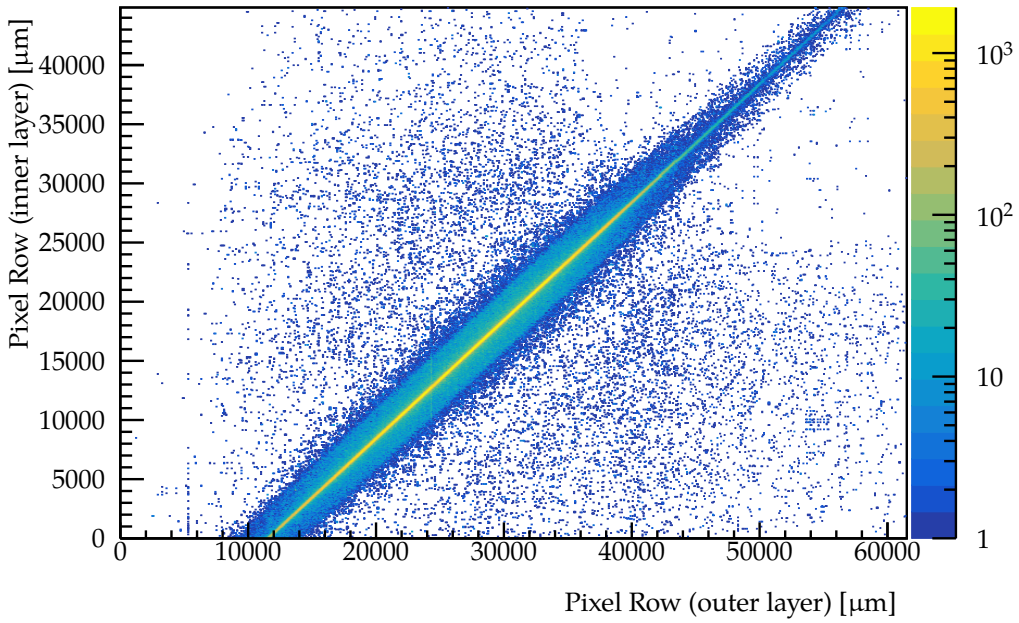

(B) Correlation between the RoI-selected pixel row coordinates. The correlation is shifted due to the different sizes of the sensitive areas in row direction.

FIGURE 5.15: Correlation between the RoI-selected pixel coordinates on the two PXD layers.

Deviations	
Pixel Column - RoI Column Centre (inner PXD layer)	Constant $9.079 \times 10^4 \pm 1.420 \times 10^2$ Mean 0.6395 ± 0.0040 Sigma 3.406 ± 0.004
Pixel Row - RoI Row Centre (inner PXD layer)	Constant $2.572 \times 10^5 \pm 3.943 \times 10^2$ Mean 0.9187 ± 0.0014 Sigma 1.218 ± 0.001
Pixel Column - RoI Column Centre (outer PXD layer)	Constant $2.935 \times 10^5 \pm 5.045 \times 10^2$ Mean 2.228 ± 0.0001 Sigma 0.9002 ± 0.0011
Pixel Row - RoI Row Centre (outer PXD layer)	Constant $4.291 \times 10^5 \pm 7.276 \times 10^2$ Mean 0.1563 ± 0.0009 Sigma 0.6911 ± 0.0009

Table 5.2: Deviations between RoI centres and pixel coordinates.

5.6.5 Correlations of RoIs and selected PXD Data

The correlations between the RoI centres and the RoI-selected PXD data are shown in figures 5.16 to 5.19 on pages 82–85. The RoI centres were calculated as described in equation 5.1. RoIs with coordinates at the edges of the modules were excluded. Two different plots are shown for each row and column, and for both layers.

The column coordinates of the RoI centres and the pixels of the inner layer are shown in figure 5.16a on the next page. Since the RoIs with coordinates at the edges of the sensitive areas of the PXD modules were not used and there was a maximum size of RoIs[3], there are areas without any data points. As expected there is a correlation between the coordinates. Figure 5.16b shows the deviation between column coordinates of the RoI centres and the pixels. The corresponding plots for the row coordinates are shown in figure 5.17 on page 83.

The plots for the outer PXD layer are shown in figures 5.18 to 5.19 on pages 84–85. The deviations show that the RoI centres were very close to the RoI-selected pixel data as one would expect. A slightly blurred correlation can be seen in the column plots. This is probably caused by the magnetic field of 1 T.

The results are summarised in table 5.2.

[3]The correlation plots show only pixel columns (rows) for those RoI centres where RoI-Column1 (-Row1)≤pixel column (row)≤RoI-Column2 (-Row2).

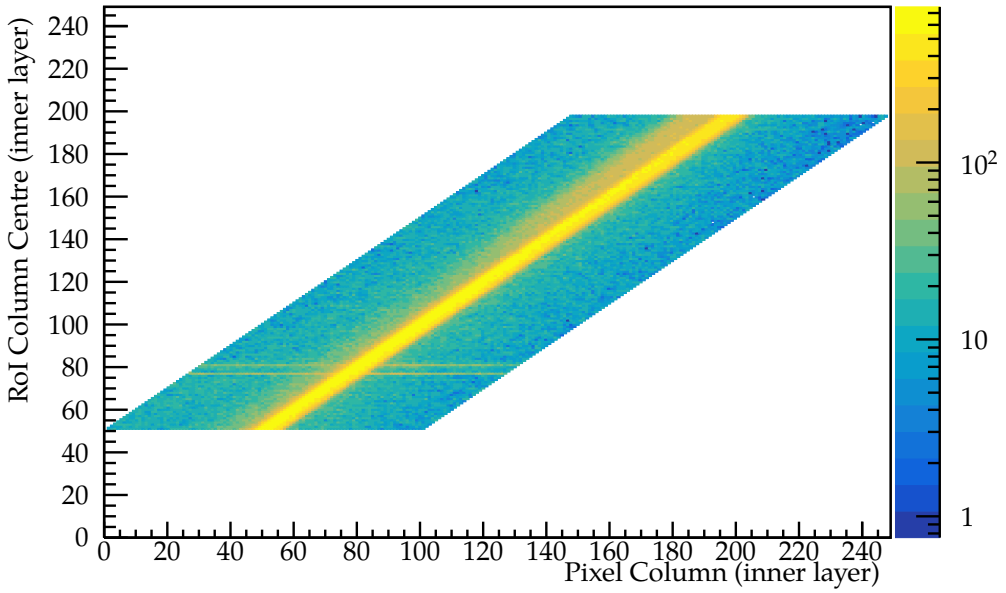

(A) Correlation between the RoI-selected pixels and the RoI centres in column direction. The maximum RoI column size was set to 100 columns in this run.

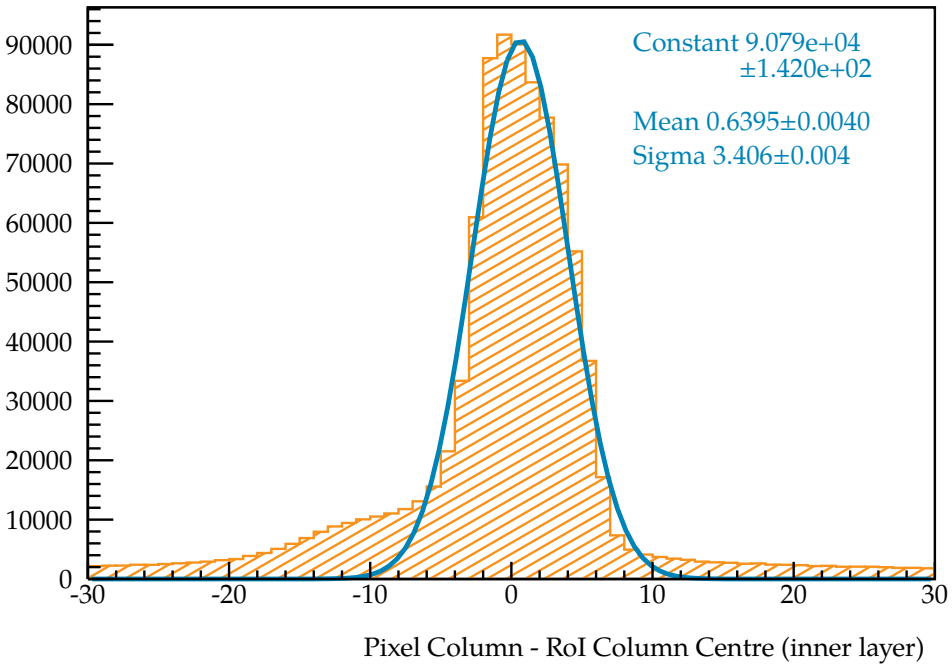

(B) Deviation between the RoI-selected pixels and the RoI centres in column direction.

FIGURE 5.16: Correlation between the RoI-selected pixels and the RoI centres in column direction of the inner PXD layer, and their deviation from each other.

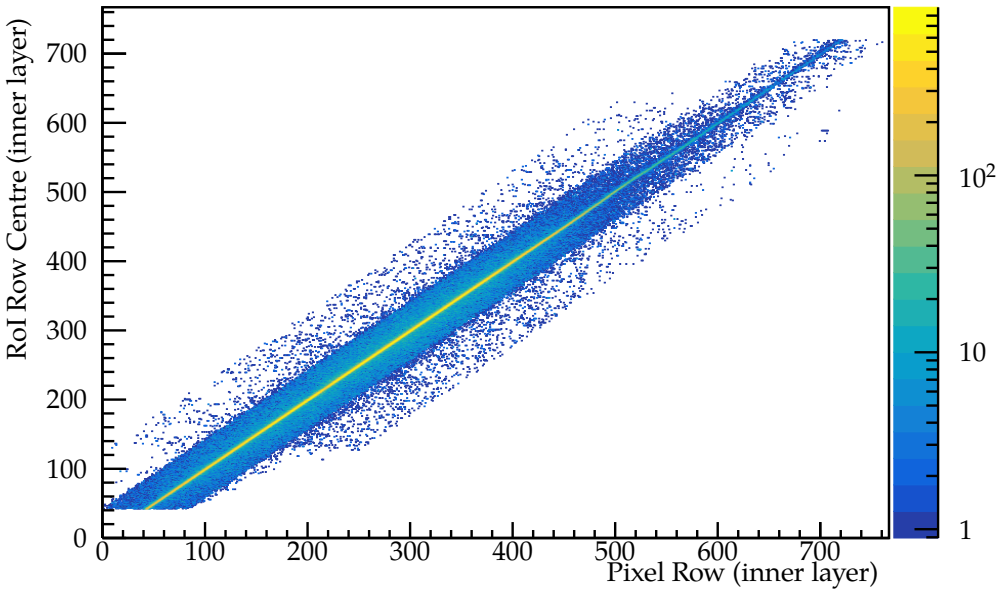

(A) Correlation between the RoI-selected pixels and the RoI centres in row direction.

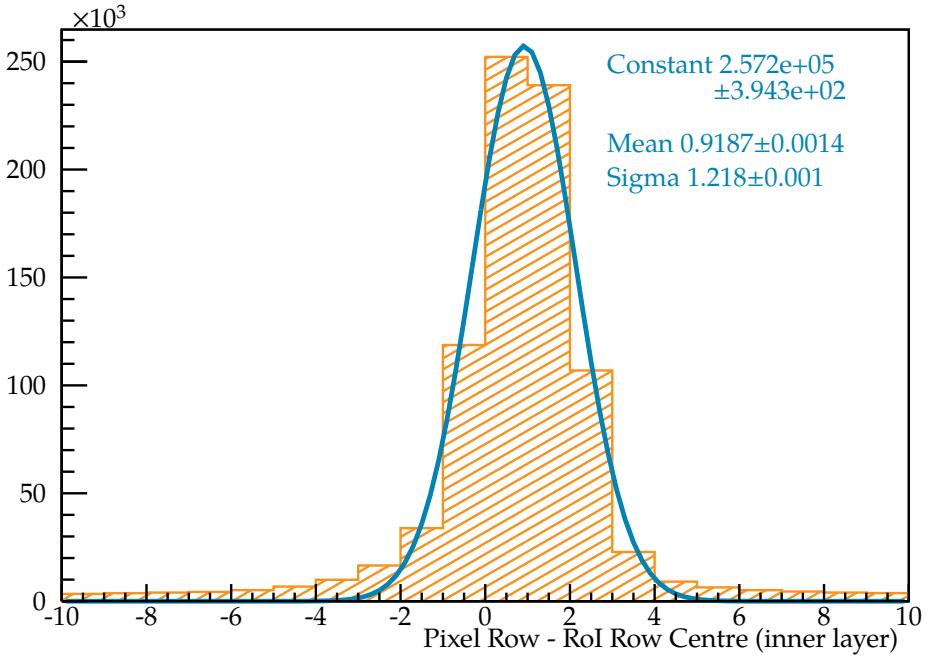

(B) Deviation between the RoI-selected pixel rows and the RoI centres in row direction.

FIGURE 5.17: Correlation between the RoI-selected pixel and the RoI centres in row direction of the inner PXD layer, and their deviation from each other.

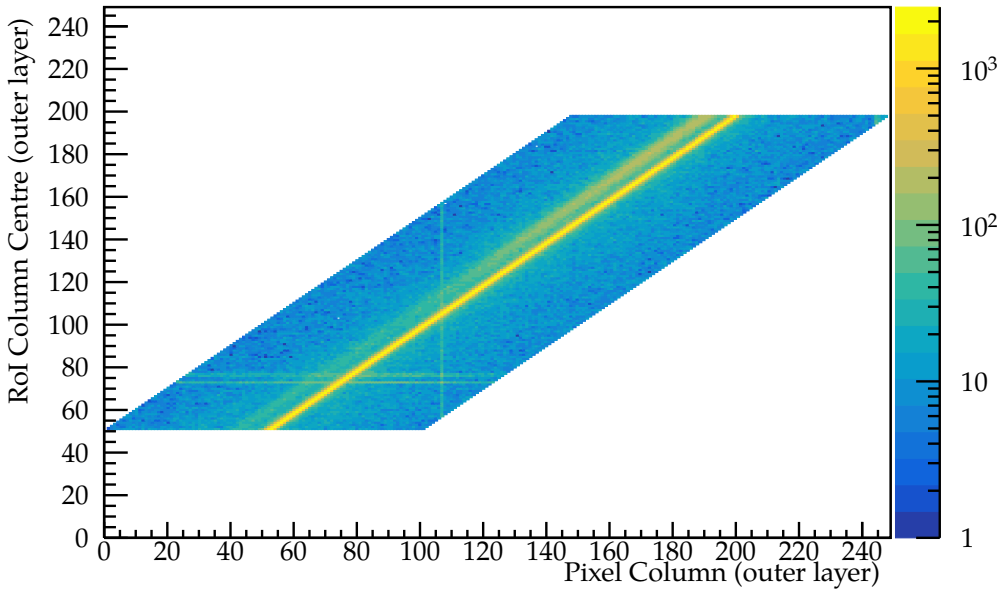

(A) Correlation between the RoI-selected pixels and the RoI centres in column direction. The maximum RoI column size was set to 100 columns in this run.

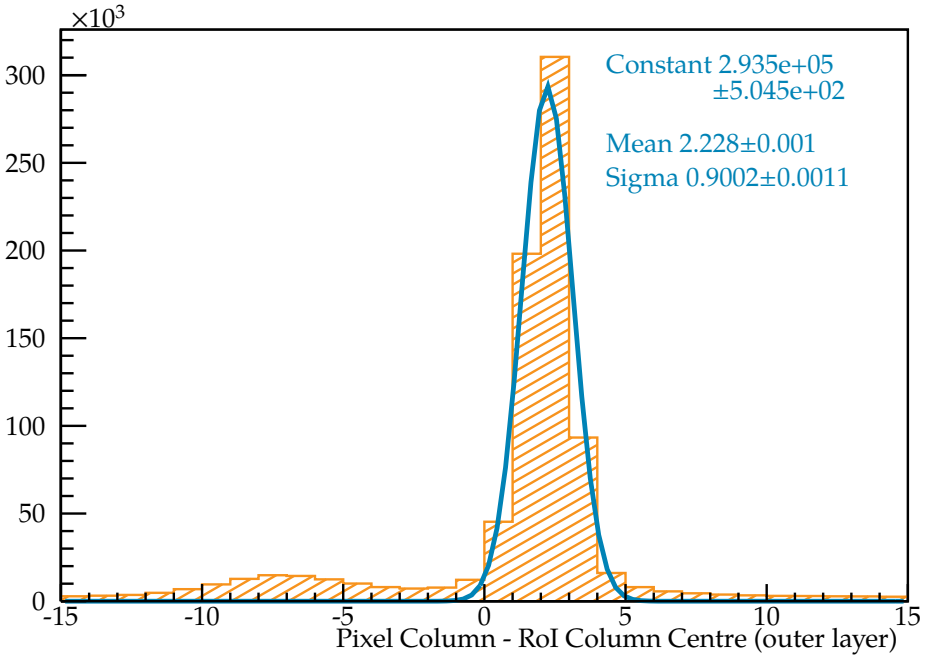

(B) Deviation between the RoI-selected pixels and the RoI centres in column direction.

FIGURE 5.18: Correlation between the RoI-selected pixels and the RoI centres in column direction of the outer PXD layer, and their deviation from each other.

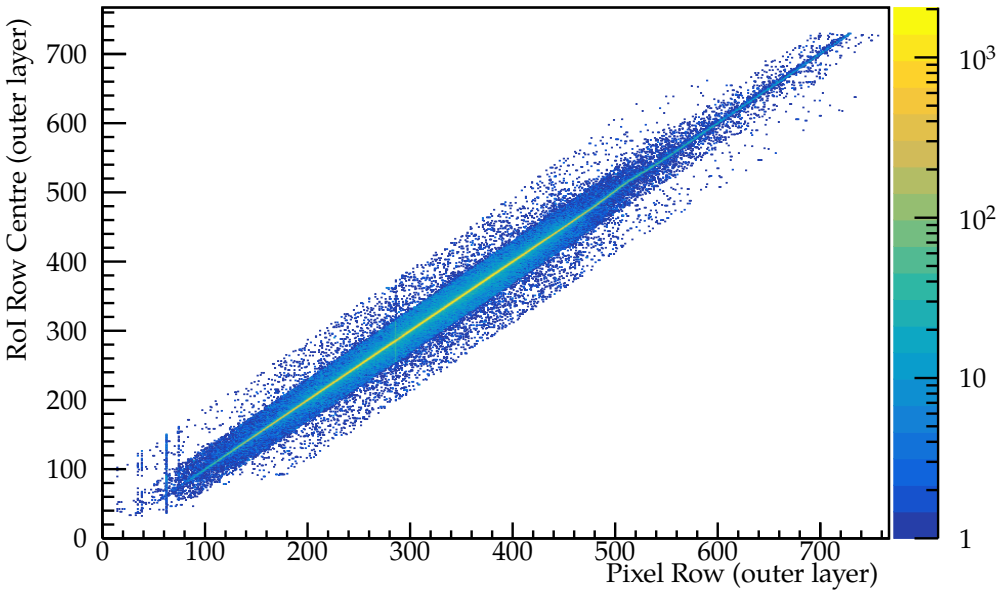

(A) Correlation of the RoI-selected pixels and the RoI centres in row direction.

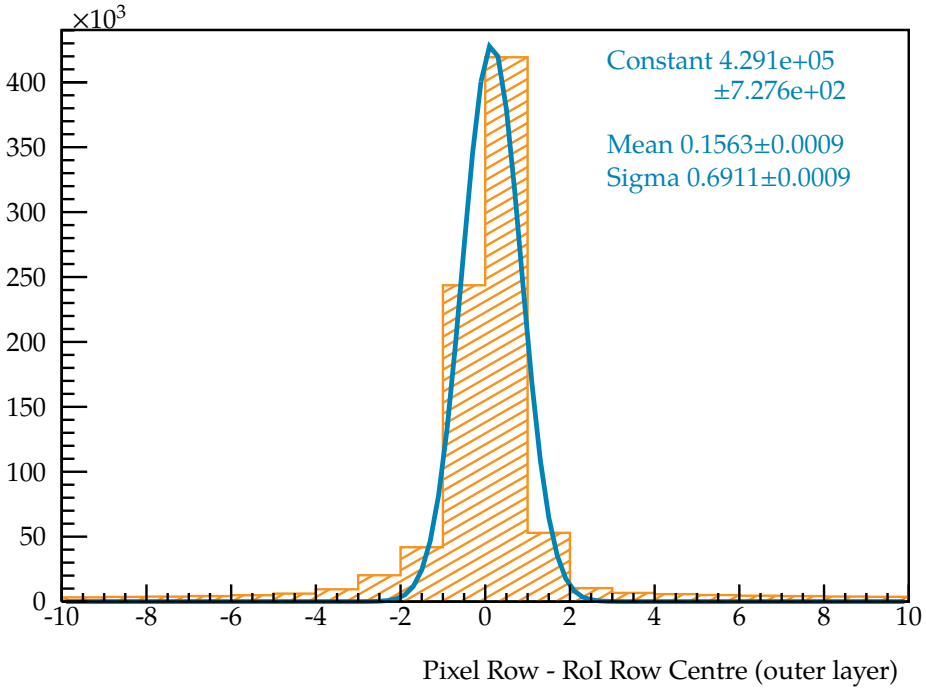

(B) Deviation between the RoI-selected pixels and the RoI centres in row direction.

FIGURE 5.19: Correlation between the RoI-selected pixels and the RoI centres in row direction of the outer PXD layer, and their deviation from each other.

Chapter 6

RoI Distribution Tests at KEK

6.1 Overview

Part of this work involved the development of the RoI distribution on CNCBs (see section 4.5). The test setup at JLU included only a few AMCs and CNCBs, as most of the ONSEN hardware had already been delivered to KEK by the time the tests described in this chapter were carried out.

Testing of the RoI distribution, using nine CNCBs and 33 AMCs, was carried out at KEK in late 2018. The test setup included a scaled-down HLT, the ONSEN (one Merger and 32 Selectors) and the event-builder-2. Specific test patterns for the HLT RoIs were defined prior to the tests.

In normal operation, the ONSEN-processed data does not contain any information about which Selector processed which data. For the RoI distribution, however, it was necessary to check that the RoIs were forwarded to the correct Selectors. Therefore, the ONSEN was adapted so that the Internet Protocol address (IP) of each Selector was added to the ONSEN-processed data making it possible to identify the Selector that had sent the data in question to the event-builder-2. The ONSEN-processed data was stored at KEK for later analysis.

6.2 Test of RoI Distribution

6.2.1 Test Setup and Data

At the time of the RoI distribution tests, a scaled-down HLT and the EB2 were available for the tests. The use of these two systems in the test setup, increased the quality of the tests compared to the setup at JLU. The test setup used at KEK is illustrated in figure 6.1.

The DHH was not part of the test setup. During the tests at JLU, PXD data was emulated and sent via a local PC and additional AMCs (for sending data via optical fibres to the Selectors). However, the ONSEN operation during the tests at KEK was performed remotely from JLU. Therefore, emulated PXD data was provided to the ONSEN in a different way.

If no DHH data was sent to ONSEN for a given trigger number, then the ONSEN adds dummy data frames to comply with the data format specification (see section

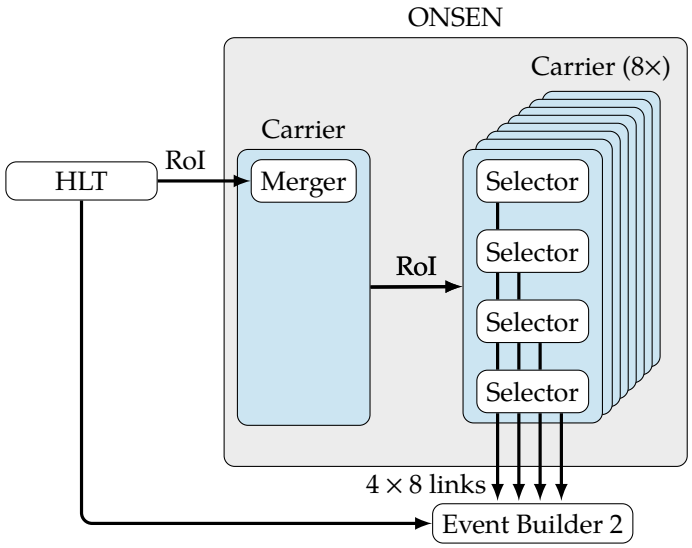

Figure 6.1: Setup for the RoI distribution tests at KEK. The ONSEN was operated and monitored remotely from JLU.

4.4.3 and appendix A). The dummy data sent in this case was adapted for these tests. The PXD data pattern shown in figure 6.2 was emulated and added to the default dummy data. The pattern represents an occupancy of ~ 2.9% (5,544 pixel coordinates) of one half-ladder. The DHE ID of the data was set to $111111_2 = 3F_{16} = 63_{10}$, an ID not used by the DHH, to ensure that the data could be easily identified as test data.

The ONSEN received 40 HLT RoIs for each trigger number with trigger rates up to 20 kHz. The RoIs differed in DHE ID.

Two RoI distribution patterns were used for the tests: the first pattern was chosen so that each of the 32 Selectors received exactly one RoI for each trigger number. The remaining eight RoIs were supposed to be discarded by ONSEN. The ONSEN data was received by EB2. The second test distribution pattern was chosen so that each Selector only sent every eighth event and the RoIs for four different DHE IDs. Both patterns are listed in table 6.1 on the next page.

6.2.2 IP Writer

The ONSEN sends the RoI-selected PXD data to the event-builder-2 where it is combined with data from other subdetectors. The EB2 receives the ONSEN data via 32 links using the TCP protocol. Each Selector must therefore have its own IP address. Since the data transmitted by the Selectors does not contain any information about the IP address, there is no direct way to associate the data with the Selector that sent it. Therefore, conclusive tests of the RoI distribution in ONSEN were only possible if each data sent to the EB2 contained an additional identifier of the sending Selector.

In the Belle II data format specification, there are bits which are not assigned to specific purposes (see appendix A). This fact was utilised for the tests. A new IP

Test Distribution Pattern 1								
Selector	21	22	23	24	31	32	33	34
DHEID	2	3	4	5	6	7	8	9
Selector	41	42	43	44	51	52	53	54
DHEID	10	11	12	13	14	15	16	17
Selector	101	102	103	104	111	112	113	114
DHEID	34	35	36	37	38	39	40	41
Selector	121	122	123	124	131	132	133	134
DHEID	42	43	44	45	46	47	48	49
Selector	✘	✘	✘	✘	✘	✘	✘	✘
DHEID	50	51	52	53	54	55	56	57

Test Distribution Pattern 2								
Selector	21	22	23	24	31	32	33	34
Trg.%8	0	0	0	0	1	1	1	1
DHEID	2–5	6–9	10–13	14–17	34–37	38–41	42–45	46–49
Selector	41	42	43	44	51	52	53	54
Trg.%8	2	2	2	2	3	3	3	3
DHEID	2–5	6–9	10–13	14–17	34–37	38–41	42–45	46–49
Selector	101	102	103	104	111	112	113	114
Trg.%8	4	4	4	4	5	5	5	5
DHEID	2–5	6–9	10–13	14–17	34–37	38–41	42–45	46–49
Selector	121	122	123	124	131	132	133	134
Trg.%8	6	6	6	6	7	7	7	7
DHEID	2–5	6–9	10–13	14–17	34–37	38–41	42–45	46–49
Selector	✘	✘	✘	✘	✘	✘	✘	✘
Trg.%8	✘	✘	✘	✘	✘	✘	✘	✘
DHEID	50	51	52	53	54	55	56	57

Table 6.1: Test pattern for RoI distribution tests. "Selector" shows the last number of the IP addresses of the Selectors and "DHEID" refers to the (expected) DHE ID in the ONSEN-processed RoI data. In tests with the first pattern, each Selector received every event. In tests with the second pattern, each Selector received only the events with the three LSBs listed in "Trg.%8" as decimal numbers, i.e. every eighth event. The RoIs with DHE ID > 49 were not expected to be sent from any Selector to EB2 in any of the test patterns.

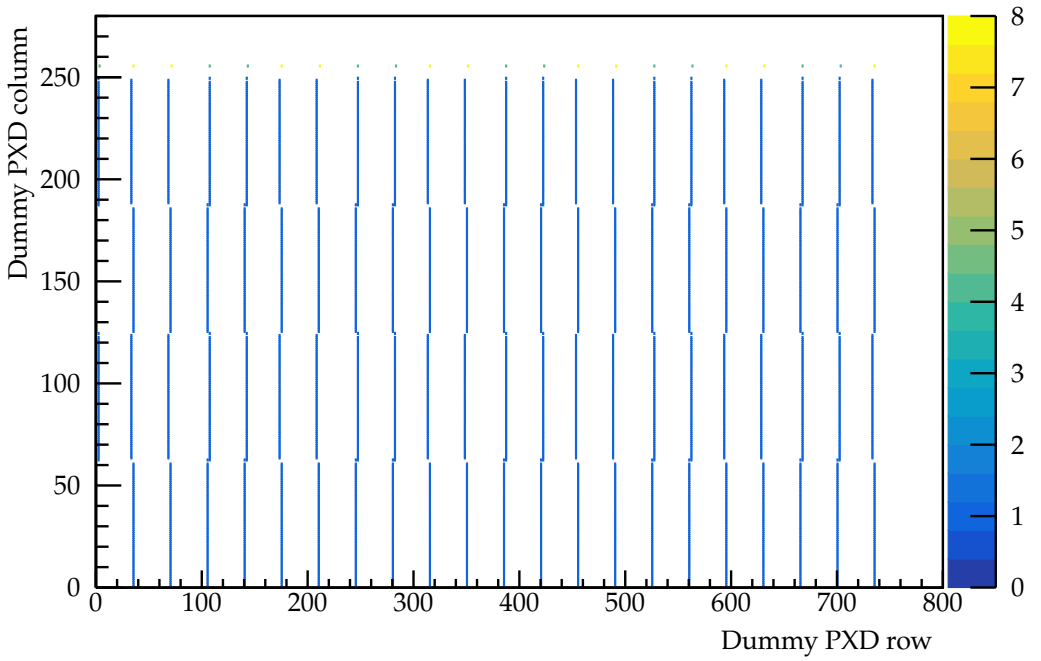

Figure 6.2: Emulated PXD data pattern representing a occupancy of ~ 2.9% of one half-ladder. The data pattern was added to the ONSEN dummy data.

core, the *IP Writer*, was designed to write the IP address of each Selector into the data before sending it to EB2. In the tests, the last digits of the Selector IP were written into a slave register used by the IP core (see appendix C.2). The core then replaced bits in the merged RoI data with the information stored in this slave register. In the ONSEN-processed data, these bits can be found in the ONSEN Trigger frame. The adjusted data format and the RoI frame sent by the Selectors are shown in figure 6.3. More informations about the Belle II data formats are given in Ref. [6, pp. 163-171]. Appendix A lists some parts of the data format specifications as well as adjustments made for the tests discussed in this thesis.

The Parsers used in ONSEN recalculate each CRC checksum to verify the data integrity. Therefore, if the IP Writer was implemented before a Parser, it would have caused a CRC error. To avoid implementing an additional CRC calculation in the IP Writer, the IP core was implemented between the RoI Parser and the Pixel Filter IP cores as shown in figure 6.4 on page 92. The Pixel Filter does not check the data integrity – this is supposed to be done by the parsers. Since the Pixel Filter discards PXD data based on the RoIs, it is mandatory to calculate CRCs checksums for certain frames that pass the Pixel Filter. Consequently, the CRC checksums of the frames manipulated by the IP Writer were also calculated in the tests discussed here, so that no CRC checksum errors caused by the IP Writer were to be expected.

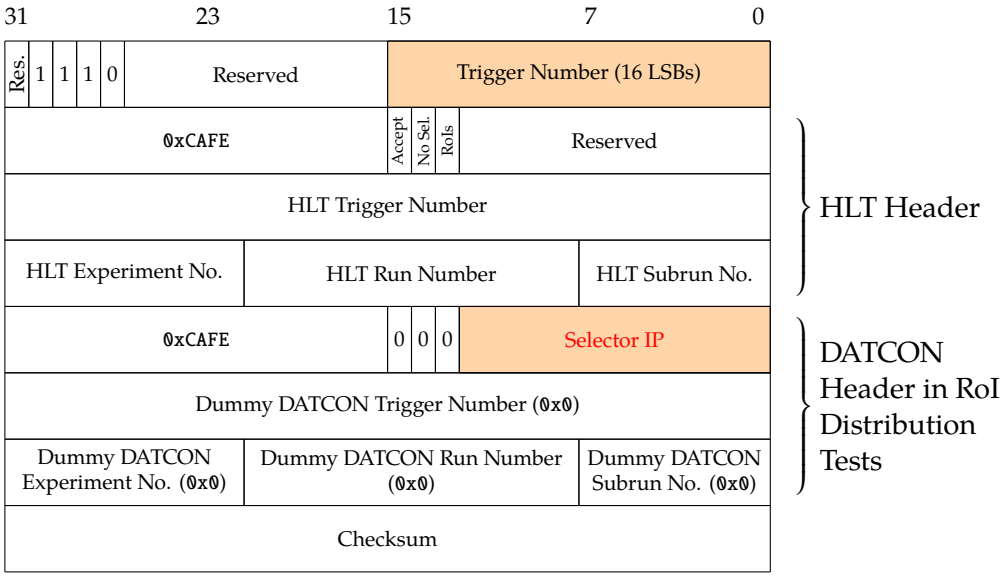

(A) ONSEN Trigger frame, adjusted for RoI distribution tests. DATCON was not included in the test setup. Therefore the DATCON header only contained dummy information about trigger number, experiment number etc. Bits reserved (but not used for particular purposes) were used to write the last digits of each Selectors IP into it. This was done for the sole purpose of testing the RoI distribution.

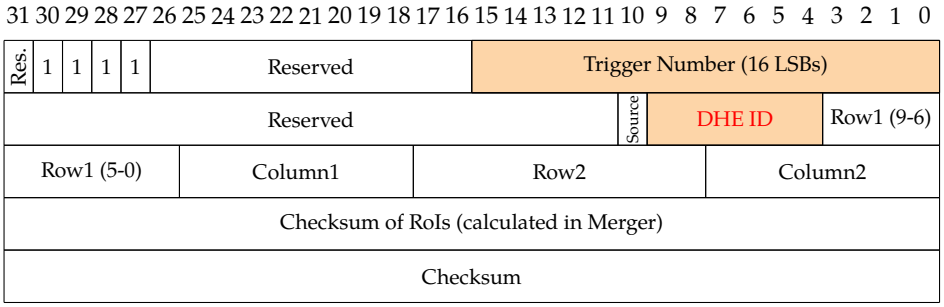

(B) ONSEN Debug RoI frame with one RoI. The data contains the DHE ID and therefore the information for which HL the RoI was calculated or, in this case, for which HL the data was emulated for testing purposes.

FIGURE 6.3: Particularly important data formats for RoI distribution tests. The data format was adapted from Ref. [6, pp. 167,171]. Note that the Selector IP is not a part of the official data format and is therefore not listed in the reference.

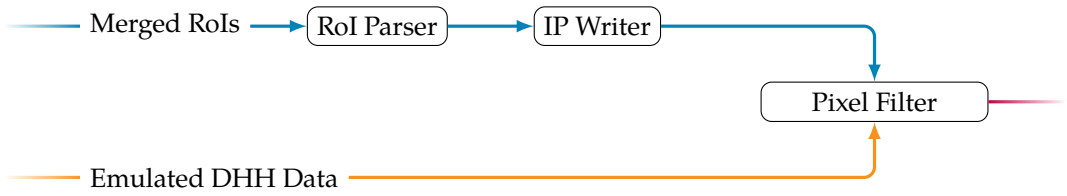

Figure 6.4: Simplified data flow in ONSEN Selector at the time of RoI distribution tests at KEK. The IP Writer core was implemented between the RoI Parser and the Pixel Filter.

6.2.3 Test Results

In first tests, we found that the HLT-ONSEN link got lost when the trigger rate was too high for this setup with a scaled-down HLT. Therefore, tests were performed at low trigger rates in a range between 1 kHz and 10 kHz on December 13th and 17th, 2018. Later, on December 20th, settings were adjusted by the HLT-team so that short tests with a trigger rate of up to ~20 kHz were possible. This was the maximum trigger rate that could be achieved at that time. We used this opportunity to verify the stability of the HLT-ONSEN link as well as the stability of the ONSEN system at KEK at those rates.

The first RoI distribution pattern was tested with trigger rates between 1 kHz and 10 kHz. Figure 6.5 shows the trigger rates of Merger and Selector as monitored in time of tests when the trigger rate was set to 5 kHz.

Figure 6.6 shows trigger rates of Merger and Selector as monitored in tests performed with the second test pattern. Here the RoIs were distributed not only based on the DHE ID but also based on the trigger number. The trigger rate of the Selector was lower by a factor of eight. This is due to the fact that only every eighth event was sent by the Merger to each Selector. The tests were performed with trigger rates of 1 kHz and 20 kHz. The test run with the trigger rate of 20 kHz served as a stability test and the data was not recorded for further analysis.

No errors in the RoI distribution were found in the analysis of the recorded data (1-10 kHz). For this analysis, the ONSEN-processed data stored in sroot-files created by EB2 was checked. One event collected in one of the test runs is shown in figure 6.7. The data was analysed using C++ programs, like in the follow-up tests discussed in section 5.5. Some snippets of these programs can be found in appendix B.

Figures 6.8 and 6.9 show snippets of the result of the data checks for the second test pattern. The data checks were performed after the test runs had been concluded. The "EvtNrErr" counters in figure 6.8 represents the number of trigger number mismatches in the data. These were expected since emulated PXD data was added to the default dummy data for the tests. The trigger number of the emulated data was set to zero in every event and therefore differed from the actual trigger number defined by the HLT RoI data. The Selector IP address counter in figure 6.9 met the expectations.

A summary of the test runs is listed in table 6.2.

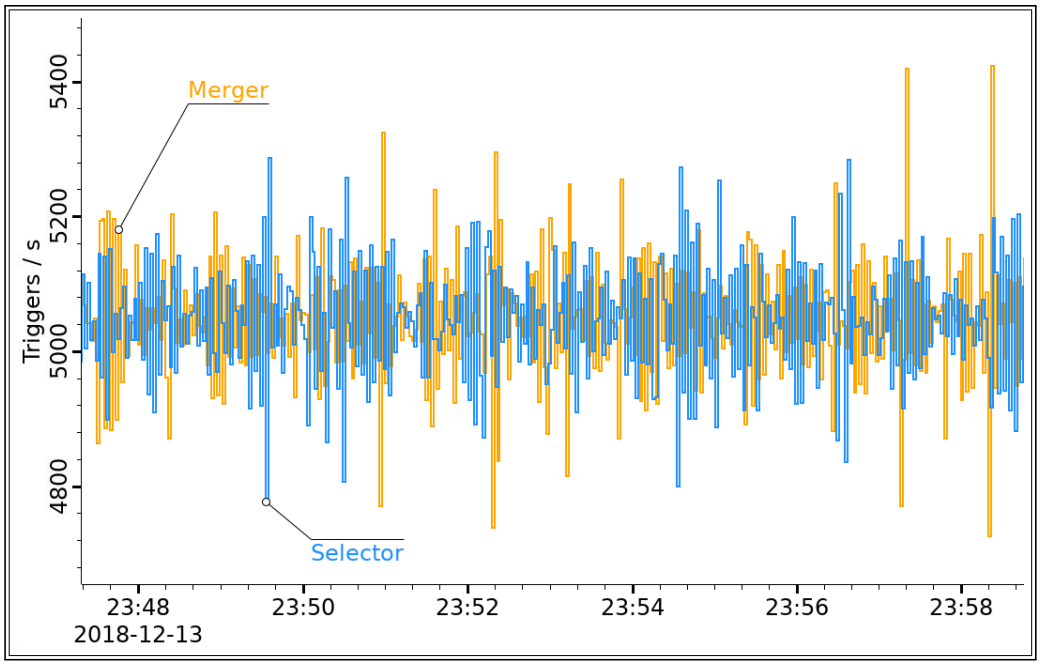

FIGURE 6.5: Test distribution pattern 1: trigger rates of the Merger and one Selector as monitored in a test run with a trigger rate of 5 kHz. The Merger and Selector trigger rates were the same because each Selector received RoIs for each trigger number. All timestamps are in JST.

Summary				
Test pattern	Events	RoIs (Input; 40 RoIs/event)	RoIs (Output)	Trigger Rates
1	18,335,882	733,435,280	586,748,224 (1 RoI/Selector in every event)	1 – 10 kHz
2	7,027,308	281,092,320	112,436,928 (4 RoIs/Selector in every eighth event)	1 kHz
2	15,755,625	630,225,000	*stability test; data not recorded*	~20 kHz

TABLE 6.2: Summary of RoI distribution tests. No error related to the RoI distribution was found. In addition to a detailed verification of the correct RoI distribution, a stability test for data processing at a trigger rate of 20 kHz was performed. All tests were performed at KEK and coordinated remotely from JLU.

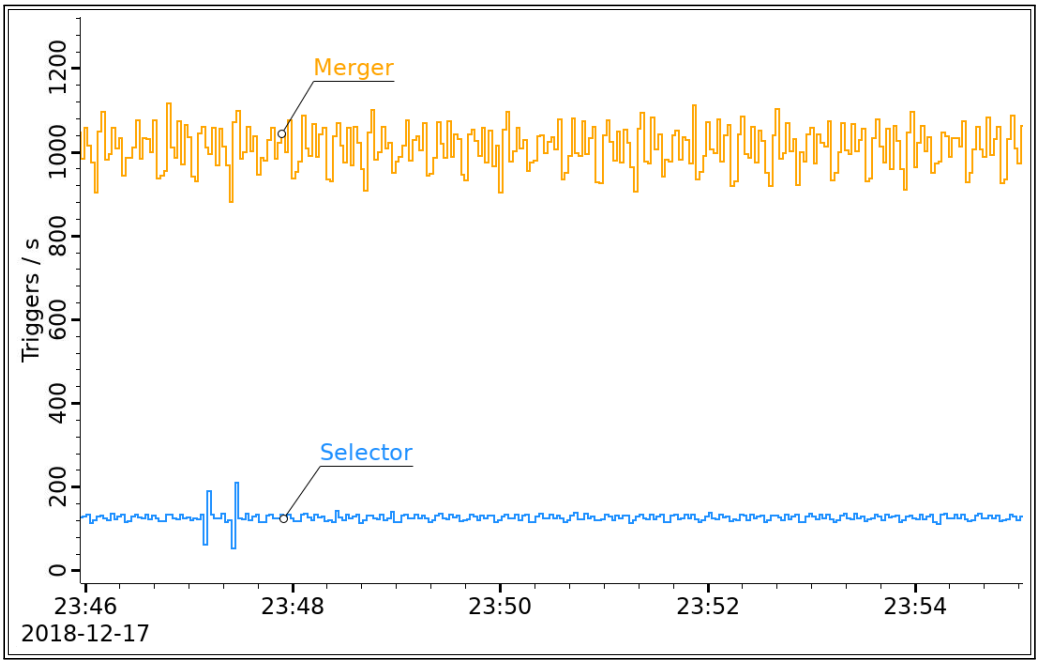

(A) Test run with a trigger rate of 1 kHz. Data was recorded and analysed. No issues were found.

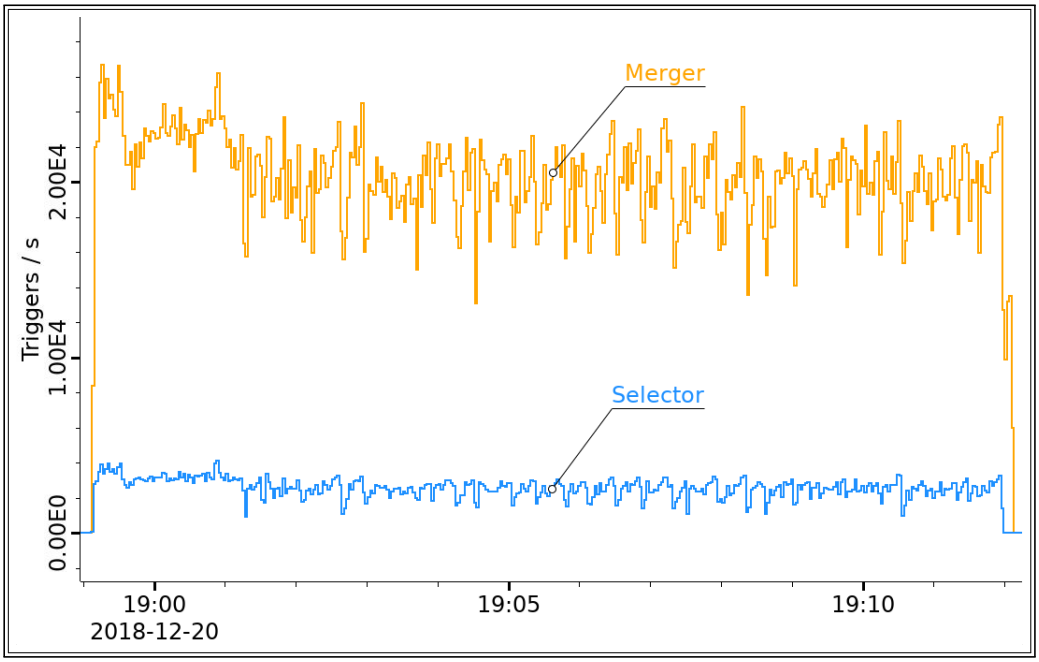

(B) Stability test run with a trigger rate of ~ 20 kHz. Data was not recorded for this run. Monitoring showed no indication for issues related to the RoI distribution during test execution.

FIGURE 6.6: Test distribution pattern 2: trigger rates of the Merger and one Selector as monitored in a test run. The Selector's rate was lower by a factor of ~ 8, as each Selector only received every eighth event from the Merger. All timestamps are in JST.

ONSEN Index Frame			
0xCAFEBABE	0x0000000A	0x00000020	0x00000014
0x00000010	0x0000000C	0x0000000C	0x0000000C
0x0000000C	0x00000010	0x00000014	0x00000010

ONSEN Trigger Frame with adjusted Dummy DATCON Data			
0x7000 EE14 (Trigger No. (16 LSBs))	0xCAFEA000	0x0014EE14 (Complete Trigger No.)	0x011BDC00
0xCAFE0 315 (Sel. IP 3.21 (last digits))	0x00000000	0x00000000	0xD7B9BE77

Dummy DHC Start Frame			
0x58000000	0x00000000	0x00000000	0x00000000
0x4D212948			

Emulated DHE Start Frame (DHE ID = 0x3F)			
0x1BFF0000	0x00000000	0x00000000	0x1D0BD102

Emulated DHP Frames w/o Zero-suppressed PXD data (DHE ID = 0x3F = 63, PXD data rejected in ONSEN)		
0x6BF00000	0xA0FC0000	0xB7BACB74
0x6BF10000	0xA0FD0000	0xF9350FE2
0x6BF20000	0xA0FE0000	0x2AA54258
0x6BF30000	0xA0FF0000	0x642A86CE

Emulated DHE End Frame (DHE ID = 0x3F)			
0x23F00000	0x00000000	0x00000000	0x95E85A03

ONSEN RoI Frame			
0x7800 EE14 (Trigger No. (16 LSBs))	0x00000 02 0 (DHE ID (6 bits))	0x0002FFF9 (RoI Coordinates)	0xA630A25B
0xF110A707			

Dummy DHC End Frame			
0x60000000	0x00000000	0x00000000	0x07A5BCF7

Figure 6.7: An ONSEN-processed event from the test runs performed at KEK on 13th of December 2018. The last digits of the Selector IP replaced unused bits in ONSEN Trigger frame. Only the eight least significant bits were relevant as only here the Selector IP addresses are different. The IP (0x315→ last number of IP is $15_{16} = 21_{10}$) was used to check whether the DHE ID (0x02→ DHE ID is 2) in ONSEN RoI frame data met the expectation. When the second test pattern was used, the trigger number was checked as well.

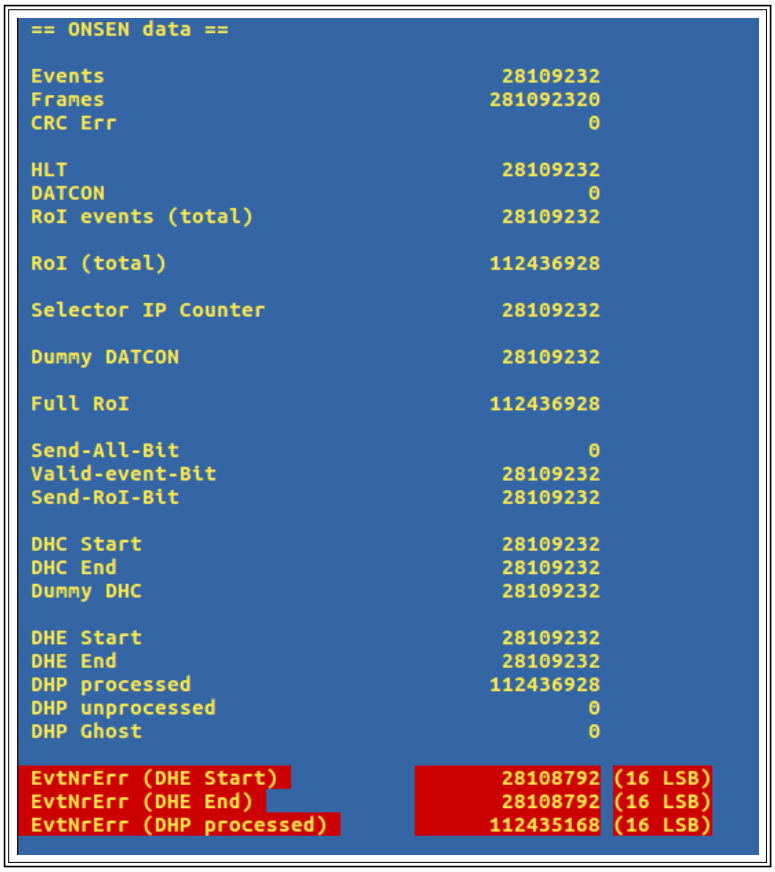

FIGURE 6.8: Snippet of the analysis of data recorded on 17th of December 2018 (test distribution pattern 2). The event number errors (EvtNrErr) are expected because emulated DHE and DHP frames were introduced. The event numbers of the emulated frames were set to `0x0`. The actual total number of events was $^{28,109,232}/_{4}$ = 7,027,308 because data for a given event number was sent from four Selectors to EB2 (see test distribution pattern 2 in table 6.1). A C++ program was used to check each output of each Selector.

```
DHC ID Start 00 (0x0):                28109232
DHC ID End 00 (0x0):                  28109232

DHE 02 (0x02):                                0
HLT for DHE 02 (0x02):                  3514598
DATCON for DHE 02 (0x02):                     0

IP  21 (0x15) for DHE 02 (0x02):         878616


IP  41 (0x29) for DHE 02 (0x02):         878664


IP 101 (0x65) for DHE 02 (0x02):         878674


IP 121 (0x79) for DHE 02 (0x02):         878644


DHE 03 (0x03):                                0
HLT for DHE 03 (0x03):                  3514598
DATCON for DHE 03 (0x03):                     0

IP  21 (0x15) for DHE 03 (0x03):         878616


IP  41 (0x29) for DHE 03 (0x03):         878664


IP 101 (0x65) for DHE 03 (0x03):         878674


IP 121 (0x79) for DHE 03 (0x03):         878644
```

FIGURE 6.9: Snippet of the IP counters of data recorded on 17th of December 2018 (test distribution pattern 2). DHEs with IDs `0x02` and `0x03` are shown as well as how many HLT / DATCON RoIs were found for these specific DHE IDs. The DHC ID is equal to zero as only dummy DHC data was used in tests. Four different IP addresses were found for each Selector, which met the expectations. In addition, the IP address sent by each Selector also matched expectations.

Chapter 7

Summary of Results

In this work I presented results of a test beam campaign performed at DESY in 2017. Results determined from 5,000,000 events, taken with a 3 GeV electron beam and a 1 T magnetic field were

- RoI reduction factor 10.38 (consistent with expected reduction factor of 10 [5])
- up to three RoIs for the same trigger number on both PXD module layers
- deviations between pixel column coordinates and RoI column centres of $\sim$ 0.64 pixel with $\sigma \sim 3.41$ pixel (2.23 pixel with $\sigma \sim 0.90$ pixel) in inner (outer) layer
- deviations between pixel row coordinates and RoI row centres of 0.92 pixel with $\sigma \sim 1.22$ pixel (0.16 pixel with $\sigma \sim 0.69$ pixel) in inner (outer) layer

The test campaigns at DESY also made it possible to evaluate the functionality of the ONSEN as part of the PXD readout system. The tests brought unexpected results despite the positive experiences during the tests at JLU. We found that the processing of incorrect data could lead to incorrect data processing requiring a complete restart of the ONSEN system. A number of tests were therefore carried out to identify problematic conditions, including

- incorrect CRC in data (ONSEN stopped receiving data correctly)
- incomplete data input (ONSEN merged two events)
- unexpected additional data (lead to trigger number mismatch in ONSEN data)

These bugs were fixed by the ONSEN developer team. To further improve the stability of the ONSEN, the developer team introduced filters to prevent corrupted data input which might cause issues.

A RoI distribution system was designed. It was tested with trigger rates up to 20 kHz at KEK. For testing purposes, the firmware was temporarily modified to write the IP addresses to the ONSEN-processed data. The tests were successful.

Chapter 8

Outlook

Belle II data acquisition and detectors are coming closer to the design specifications. At the time of this thesis, the RoI distribution on CNCBs has been successfully tested at KEK with a scaled-down HLT and with trigger rates up to 20 kHz. An integration test is to be performed with the maximum trigger rate expected (30 kHz) and with all the hardware required by design. This setup would include the ONSEN, all HLT units, the DATCON, all 40 PXD modules installed and connected to DHH hardware, and the event-builder-2. Such tests can be performed latest when Belle II detectors and data acquisition systems meet the design specifications. Other firmware adaptations for handling faulty or HLT-rejected events, as discussed in this thesis, are available in the ONSEN repositories. For certain testing purposes, it might be reasonable not to use the faulty-data discarding feature as developed for this thesis.

In case of any changes affecting ONSEN data inputs and outputs, or the firmware itself (e.g. the high-speed data multiplexer which was presented in Ref. [83]), it might be reasonable to test the entire ONSEN functionality to verify proper data processing and to avoid any unintended behaviour. In the long term, the ONSEN hardware may be modified. In this case, the entire ONSEN firmware must be adapted so that it can be used on the new hardware. Such changes require extensive testing.

Chapter 9

Acknowledgements

In 2014, I started working on the ONSEN system. My colleagues in the Belle II research group, especially Björn Spruck, helped me with questions that came up while I was working with the system as part of my master thesis. After completing my Master's degree, I had the opportunity to travel to KEK in Japan several times as part of the JENNIFER programme[1]. At KEK, I was involved in setting up and testing the ONSEN system. I also supported the activities around the first data acquisitions with PXD modules and I was even the PXD operator on the night of the very first Belle II collision runs.

For these great experiences and much more, I thank all Belle II colleagues, whether they work at JLU or elsewhere. My thanks also go to the Bundesministerium für Bildung und Forschung (BMBF) and the JENNIFER programme. I would especially like to thank the Belle II colleagues at the 2nd Physics Institute of JLU, who have always supported me, be it with questions about the ONSEN system, the Belle II experiment, or questions about the best way to implement firmware changes. Without their help with the development, data emulation and testing, I would not have been able to complete this work. Therefore I would like to thank in alphabetical order of the surnames: Thomas Geßler, Wolfgang Kühn, Sören Lange, Klemens Lautenbach, David Münchow, Simon Reiter and Björn Spruck. In particular, Thomas Geßler and Simon Reiter were always available to answer any questions I had during the testing and firmware development phases and when setting up the CSS user interfaces. They were a great support in testing, debugging and code review during my time at university, many thanks for that.

I am also grateful to my wife, who has always been a pillar of support for me.

This thesis was written using pdfLaTeXversion 3.14159265-2.6-1.40.16. For the precompilation of TIKZ drawings, I used luaLaTeXversion beta-0.80.0. For the bibliography I used JabRef version 2.10 and biber version 2.4. For translations, alternative wording, spell checks, etc., I used DeepL Translator (`https://www.deepl.com/de/translator`) and DeepL Write (beta version) (`https://www.deepl.com/write`).

[1] see official website [94]

Appendices

Appendix A

Data Formats

A.1 Overview

The information about the data formats provided in this chapter, except certain adjustments for RoI distribution tests, is based on thesis *Development of FPGA-Based Algorithms for the Data Acquisition of the Belle II Pixel Detector* [6, pp. 163-171], where a similar presentation of the data frames can be found. Since the Belle II data format specification is relevant for this dissertation, some parts of it are also listed here. For DHH data, only the dummy and emulated data formats are listed. For more details, the reader is referred to Ref. [6] or (internal) Belle II documentations. It should be noted that there might have been updates to the data format in most recent official Belle II data format specification.

Figures A.1 and A.2 show the frames which are received and sent out, respectively, by the ONSEN. Note that similar illustrations of the data frames can be found in Ref. [6, p. 170] and Ref. [7, p. 59].

The ONSEN sends frames with DHE and DHP data only when the ONSEN has received DHH data. The DHC frames are mandatory part of the data format, whether or not DHH data has been provided to the ONSEN system. The ONSEN sends dummy DHC frames as a substitute if needed. The RoI frame is primarily a debugging option. It was indispensable for testing the RoI distribution on the CNCBs.

More details about the 32-bit aligned frames are given in the following sections. There are many "reserved" / "Res." bits in the data format specification which are set to zero by default. Frames can be distinguished by header words or at least a fixed bit-pattern. Hereinafter, such mandatory identifiers are referred to as "magic word".

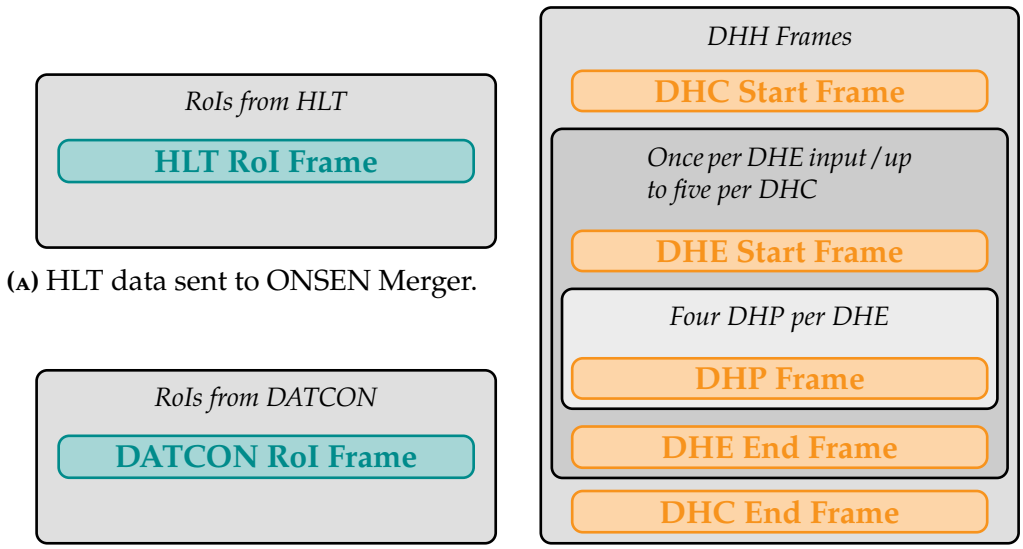

(A) HLT data sent to ONSEN Merger.

(B) DATCON data sent to ONSEN Merger.

(C) DHH / PXD data sent to ONSEN Selectors.

FIGURE A.1: Input data for the ONSEN Merger and Selector. There are inputs from the HLT, the DATCON and the DHH system.

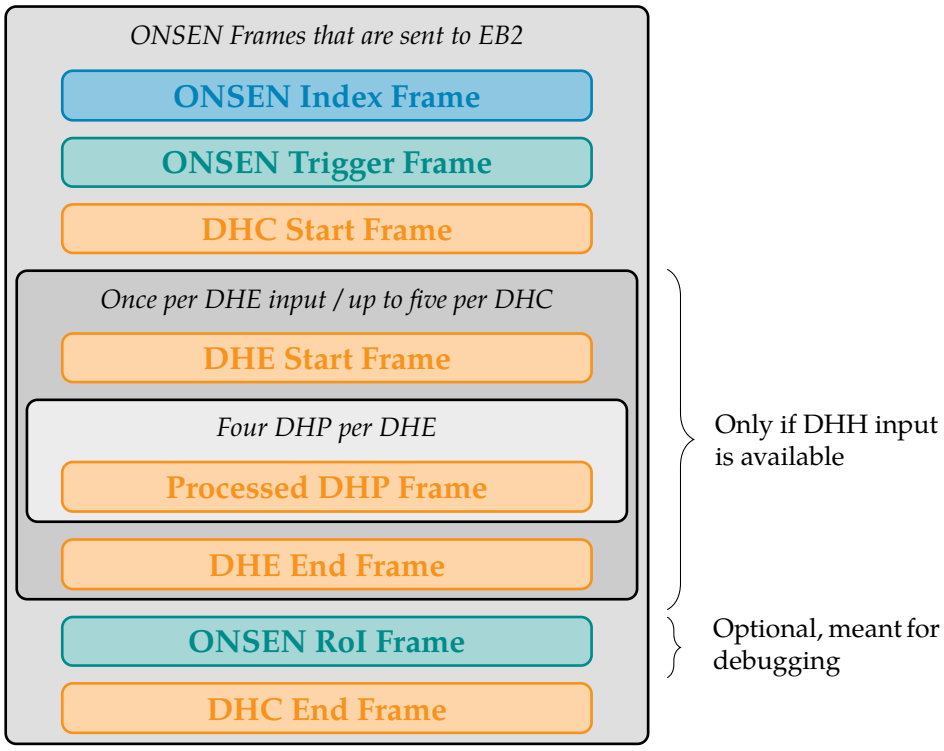

Figure A.2: Data frames sent by ONSEN Selectors to EB2. The data consists of DHH data and RoI-selected PXD data. If no DHH data has been provided to ONSEN, dummy DHC frames are sent instead. The ONSEN Trigger frame contains information from the RoI sources HLT and DATCON. The RoIs can be sent by ONSEN in a frame as a debug option. The ONSEN Index frame contains the lengths of all frames.

A.2 ONSEN Frames

This section focuses on the frames that are generated in the ONSEN system itself [6, pp. 169-171].

The Index frame contains the information about how many frames of what size (in bytes) will be sent for the event. The Index frame, and thus the ONSEN-data, starts with `0xCAFEBABE` as the magic word.

ONSEN Index Frame

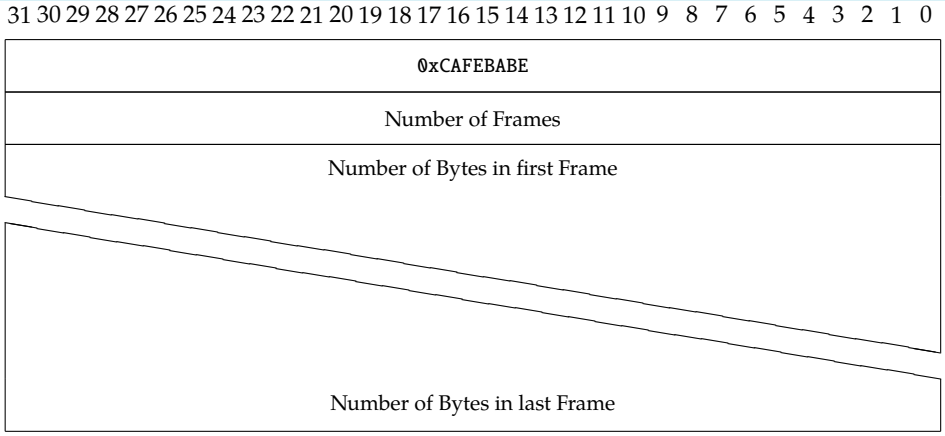

The Trigger frame is basically a combination of the HLT and the DATCON header words with a preceding magic word. It is sent after the Index frame and the first frame which contains the trigger number. The HLT and DATCON frames are discussed in section A.3. The very first trigger number in the Trigger frame is a copy of the 16 LSBs of the HLT trigger number. Each word in this frame is mandatory. This is also true for the DATCON information. If no actual DATCON data is available, a dummy DATCON data substitute is added instead (see section A.4).

ONSEN Trigger Frame

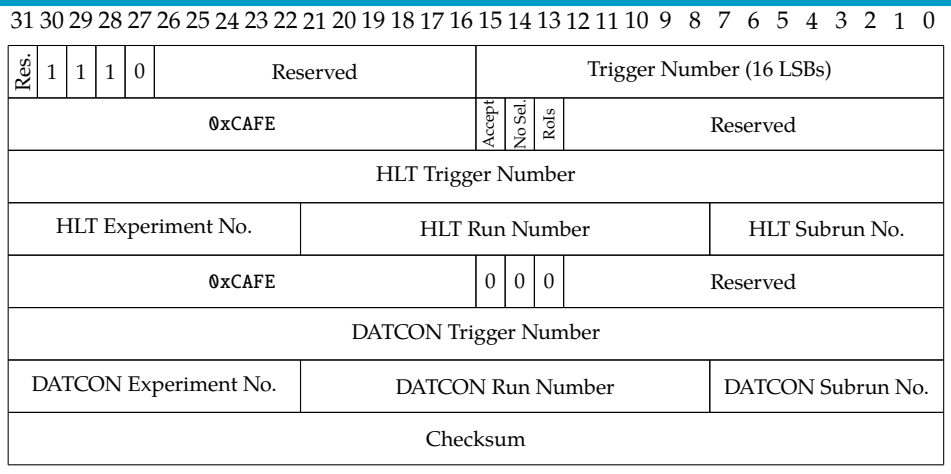

The RoI frame lists all RoIs received by the Selector. The original CRC checksum of the merged RoI packet (HLT RoIs + DATCON RoIs), calculated on the Merger, is preserved as second last word in this frame.

Optional ONSEN RoI Frame

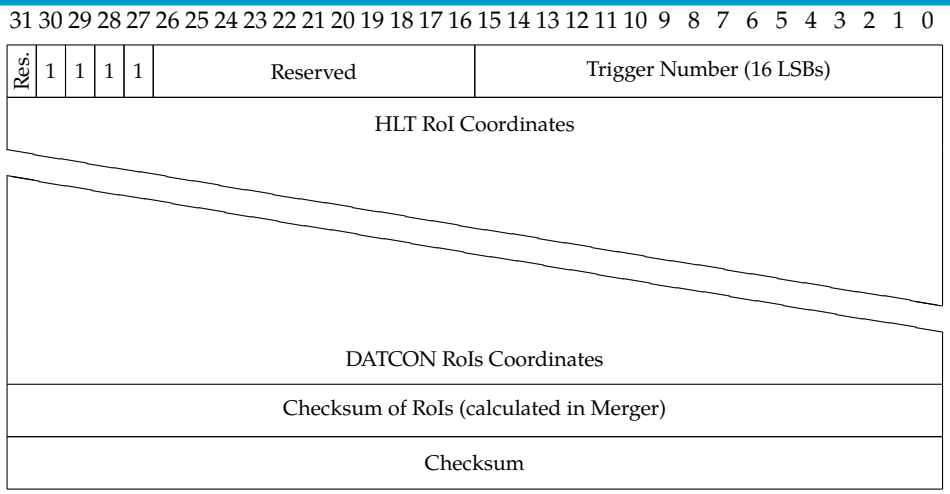

A.3 Region of Interest Data Frames

The two RoI coordinates (Row1, Column1) and (Row2, Column2) define a rectangular area on sensitive area of the PXD module. There are 768 rows and 250 columns on each PXD module. As a consequence, there are ten bits reserved for each row coordinate, while only eight bits are reserved for each column coordinate. The DHE ID is used as identifier for the half-ladder or rather the DHE. The "Source" flag is used to distinguish RoIs from HLT (Source = 0) and DATCON (Source = 1). The RoI coordinates are sent as part of the HLT RoI frame and DATCON RoI frame. These are discussed below.

Region of Interest Coordinates

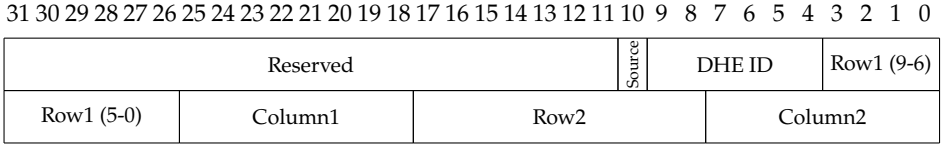

The data formats discussed in this section are adapted from Ref. [6, pp. 166-168] with the exception of the magic word `0xBE12DA7A` in the HLT RoI frame. This magic word was introduced after publication of Ref. [6].

The "Accept" flag is set by the HLT. It indicates whether an event should be discarded (Accept=0) or not (Accept=1). "No Sel."=1 disables the RoI selection in ONSEN for the given event. In that case, all PXD data received by the Selectors will be sent to

EB2. When the "RoIs"-flag is set to "1", the RoIs received by the Selectors will be forwarded to the EB2 as additional information which is mainly used for debugging.

The HLT RoI frame also provides the current experiment-, run- and subrun-numbers as well as the HLT-RoI coordinates mentioned above.

HLT RoI Frame

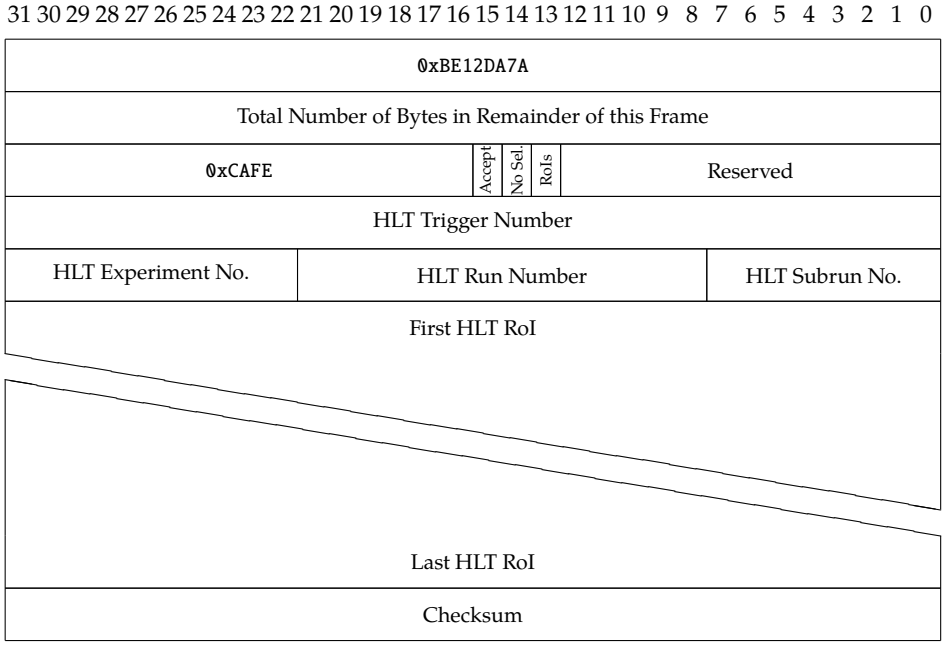

The DATCON RoI frame format is almost identical to the HLT RoI frame format but with DATCON-calculated RoIs. The DATCON system sets neither "Accept"-, "No Sel."- nor "RoIs"- bits. There is also no magic word like `0xBE12DA7A` and no information about the trailing data needed as the DATCON RoI frame is transmitted using the Aurora Protocol [6, p. 167].

DATCON RoI Frame

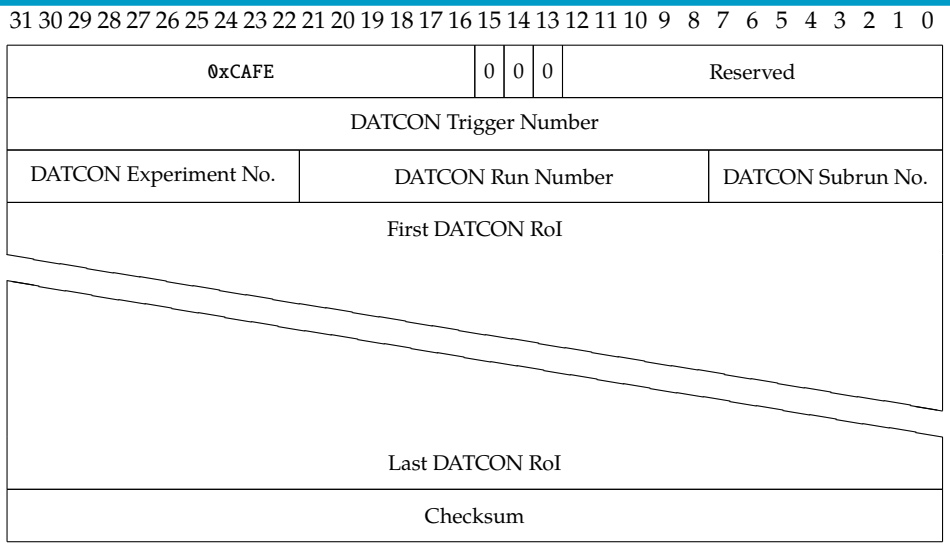

A.4 Dummy Data Formats

The dummy data frames are sent as substitutes by the ONSEN if no DHH and / or no DATCON data has been received. All variable entries such as the trigger number are set to zero in dummy data. An exception is made for the checksum, which must be correct even if dummy data is used.

There are dummy data for DATCON and DHC data but no dummy data for missing DHE or DHP data (see figure A.2 on page 109).

Dummy DATCON Frame

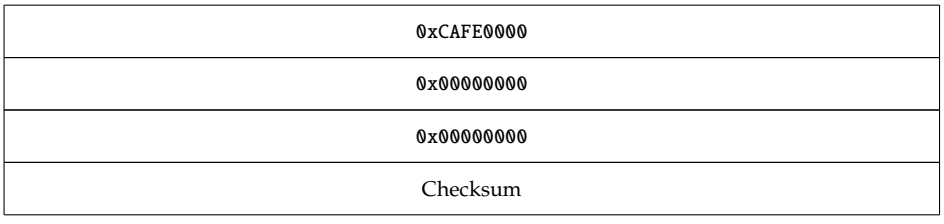

Dummy DHC Start

31 30 29 28 27 26 25 24 23 22 21 20 19 18 17 16 15 14 13 12 11 10 9 8 7 6 5 4 3 2 1 0
0x58000000
0x00000000
0x00000000
0x00000000
Checksum

Dummy DHC End

31 30 29 28 27 26 25 24 23 22 21 20 19 18 17 16 15 14 13 12 11 10 9 8 7 6 5 4 3 2 1 0
0x60000000
0x00000000
0x00000000
Checksum

A.5 Adjustments of Dummy Data for RoI Distribution Tests

For RoI distribution tests, reserved (undefined) bits in the dummy DATCON data in the ONSEN Trigger frame were adjusted temporarily. Since the DATCON was not part of the test setup, no input data has to be transformed but only dummy data. For testing purpose described in section 6.2.2, reserved bits were replaced by the last two numbers of the Selector IP. For example, the IP `10.18.3.21` replaced reserved bits with `0x315` (last digits of IP: 21_{10}=`0x15`).

ONSEN Trigger Frame with Adjustments for RoI Distribution Tests

31	30	29	28	27	26	25	24	23	22	21	20	19	18	17	16	15	14	13	12	11	10	9	8	7	6	5	4	3	2	1	0
Res.	1	1	1	0	Reserved											Trigger Number (16 LSBs)															
0xCAFE																Accept	No Sel.	RoIs	Reserved												
HLT Trigger Number																															
HLT Experiment No.											HLT Run Number															HLT Subrun No.				
0xCAFE																0	0	0	Selector IP												
Dummy DATCON Trigger Number																															
Dummy DATCON Experiment No.											Dummy DATCON Run Number															Dummy DATCON Subrun No.				
Checksum																															

In the emulated DHE Start frame, as well as in the emulated DHE End frame and the emulated DHP data frames, the DHE ID was set to 63, which is the highest possible value for a DHE ID. In addition, this DHE ID does not represent an existing DHE. This ID used in tests translates to the fifteenth module in the outer PXD layer in backward direction. However, there are only twelve modules in each direction.

The DHP mask was set to `0xF` to emulate the existence of four connected DHPs.

Emulated DHE Start (added to Dummy Data)

31	30	29	28	27	26	25	24	23	22	21	20	19	18	17	16	15	14	13	12	11	10	9	8	7	6	5	4	3	2	1	0
0x1											1	0	DHE ID = 63							DHP Mask = 0xF				0x0000							
0x00000000																															
0x00000000																															
Checksum																															

Emulated DHE End (added to Dummy Data)

31	30	29	28	27	26	25	24	23	22	21	20	19	18	17	16	15	14	13	12	11	10	9	8	7	6	5	4	3	2	1	0
0x2											0	0	DHE ID = 63							0x00000											
0x00000000																															
0x00000000																															
Checksum																															

Emulated DHP Data Frame (added to Dummy Data)

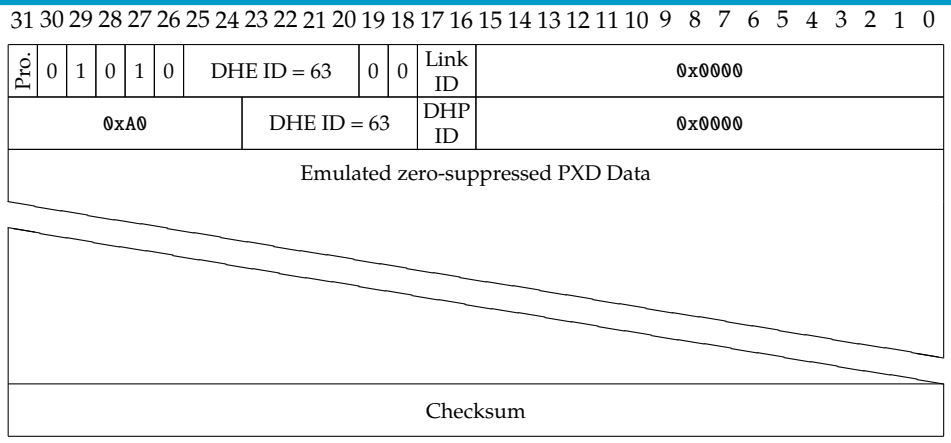

The processed-bit ("Pro.") was set by the Pixel Filter. The DHP ID (here: equal to "Link ID"), was ascending in test data so that the pixels were distributed over the sensitive area of a module as shown in figure 6.2 on page 90.

In emulated PXD data, the ADC value of the pixels was replaced by the column coordinate. This was done to simplify the check of the data.

Emulated Zero-suppressed PXD Data (added to Dummy Data)

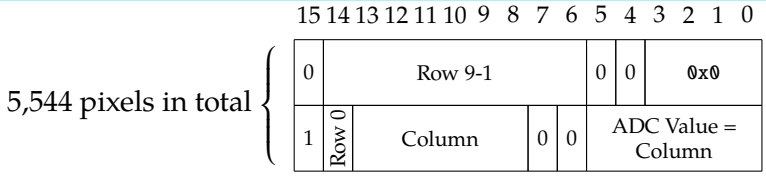

Appendix B

Data Validation with C++

B.1 Overview

The ONSEN data has been analysed for technical validity in numerous tests. The tool of choice for that purpose is the BASF2. However, in tests discussed in this dissertation C++ programs were used as well. These provided a convenient option to check the CRC checksums of the frames or to check specific parts of the data stream.

The C++ program as used while working on this dissertation started as a tool developed by ONSEN developers to recalculate CRCs checksums. Based on that, additional checks and counters have been introduced. These made it possible to analyse specific conditions in the tests, thus supporting the testing activities described in chapter 5 and chapter 6. Similar programs were also used for data checks when I was working on my Master thesis [81].

The program remained simple and was often adapted to the current situation. When the test data for the ONSEN Merger or Selector was emulated, it was easy to add a check for the expectations at hand, for example a certain appearance of the ONSEN Index frame which is variable in size in normal operation.

In general, the program was used to check the number of frames, the number of different types of frames (e.g. Trigger frame, DHC frame etc.) and the number of certain bits (e.g number of specific DHE IDs in the data). In the following a brief overview of some checks in the program will be presented. The code snippets shown have been simplified for this thesis. In some parts the code has been replaced with place holders like "[...]" or "<*a certain frame*>".

B.2 Code Snippets

The data of each frame which has been forwarded to the program is temporarily stored in 32 bit array `buffer`. In the `length` array, the frame lengths as provided by the ONSEN Index frame are stored temporarily. This information is necessary to determine the number of 32 bit words in a frame, see code snippet B.1.

Listing B.1: Read each 32-bit word of the frame and store it in the buffer-array

```
#include <cstdio>
...
```

```
//Array to store the content of each frame
uint32_t buffer[1000000];

//Array to store the length of each frame; the length is available in
    ONSEN Index Frame
uint32_t length[64];
...

fread( &buffer, 1, length[<Current Frame>], stdin );
...
```

The frame lengths are needed in particular for the CRC checksum calculations shown below in snippet B.2. If a mismatch between the calculated CRC checksum and those in the data frame has been found, an error message is printed.

Note that the checksum format was also discussed in Ref. [6, p. 172]. Further information about the boost library can be found on the *boost* website [95].

Listing B.2: Recalculate / verify CRC of frame

```
#include <boost/crc.hpp>
#include <arpa/inet.h>
#include <cstdio>
...

uint32_t crc_value;
boost::crc_optimal<32, 0x04C11DB7, 0, 0, false, false> crc_out;
...

//Calculate CRC of current frame ("-4" to exclude the CRC of the frame)
crc_out.process_bytes( buffer,length[<Current Frame>]-4 );

//Get CRC of current frame
crc_value = ntohl( buffer[( length[<Current Frame>]/4 )-1] );
...

//Compare calculated CRC and CRC of current frame
if( crc_value != crc_out() ){
  printf( "␣CRC␣Error␣in␣frame␣with␣header␣0x%08X␣in␣event␣%08X␣[...]",
      ntohl( buffer[0] ), current_event [...]);
}
...
```

Since `buffer[0]` always contains the header of each frame, it is possible to identify the frame type, see snippet B.3. In the case of DHP frames, the ONSEN-processed and unprocessed data, starting with `0x6800` and `0x2800`, respectively (only one bit difference), are distinguished. In addition, whether the lengths fulfilled ≥ 12 byte is checked. A size of just 12 byte is only expected if no PXD data is available in the DHP frame, see Ref. [6, pp. 164-165] for more details.

Listing B.3: Identify frame type in Belle II data from 16 first bits in each frame

```
#include <arpa/inet.h>
#include <cstdio>
...
```

```
fread( &buffer, 1, length[<Current Frame>], stdin );
...

//Trigger Frame
if( ( ( ntohl( buffer[0] )&0xFFFF0000 )>>16 ) == 0x7000 )
...

//RoI Data Frame
if( ( ( ntohl( buffer[0] )&0xFFFF0000 )>>16 )== 0xCAFE )
...

// DHC Start Frame
if( ( ( ntohl( buffer[0] )&0xF8000000 )>>16 )== 0x5800 )
...

// DHE Start Frame
if( ( ( ntohl( buffer[0] )&0xF8000000 )>>16 ) == 0x1800 )
...

// DHE Zero Suppressed Data (ZSD) Frame
if( ( ( ( ( ntohl( buffer[0] )&0xF8000000 )>>16 ) == 0x2800 ) ||
  ( ( ( ntohl( buffer[0] )&0xF8000000 )>>16 ) == 0x6800 ) )
  && length[<DHE ZSD Frame>] >= 12 )
...

// DHE End Frame
if( ( ( ntohl( buffer[0] )&0xF8000000 )>>16 ) == 0x2000 )
...

// Debug RoI Frame
if( ( ( ntohl( buffer[0] )&0xF8000000 )>>16 ) == 0x7800 )
...

// DHC End Frame
if( ( ( ntohl( buffer[0] )&0xF8000000 )>>16 ) == 0x6000 )
...
```

Aside from correct CRC checksums, consistent trigger numbers / event numbers are expected. The source of truth for the trigger number is the number provided in HLT data. An example for the check is shown in the following snippet B.4. Only the 16 LSBs are compared in most cases.

Listing B.4: Comparison of trigger numbers in different frames of the same event (example for Trigger frame, HLT and DATCON trigger numbers)

```
#include <arpa/inet.h>
#include <cstdio>
...

//Compare 16 LSBs of trigger number in first 32-bit word of the frame
    with 16 LSBs of trigger number of third 32-bit word (here: HLT trigger
     number)
if( ( ntohl( buffer[0] ) & 0xFFFF ) != ( ntohl( buffer[2] ) & 0xFFFF ) )
    {
  printf( "␣Mismatch␣of␣HLT␣and␣Trigger␣event␣numbers␣[...]" );
}
...
```

```
//Compare trigger number in third 32-bit word of frame (here: HLT trigger
     number) with trigger number of sixth 32-bit word (here: DATCON
    trigger number)
if( ntohl( buffer[2] ) != ntohl( buffer[5] ) ) {
  printf( "␣Mismatch␣of␣event␣number␣in␣Trigger␣Frame␣[...]" );
}
...
```

Another important requirement of the ONSEN is the correct order of the DHE IDs in the data stream. The ONSEN expects an ascending order of DHE IDs in the DHH data. This is addressed in snippet B.5.

Listing B.5: Verification of proper DHE ID order

```
#include <arpa/inet.h>
#include <cstdio>
...

//Compare DHE ID in data with highest DHE ID read in this event so far
dhe_id_current = ( ntohl( buffer[0] )&0x03F00000 )>>20;

if( dhe_id_current < dhe_id_highest ) {
  printf( "␣DHE␣Frame:␣wrong␣DHE␣ID␣[...]" );
}
else {
  dhe_id_highest = dhe_id_current;
}
...
```

In the DESY test campaigns we found that the "Start-of-Row" information in DHP frames (the first 2 Byte of the pixel coordinates, see figure 4.15 on page 57) had been sent twice unexpectedly in certain events. Therefore another check is implemented in the C++ program, see snippet B.6.

Listing B.6: Check for double Start-of-Row information

```
#include <arpa/inet.h>
...

//Check if PXD data starts with double Start-of-Row (which is unexpected;
     observed in tests)
if( ( ( ntohl( buffer[2] )&0x80008000 ) == 0x00000000 ) )
...
```

Another checks were introduced whenever needed but not necessarily kept for later. Some of these checks will be addressed in the next section.

B.3 Check of RoI Distribution in Tests at KEK

The IP Writer core was utilized for tests of the RoI distribution at KEK. The tests required confirmation that all RoIs for specific trigger numbers and DHE IDs were

sent to the correct Selector. The code snippets shown below provide an overview how the ONSEN data was checked for unexpected behaviour of the RoI distribution.

Important information in the data frames were the IP addresses of the ONSEN Selectors and the DHE IDs, see code snippets in B.7 and B.8.

Listing B.7: Get IP from DATCON data in Trigger frame

```
//Get IP from fifth 32-bit word in Trigger frame (written to buffer[4],
    manipulated DATCON data)
if( ( ntohl( buffer[4] ) & 0x00001FFF ) != 0x00000000 ) {
  output_ip = ( ntohl( buffer[4] ) & 0x000000FF );
}
...
```

Listing B.8: Get RoI DHE ID from ONSEN Debug RoI frame

```
//ONSEN Debug RoI Frame: read DHE ID from second 32-bit word
if( ( ntohl( buffer[0] )&0xF8000000 ) == 0x78000000 ) {
  roi_id_current = (ntohl(buffer[1] )&0x3F0) >> 4;
...
```

Two test patterns were defined for the tests at KEK (see chapter 6). In snippet B.9 the first two (possible) DHE IDs in the HLT data (`roi_id_current`) and the (unexpected) IP addresses (`output_ip`) are compared.

Listing B.9: Testpattern 1: Check of DHE ID in RoI sent by the Selector (identified by its IP)

```
//Testpattern 1 in RoI Distribution Tests at KEK
//Check if DHE ID in RoI (roi_id_current) meets expectations for current
    IP (output_ip)
if( ( ntohl( buffer[0] )&0xF8000000 ) == 0x78000000 )
{
  roi_id_current = (ntohl(buffer[1] )&0x3F0) >> 4;

  if( (roi_id_current == 0x2) && (output_ip != 21) )
      printf("ERROR␣[...]" );
  if( (roi_id_current == 0x3) && (output_ip != 22) )
      printf("ERROR␣[...]" );
...
}
...
```

The snippet B.10 illustrates how the trigger numbers and Selector IPs were compared. Again, an error message was printed in case of unexpected mismatches.

Listing B.10: Testpattern 2: Check of trigger number in data sent by a specific Selector (identified by its IP)

```
//Testpattern 2 in RoI Distribution Tests at KEK
//Check if IP (output_ip) meets expectations for trigger number (
    current_event)
if( ( ntohl( buffer[0] )&0xF8000000 ) == 0x78000000 ) {
  ...
  if( (output_ip == 21) || (output_ip == 22) || (output_ip == 23) || (
      output_ip == 24) ) {
```

```
    if( current_event % 8 != 0) {
      printf( "ERROR [...]" );
    }
  }
  ...
}
...
```

For the second test pattern the comparison of DHE IDs with the Selector IPs had to be adjusted as shown in code B.11.

Listing B.11: Testpattern 2: Check of DHE ID in RoI sent by the Selector (identified by its IP) as used for tests at KEK

```
//Testpattern 2 in RoI Distribution Tests
//Check if DHE ID in RoI (roi_id_current) meets expectations for current
    IP (output_ip)
if( ( ntohl( buffer[0] )&0xF8000000 ) == 0x78000000 ) {
  roi_id_current = (ntohl(buffer[1] )&0x3F0) >> 4;

  if( (output_ip == 21) || (output_ip == 41) || (output_ip == 101) || (
      output_ip == 121) ) {
    if( !( (roi_id_current == 0x2) || (roi_id_current == 0x3) || (
        roi_id_current == 0x4) || (roi_id_current == 0x5)) ) {
      printf("ERROR [...]" );
    }
  }
...
}
...
```

Appendix C

Slave Registers

C.1 Slave Registers used in RoI Distribution

In this section the slave registers as implemented for the RoI distribution on CNCBs are listed in figures C.1 to C.4 on pages 123–125.

	Bit	
Slave Register 0	31	Link 1 Out: Destination Not Ready
	30	Link 2 Out: Destination Not Ready
	29	Link 3 Out: Destination Not Ready
	⋮	
	24	Link 8 Out: Destination Not Ready
	23	Link 1 Out: Source Not Ready
	22	Link 2 Out: Source Not Ready
	21	Link 3 Out: Source Not Ready
	⋮	
	16	Link 8 Out: Source Not Ready
	8	Link In: Destination Not Ready
	0	Link In: Source Not Ready

Figure C.1: Slave registers for the LocalLink status. Used for debugging the IP core in development phase. Status bits can be read out via slow control in a CSS user interface.

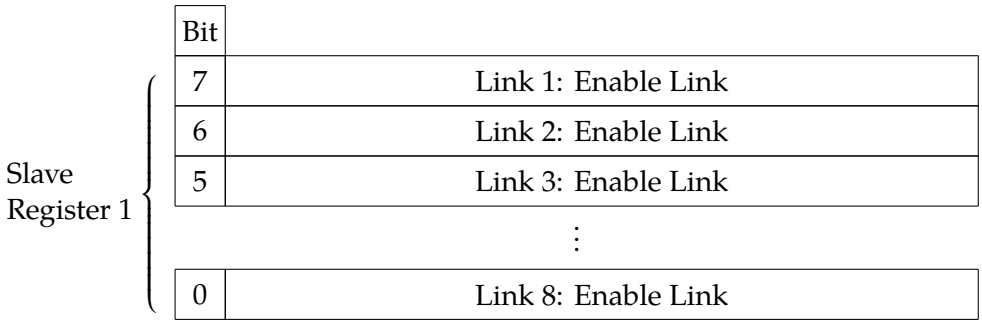

FIGURE C.2: RoI Fork: slave register to enable the links from the Merger CNCB to the Selector CNCBs and from the Selector CNCB to the Selector AMCs. Settings can be changed in a CSS user interface.

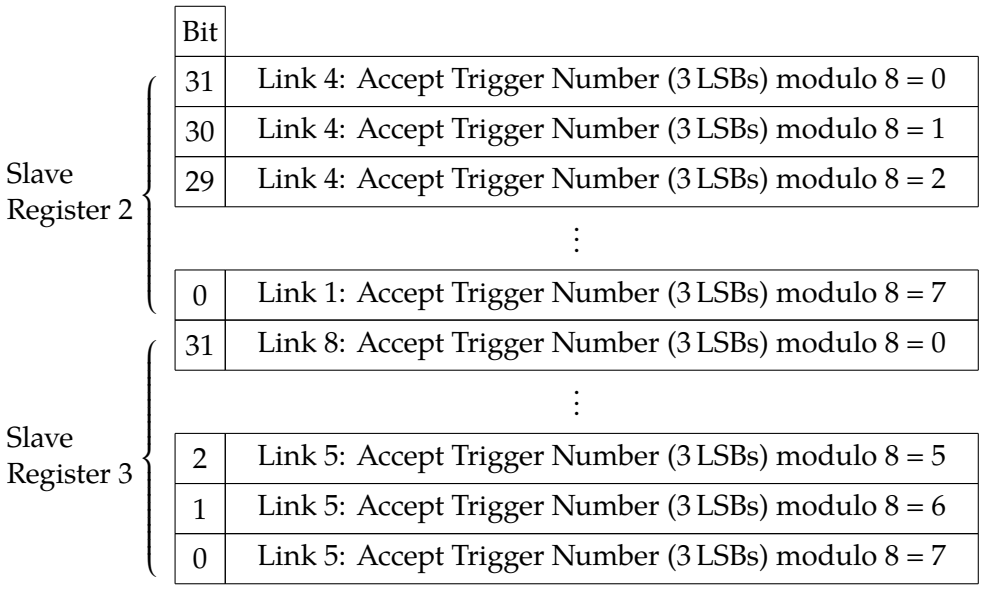

FIGURE C.3: Slave registers for the trigger number selection. Settings can be changed in a CSS user interface. This selection is performed on the Merger CNCB.

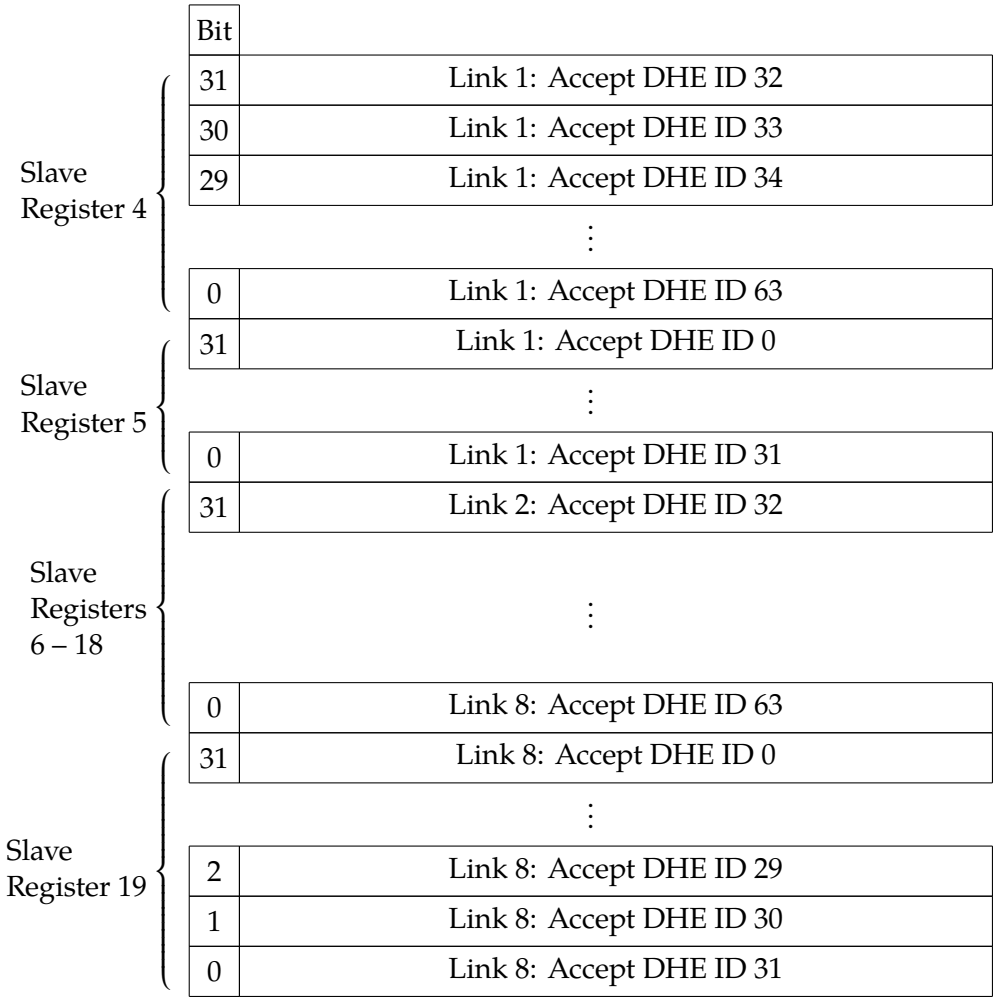

Figure C.4: Slave registers for the selection of RoIs based on DHE IDs. Settings can be changed in a CSS user interface. This selection is performed on the Selector CNCBs.

C.2 Slave Registers used in IP Writer

For the tests of the RoI distribution an IP Writer IP core was used. The core used slave registers as listed in figures C.5 and C.6.

	Bit	
Slave Register 0	24	Link Out: Destination Not Ready
	16	Link Out: Source Not Ready
	8	Link In: Destination Not Ready
	0	Link In: Source Not Ready

Figure C.5: Slave registers for the LocalLink status of the IP Writer used for RoI distribution tests in December 2018 at KEK.

	Bit	
Slave Register 1	31	Last three hexadecimal digits of IP address of Selector AMC
	⋮	
	19	

Figure C.6: Slave register for the last digits of the IP address of the Selector AMC.

List of Figures

List of Tables

Acronyms

AMC Advance Mezzanine Card

ARICH Aerogel Ring-Imaging Cherenkov Detector

ASIC Application Specific Integrated Circuit

ATCA Advanced Telecommunications Computing Architecture

BASF2 Belle II Analysis and Software Framework

BKLM Barrel KLM

BMBF Bundesministerium für Bildung und Forschung

B2GM Belle II General Meeting

CDC Central Drift Chamber

CKM Cabibbo-Kobayashi-Maskawa

CNCB Compute Node Carrier Board

CP charge-conjugation parity

CRC Cyclic Redundancy Check

CSS Control System Studio

DAQ data acquisition

DATCON Data Acquisition Tracking Concentrator Online Node

DCD Drain Current Digitizer

DEPFET Depleted Field Effect Transistor

DESY Deutsches Elektronen-Synchrotron

DHC Data Handling Concentrator

DHE Data Handling Engine

DHH Data Handling Hub

DHP Data Handling Processor

DPG Deutsche Physikalische Gesellschaft

DSSD double-sided silicon microstrip detector

EB2 event-builder-2

ECL Electromagnetic Calorimeter

EKLM Endcap KLM

EPICS Experimental Physics and Industrial Control System

FPGA Field Programmable Gate Array

HEPHY Institut für Hochenergiephysik

HL half-ladder

HLT High Level Trigger

IHEP Institute of High Energy Physics

IP interaction point

IP Intellectual Property

IP Internet Protocol address

JENNIFER Japan and Europe Network for Neutrino and Intensity Frontier Experimental Research

JFET junction field effect transistor

JLU Justus-Liebig-University

JTAG Joint Test Action Group

KEK High Energy Accelerator Research Organization

KLM K_L^0 and μ Detector

LEP Large Electron Positron Collider

LHC Large Hadron collider

LSB least significant bit

LUT look-up table

LVDS Low Voltage Differential Signaling

MGT Multi Gigabit Transceiver

MOSFET metal-oxide-semiconductor field-effect transistor

ONSEN Online Selection Nodes

PSU power supply unit

PXD Pixel Detector

RAM Random Access Memory

QCS final-focus superconducting magnet system

RoI Region of Interest

RPC resitive plate chamber

RTM rear transition module

SFP+ Small Form-factor Pluggable

SM Standard Model

SVD Silicon Vertex Detector

TCA Telecommunications Computing Architecture

TOP Time-Of-Propagation counter

VXD Vertex Detector

Bibliography

[1] *Promotionsordnung der Gemeinsamen Kommission Naturwissenschaften für die Naturwissenschaftlichen Fachbereiche der Justus-Liebig-Universität Gießen vom 4. Februar 2005*. accessed December 15th, 2023. Justus-Liebig-Universität. URL: https://www.uni-giessen.de/de/mug/7/pdf/7_40/7_40_12_1.pdf.

[2] Tetsuo Abe et al. "Achievements of KEKB". In: *Progress of Theoretical and Experimental Physics* 2013.3 (Mar. 2013). 03A001, accessed October 16th, 2023. ISSN: 2050-3911. DOI: 10.1093/ptep/pts102. eprint: https://academic.oup.com/ptep/article-pdf/2013/3/03A001/4440618/pts102.pdf. URL: https://doi.org/10.1093/ptep/pts102.

[3] T. Abe et al. *Belle II Technical Design Report*. accessed October 16th, 2023. 2010. DOI: 10.48550/ARXIV.1011.0352. URL: https://arxiv.org/abs/1011.0352.

[4] Thomas Geßler et al. "The ONSEN Data Reduction System for the Belle II Pixel Detector". In: *IEEE Transactions on Nuclear Science* 62.3 (June 2015). (version 3 as available at arxiv.org has been used in this dissertation (see URL); accessed December 17th, 2023), pp. 1149–1154. DOI: 10.1109/tns.2015.2414713. URL: https://doi.org/10.48550/arXiv.1406.4028.

[5] M. Nakao et al. "Data acquisition system for Belle II". In: *Journal of Instrumentation* 5.12 (Dec. 2010). accessed October 16th, 2023, p. C12004. DOI: 10.1088/1748-0221/5/12/C12004. URL: https://dx.doi.org/10.1088/1748-0221/5/12/C12004.

[6] Thomas Geßler and Justus Liebig University Giessen. "Development of FPGA-based algorithms for the data acquisition of the Belle II pixel detector". engl. accessed October 16th, 2023. PhD thesis. Justus Liebig University Giessen, 2015. DOI: 10.22029/JLUPUB-9710. URL: https://jlupub.ub.uni-giessen.de//handle/jlupub/10326.

[7] David Münchow and Justus Liebig University Giessen. "Development of the online data reduction system and feasibility studies of 6-layer tracking for the Belle II pixel detector". engl. accessed October 16th, 2023. PhD thesis. Justus Liebig University Giessen, 2015. DOI: 10.22029/JLUPUB-9690. URL: https://jlupub.ub.uni-giessen.de//handle/jlupub/10306.

[8] Prof.Dr. Jörn Bleck-Neuhaus. *Elementare Teilchen - Moderne Physik von den Atomen bis zum Standard-Modell*. Ed. by Springer. 1st ed. Springer, 2010.

[9] Bodgan Povh et al. *Particles and Nuclei - An Introduction to the Physical Concepts*. Ed. by Springer. 5th ed. Springer, 2006.

[10] Murray Gell-Mann. "A Schematic Model of Baryons and Mesons". In: *Phys. Lett.* 8 (1964). accessed November 1st, 2023, pp. 214–215. DOI: 10.1016/S0031-9163(64)92001-3.

[11] G. Zweig. *An SU_3 model for strong interaction symmetry and its breaking; Version 1*. Tech. rep. An updated version of the paper is available as CERN-TH-412, Feb. 1964. Accessed October 16th. 2023. Geneva: CERN, 1964. DOI: 10.17181/CERN-TH-401. URL: http://cds.cern.ch/record/352337.

[12] R.L. Workman et al. (Particle Data Group). "Review of Particle Physics". In: *Prog. Theor. Exp. Phys.* 2022 (2022). accessed October 16th, 2023, p. 083C01. DOI: 10.1093/ptep/ptac097.

[13] Y. Fukuda et al. "Evidence for Oscillation of Atmospheric Neutrinos". In: *Phys. Rev. Lett.* 81 (8 Aug. 1998). accessed October 16th, 2023, pp. 1562–1567. DOI: 10.1103/PhysRevLett.81.1562. URL: https://link.aps.org/doi/10.1103/PhysRevLett.81.1562.

[14] *Press release. NobelPrize.org. Nobel Prize Outreach AB 2023. Fri. 8 Sep 2023.* accessed September 9th, 2023. 2015. URL: https://www.nobelprize.org/prizes/physics/2015/press-release/.

[15] The ALEPH and DELPHI and L3 and OPAL and SLD Collaborations and the LEP Electroweak Working Group and the SLD Electroweak and Heavy Flavour Groups. "Precision Electroweak Measurements on the Z Resonance". In: *Physics Reports* 427.5–6 (May 2006). (version 3 as available at arxiv.org has been used in this dissertation (see URL); accessed December 2nd, 2023), pp. 257–454. ISSN: 0370-1573. DOI: 10.1016/j.physrep.2005.12.006. URL: https://doi.org/10.48550/arXiv.hep-ex/0509008.

[16] Patrick Janot and Stanisław Jadach. "Improved Bhabha cross section at LEP and the number of light neutrino species". In: *Physics Letters B* 803 (Apr. 2020). accessed October 16th, 2023, p. 135319. DOI: 10.1016/j.physletb.2020.135319. URL: https://doi.org/10.1016%2Fj.physletb.2020.135319.

[17] S. Chatrchyan et al. "Observation of a new boson at a mass of 125 GeV with the CMS experiment at the LHC". In: *Physics Letters B* 716.1 (2012). accessed October 16th, 2023, pp. 30–61. ISSN: 0370-2693. DOI: https://doi.org/10.1016/j.physletb.2012.08.021. URL: https://www.sciencedirect.com/science/article/pii/S0370269312008581.

[18] G. Aad et al. "Observation of a new particle in the search for the Standard Model Higgs boson with the ATLAS detector at the LHC". In: *Physics Letters B* 716.1 (2012). accessed October 16th, 2023, pp. 1–29. ISSN: 0370-2693. DOI: https://doi.org/10.1016/j.physletb.2012.08.020. URL: https://www.sciencedirect.com/science/article/pii/S037026931200857X.

[19] F. Englert and R. Brout. "Broken Symmetry and the Mass of Gauge Vector Mesons". In: *Phys. Rev. Lett.* 13 (9 Aug. 1964). accessed November 17th, 2023, pp. 321–323. DOI: 10.1103/PhysRevLett.13.321. URL: https://link.aps.org/doi/10.1103/PhysRevLett.13.321.

[20] Peter W. Higgs. "Broken symmetries and the masses of gauge bosons". In: *Phys. Rev. Lett.* 13 (16 Oct. 1964). accessed October 16th, 2023, pp. 508–509. DOI: 10.1103/PhysRevLett.13.508. URL: https://link.aps.org/doi/10.1103/PhysRevLett.13.508.

[21] *Prize announcement. NobelPrize.org. Nobel Prize Outreach AB 2023.Fri. 17 Nov 2023.* accessed November 17th, 2023. 2013. URL: https://www.nobelprize.org/prizes/physics/2013/prize-announcement/.

[22] *Press release. NobelPrize.org. Nobel Prize Outreach AB 2023.Fri. 8 Sep 2023.* accessed September 9th, 2023. 2013. URL: https://www.nobelprize.org/prizes/physics/2013/press-release/.

[23] M. Gell-Mann and A. Pais. "Behavior of Neutral Particles under Charge Conjugation". In: *Phys. Rev.* 97 (5 Mar. 1955). accessed November 1st, 2023, pp. 1387–1389. DOI: 10.1103/PhysRev.97.1387. URL: https://link.aps.org/doi/10.1103/PhysRev.97.1387.

[24] T. D. Lee and C. N. Yang. "Question of Parity Conservation in Weak Interactions". In: *Phys. Rev.* 104 (1 Oct. 1956). accessed October 16th, 2023, pp. 254–258. DOI: 10.1103/PhysRev.104.254. URL: https://link.aps.org/doi/10.1103/PhysRev.104.254.

[25] C. S. Wu et al. "Experimental Test of Parity Conservation in Beta Decay". In: *Phys. Rev.* 105 (4 Feb. 1957). accessed October 16th, 2023, pp. 1413–1415. DOI: 10.1103/PhysRev.105.1413. URL: https://link.aps.org/doi/10.1103/PhysRev.105.1413.

[26] *The Nobel Prize in Physics 1957. NobelPrize.org. Nobel Prize Outreach AB 2023. Fri. 8 Sep 2023.* accessed September 9th, 2023. 1957. URL: https://www.nobelprize.org/prizes/physics/1957/summary/.

[27] J. H. Christenson et al. "Evidence for the 2π Decay of the K_2^0 Meson". In: *Phys. Rev. Lett.* 13 (4 July 1964). accessed October 16th, 2023, pp. 138–140. DOI: 10.1103/PhysRevLett.13.138. URL: https://link.aps.org/doi/10.1103/PhysRevLett.13.138.

[28] *Press release. NobelPrize.org. Nobel Prize Outreach AB 2023. Fri. 8 Sep 2023.* accessed September 9th, 2023. 1980. URL: https://www.nobelprize.org/prizes/physics/1980/press-release/.

[29] Makoto Kobayashi and Toshihide Maskawa. "CP-Violation in the Renormalizable Theory of Weak Interaction". In: *Progress of Theoretical Physics* 49.2 (Feb. 1973). accessed October 16th, 2023, pp. 652–657. ISSN: 0033-068X. DOI: 10.1143/PTP.49.652. eprint: https://academic.oup.com/ptp/article-pdf/49/2/652/5257692/49-2-652.pdf. URL: https://doi.org/10.1143/PTP.49.652.

[30] *The Nobel Prize in Physics 2008. NobelPrize.org. Nobel Prize Outreach AB 2023. Fri. 8 Sep 2023.* accessed September 9th, 2023. 2008. URL: https://www.nobelprize.org/prizes/physics/2008/prize-announcement/.

[31] Lincoln Wolfenstein. "Parametrization of the Kobayashi-Maskawa Matrix". In: *Phys. Rev. Lett.* 51 (21 Nov. 1983). accessed November 1st, 2023, pp. 1945–1947. DOI: 10.1103/PhysRevLett.51.1945. URL: https://link.aps.org/doi/10.1103/PhysRevLett.51.1945.

[32] E Kou et al. "The Belle II Physics Book". In: *Progress of Theoretical and Experimental Physics* 2019.12 (Dec. 2019). 123C01, accessed October 16th, 2023. ISSN: 2050-3911. DOI: 10.1093/ptep/ptz106. eprint: https://academic.oup.com/ptep/article-pdf/2019/12/123C01/32693980/ptz106.pdf. URL: https://doi.org/10.1093/ptep/ptz106.

[33] CKMfitter Group (J. Charles et al.) "CP Violation and the CKM Matrix: Assessing the Impact of the Asymmetric B Factories". In: *Eur. Phys. J. C41* (2005). Figure "The global CKM fit in the small (ρ-bar,η-bar) plane (zoom)" (see URL) accessed on September 6th, 2023; [hep-ph/0406184], updated results and plots available at: http://ckmfitter.in2p3.fr, pp. 1–131. DOI: 10.1140/epjc/s2005-02169-1. URL: http://ckmfitter.in2p3.fr/www/results/plots_spring21/eps/belle_rhoeta_small_global.eps.gz.

[34] Jake Bennett et al. *Belle II Luminosity*. accessed December 3rd, 2023. Belle II. 2023. URL: https://confluence.desy.de/display/BI/Belle+II+Luminosity.

[35] Kazunori Akai, Kazuro Furukawa, and Haruyo Koiso. "SuperKEKB collider". In: *Nuclear Instruments and Methods in Physics Research Section A: Accelerators, Spectrometers, Detectors and Associated Equipment* 907 (Nov. 2018). (version 2 as available at arxiv.org has been used in this dissertation (see URL), accessed December 17th, 2023), pp. 188–199. DOI: 10.1016/j.nima.2018.08.017. URL: https://doi.org/10.48550/arXiv.1809.01958.

[36] I. Bigi et al. "Production and decay properties of ultra-heavy quarks". In: *Physics Letters B* 181.1 (1986). accessed November 1st, 2023, pp. 157–163. ISSN: 0370-2693. DOI: https://doi.org/10.1016/0370-2693(86)91275-X. URL: https://www.sciencedirect.com/science/article/pii/037026938691275X.

[37] R.L. Workman et al. (Particle Data Group). "Review of Particle Physics". In: *Prog. Theor. Exp. Phys.* 2022 (2022). Figure "The charmonium system" licensed under CC BY-NC 4.0 (see https://creativecommons.org/licenses/by-nc/4.0/), URL to "The charmonium system" was accessed January 6th, 2023, p. 083C01. DOI: 10.1093/ptep/ptac097. URL: https://pdg.lbl.gov/2022/figures/charmonium/figures/charmonium-2022.eps.

[38] R.L. Workman et al. (Particle Data Group). "Review of Particle Physics". In: *Prog. Theor. Exp. Phys.* 2022 (2022). Figure "The bottomonium system" licensed under CC BY-NC 4.0 (see https://creativecommons.org/licenses/by-nc/4.0/), URL to "The bottomonium system" was accessed January 6th, 2023, p. 083C01. DOI: 10.1093/ptep/ptac097. URL: https://pdg.lbl.gov/2022/figures/bottomonium/figures/bottomonium-2021.eps.

[39] S.-K. Choi et al. "Observation of a Narrow Charmoniumlike State in Exclusive $B^{\pm} \to K^{\pm}\pi^{+}\pi^{-}J/\psi$ Decays". In: *Phys. Rev. Lett.* 91.26 (Dec. 2003). accessed November 1st, 2023, p. 262001. ISSN: 1079-7114. DOI: 10.1103/physrevlett.91.262001. URL: http://dx.doi.org/10.1103/PhysRevLett.91.262001.

[40] R. Aaij et al. "Determination of the $X(3872)$ Meson Quantum Numbers". In: *Phys. Rev. Lett.* 110 (22 May 2013). accessed October 16th, 2023, p. 222001. DOI: 10.1103/PhysRevLett.110.222001. URL: https://link.aps.org/doi/10.1103/PhysRevLett.110.222001.

[41] S.-K. Choi et al. "Observation of a Resonancelike Structure in the $\pi^{+-}\psi'$Mass Distribution in Exclusive $B \to K\pi^{+-}\psi'$Decays". In: *Phys. Rev. Lett.* 100.14 (Apr. 2008). accessed November 1st, 2023, p. 142001. DOI: 10.1103/physrevlett.100.142001. URL: https://doi.org/10.1103%2Fphysrevlett.100.142001.

[42] K. Chilikin et al. "Experimental constraints on the spin and parity of the $Z(4430)^+$". In: *Physical Review D* 88.7 (Oct. 2013). accessed November 1st, 2023. DOI: 10.1103/physrevd.88.074026. URL: https://doi.org/10.1103%2Fphysrevd.88.074026.

[43] R. Aaij et al. "Observation of the Resonant Character of the $Z(4430)^-$ State". In: *Phys. Rev. Lett.* 112 (22 June 2014). accessed October 16th, 2023, p. 222002. DOI: 10.1103/PhysRevLett.112.222002. URL: https://link.aps.org/doi/10.1103/PhysRevLett.112.222002.

[44] R. P. Feynman. "Space-Time Approach to Quantum Electrodynamics". In: *Phys. Rev.* 76 (6 Sept. 1949). accessed October 16th, 2023, pp. 769–789. DOI: 10.1103/PhysRev.76.769. URL: https://link.aps.org/doi/10.1103/PhysRev.76.769.

[45] Fermilab. *First Published Feynman Diagram, 1949*. accessed September 6th, 2023. URL: https://history.fnal.gov/virtual/feynman_diagram.html.

[46] Joshua Ellis. "TikZ-Feynman: Feynman diagrams with TikZ". In: *Computer Physics Communications* 210 (Jan. 2017). (version 1.0.0 from 2016 is available at arxiv.org (see URL)), pp. 103–123. ISSN: 0010-4655. DOI: 10.1016/j.cpc.2016.08.019. URL: https://doi.org/10.48550/arXiv.1601.05437.

[47] Karen Lingel, Tomasz Skwarnicki, and James G. Smith. "PENGUIN DECAYS OF B MESONS". In: *Annual Review of Nuclear and Particle Science* 48.1 (1998). accessed November 1st, 2023, pp. 253–306. DOI: 10.1146/annurev.nucl.48.1.253. eprint: https://doi.org/10.1146/annurev.nucl.48.1.253. URL: https://doi.org/10.1146/annurev.nucl.48.1.253.

[48] S.-W. Lin et al. "Difference in direct charge-parity violation between charged and neutral B meson decays". In: *Nature* 452.20 (Mar. 2008). accessed November 1st, 2023. DOI: 10.1038/nature06827. URL: https://doi.org/10.1038/nature06827.

[49] K. Abe et al. "Observation of Large CP Violation in the Neutral B Meson System". In: *Physical Review Letters* 87.9 (Aug. 2001). accessed November 1st, 2023. ISSN: 1079-7114. DOI: 10.1103/physrevlett.87.091802. URL: http://dx.doi.org/10.1103/PhysRevLett.87.091802.

[50] Y. Amhis et al. (Heavy Flavor Averaging Group Collaboration). "Averages of b-hadron, c-hadron, and τ-lepton properties as of 2021". In: *Physical Review D* 107.5 (Mar. 2023). accessed October 16th, 2023. DOI: 10.1103/physrevd.107.052008. URL: https://doi.org/10.1103%2Fphysrevd.107.052008.

[51] CKMfitter Group (J. Charles et al.) *[title on website (see URL):] CKMfitter global fit results as of Spring 21*. Eur. Phys. J. C41, 1-131 (2005) [hep-ph/0406184], updated results and plots available at: http://ckmfitter.in2p3.fr; accessed September 6th, 2023. URL: http://ckmfitter.in2p3.fr/www/results/plots_spring21/num/ckmEval_results_spring21.html.

[52] *SuperKEKB has renewed the luminosity world records again!* accessed October 2nd, 2022. KEK. 2021. URL: https://www2.kek.jp/accl/eng/topics/topics211224.html.

[53] *Belle II*. Official website of Belle II experiment, accessed September 29th, 2022. Belle II. URL: https://www.belle2.org/.

[54] *History of Peak Luminosity (e+/e- colliders)*. Image ID 12533, accessed January 7th, 2023. KEK. Mar. 2018. URL: https://www.kek.jp/wp-content/uploads/2021/10/20180319-luminosity-600x404.png.

[55] KEK. *Schematic drawing of SuperKEKB/Belle II facility*. Image ID 13827, accessed March 15th, 2022. KEK. Mar. 2018. URL: https://www.kek.jp/ja/imagearchive/images/20180320_superkekb_002.png.

[56] *Projection of integrated Luminosity delivered by SuperKEKB to Belle II*. accessed September 29th, 2022. Belle II. URL: https://confluence.desy.de/display/BI/Belle+II+Luminosity?preview=/145589871/247173899/Belle2_Luminosity_2022Mar.jpg.

[57] *Belle II Detector 3D model*. accessed March 15th, 2022. Belle II. URL: https://www.belle2.org/e21595/e21770/infoboxContent25427/BelleII3D2people.pdf.

[58] *Closeup of the Belle II Detector*. accessed March 15th, 2022. Belle II. URL: https://www.belle2.org/e21595/e21770/infoboxContent25433/BelleII_IR3D.pdf.

[59] Dehui Sun et al. "Belle2Link: A Global Data Readout and Transmission for Belle II Experiment at KEK". In: *Physics Procedia* 37 (2012). Proceedings of the 2nd International Conference on Technology and Instrumentation in Particle Physics (TIPP 2011), accessed October 16th, 2023, pp. 1933–1939. ISSN: 1875-3892. DOI: https://doi.org/10.1016/j.phpro.2012.01.036. URL: https://www.sciencedirect.com/science/article/pii/S1875389212019104.

[60] K. Adamczyk et al. "Belle II silicon vertex detector". In: *Nuclear Instruments and Methods in Physics Research Section A: Accelerators, Spectrometers, Detectors and Associated Equipment* 831 (2016). Proceedings of the 10th International "Hiroshima" Symposium on the Development and Application of Semiconductor Tracking Detectors, accessed November 1st, 2023, pp. 80–84. ISSN: 0168-9002. DOI: https://doi.org/10.1016/j.nima.2016.04.013. URL: https://www.sciencedirect.com/science/article/pii/S0168900216301760.

[61] Bernlochner, Florian et al. "Online Data Reduction for the Belle II Experiment using DATCON". In: *EPJ Web Conf.* 150 (2017). accessed November 19th, 2023, p. 00014. DOI: 10.1051/epjconf/201715000014. URL: https://doi.org/10.1051/epjconf/201715000014.

[62] N. Taniguchi. "Central Drift Chamber for Belle-II". In: *Journal of Instrumentation* 12.06 (June 2017). accessed November 1st, 2023. DOI: 10.1088/1748-0221/12/06/c06014. URL: https://doi.org/10.1088%2F1748-0221%2F12%2F06%2Fc06014.

[63] Dmitri Kotchetkov et al. "Front-end electronic readout system for the Belle II imaging Time-Of-Propagation detector". In: *Nuclear Instruments and Methods in Physics Research Section A: Accelerators, Spectrometers, Detectors and Associated Equipment* 941 (Oct. 2019). accessed November 1st, 2023. DOI: 10.1016/j.nima.2019.162342. URL: https://doi.org/10.1016%2Fj.nima.2019.162342.

[64] S. Iwata et al. "Particle identification performance of the prototype aerogel RICH counter for the Belle II experiment". In: *Progress of Theoretical and Experimental Physics* 2016.3 (Mar. 2016). accessed October 16th, 2023, 033H01. DOI: 10.1093/ptep/ptw005. URL: https://doi.org/10.1093%2Fptep%2Fptw005.

[65] B. Shwartz on behalf of BELLE II calorimeter group. "Electromagnetic calorimeter of the Belle II detector". In: *Journal of Physics: Conference Series* 928.1 (Nov. 2017). accessed October 16th, 2023, p. 012021. DOI: 10.1088/1742-6596/928/1/012021. URL: https://dx.doi.org/10.1088/1742-6596/928/1/012021.

[66] H. Ye et al. "Commissioning and performance of the Belle II pixel detector". In: *Nuclear Instruments and Methods in Physics Research Section A: Accelerators, Spectrometers, Detectors and Associated Equipment* 987 (2021). accessed November 1st, 2023, p. 164875. ISSN: 0168-9002. DOI: https://doi.org/10.1016/j.nima.2020.164875. URL: https://www.sciencedirect.com/science/article/pii/S0168900220312729.

[67] C. Marinas and K. Nakamura. *VXD Test Beam*. accessed March 15th, 2022. 2016. URL: https://indico.mpp.mpg.de/event/4247/contributions/9626/attachments/7621/8417/VXDTestBeam.pdf.

[68] Dmytro Levit et al. "FPGA Based Data Read-Out System of the Belle II Pixel Detector". In: *IEEE Transactions on Nuclear Science* 62.3 (June 2015). (version 1 from 2014 as available at arxiv.org has been used in this dissertation (see URL), accessed December 17th, 2023), pp. 1033–1039. DOI: 10.1109/tns.2015.2424713. URL: https://doi.org/10.48550/arXiv.1406.3864.

[69] T. Bilka et al. "Demonstrator of the Belle II Online Tracking and Pixel Data Reduction on the High Level Trigger System". In: *IEEE Transactions on Nuclear Science* 62.3 (June 2015). (version 2 as available at arxiv.org has been used in this dissertation (see URL), accessed November 26th, 2023), pp. 1155–1161. ISSN: 1558-1578. DOI: 10.1109/tns.2015.2419879. URL: https://doi.org/10.48550/arXiv.1406.4955.

[70] *Virtex-4 Family Overview*. DS112 (v3.1), accessed March 15th, 2022. Aug. 2010. URL: https://www.xilinx.com/support/documentation/data_sheets/ds112.pdf.

[71] *Virtex-5 Family Overview*. DS100 (v5.1), accessed March 15th, 2022. Aug. 2015. URL: https://www.xilinx.com/support/documentation/data_sheets/ds100.pdf.

[72] This is the database used by the semiconductor/electronics-group from the Institute of High Energy Physics, to store logistical and measurement data about sensors, moduls and other components., accessed January 6th, 2023. HEPHY. URL: https://www.hephy.at/hephydb/hephydb/users/login.

[73] Dennis Getzkow et al. *Tests of final hardware revision of the Belle II PXD data reduction system*. T 72.5 Postersitzung Teilchenphysik, accessed October 16th, 2023. Mar. 2017. URL: https://www.dpg-verhandlungen.de/year/2017/conference/muenster/part/t/session/72/contribution/5.

[74] Dennis Getzkow et al. *Test Runs of a Belle II PXD Prototype Readout System*. T 42.2 Vortrag, accessed October 16th, 2023. Feb. 2016. URL: https://www.dpg-verhandlungen.de/year/2016/conference/hamburg/part/t/session/42/contribution/2.

[75] Tomohisa Uchida. *SiTCP Manual*. Version 3.0, accessed on March 15th, 2022. May 2021. URL: https://www.sitcp.net/doc/SiTCP_eng.pdf.

[76] *SiTCP*. Japanese. "SiTCP Home Page" created by Dr. Tomohisa Uchida, accessed January 3rd, 2023; (SiTCP library available from Bee Beans Technologies Co.,Ltd.) URL: https://www.sitcp.net/.

[77] *Aurora 8B/10B Protocol Specification*. v2.3. SP002, accessed October 16th, 2023. Xilinx Inc. Oct. 2014. URL: https://docs.xilinx.com/v/u/en-US/aurora_8b10b_protocol_spec_sp002.

[78] *PlanAhead User Guide*. v14.6. UG632, accessed November 6th, 2023. Xilinx Inc. June 2013. URL: https://www.xilinx.com/content/dam/xilinx/support/documents/sw_manuals/xilinx14_7/PlanAhead_UserGuide.pdf.

[79] *ChipScope Pro Software and Cores User Guide*. v14.3. UG029, accessed October 16th, 2023. Xilinx Inc. Oct. 2012. URL: http://www.xilinx.com/support/documentation/sw_manuals/xilinx14_7/chipscope_pro_sw_cores_ug029.pdf.

[80] *LocalLink Interface Specification*. v2.0. SP006. Xilinx Inc. July 2005.

[81] Dennis Getzkow. "High Level Trigger Interface for PXD-Event Filtering". unpublished thesis. MA thesis. Justus Liebig University Giessen, 2015.

[82] *Control System Studio*. accessed January 2nd, 2023. URL: https://controlsystemstudio.org/.

[83] Klemens Lautenbach and Justus Liebig University Giessen. "High Speed Data Multiplexer for the Belle II Pixel Detector & Search for an Exotic Resonance at the D*0 anti-D*0 Threshold in Charged B Meson Decays". engl. accessed October 16th, 2023. PhD thesis. Justus Liebig University Giessen, 2020. DOI: 10.22029/JLUPUB-9840. URL: https://jlupub.ub.uni-giessen.de//handle/jlupub/10456.

[84] *Belle II Official ELOG for Tests and Operation*. ELOG for Tests and Operation at KEK (restricted access). Belle II. URL: https://elog.belle2.org/elog/.

[85] R. Diener et al. "The DESY II test beam facility". In: *Nuclear Instruments and Methods in Physics Research Section A: Accelerators, Spectrometers, Detectors and Associated Equipment* 922 (2019). accessed November 1st, 2023, pp. 265–286. ISSN: 0168-9002. DOI: https://doi.org/10.1016/j.nima.2018.11.133. URL: https://www.sciencedirect.com/science/article/pii/S0168900218317868.

[86] Tomoyuki Konno et al. "Integration of Readout of Vertex Detector in Belle II DAQ System". In: *Proceedings of International Conference on Technology and Instrumentation in Particle Physics 2017*. Ed. by Zhen-An Liu. Vol. 1. Springer Singapore, 2018.

[87] K. Lautenbach et al. "The Belle II Pixel Detector Data Acquisition and Background Suppression System". In: *Journal of Instrumentation* 12.06 (June 2017), p. C06023. DOI: 10.1088/1748-0221/12/06/C06023. URL: https://dx.doi.org/10.1088/1748-0221/12/06/C06023.

[88] Florian Lütticke on behalf of the test beam crew. "Session: "Pedestal calculation and Mapping alternatives": Mysterious Mapping Mess". In: *20th International Workshop on DEPFET Detectors and Applications*. accessed January 2nd, 2023. May 2016. URL: https://indico.mpp.mpg.de/event/4247/sessions/1834/#20160513.

[89] Andreas Moll et al. "The vertex detector numbering scheme". Belle II Note Number 0010, Belle II internal document. Sept. 2016.

[90] Sören Lange. *ONSEN phase 2 readiness*. accessed January 4th, 2023. Belle II. June 2017. URL: https://kds.kek.jp/event/24563/contributions/76778/attachments/61434/72859/lange_B2GM062017_pxd.pdf.

[91] Thomas Geßler et al. *ONSEN Lab Tests and Development*. accessed January 4th, 2023. 2017. URL: https://indico.mpp.mpg.de/event/5220/contributions/11886/attachments/9068/10066/170529_depfet_ringberg.pdf.

[92] René Brun and Fons Rademakers. "ROOT - An Object-Oriented Data Analysis Framework." In: *Proceedings AIHENP'96 Workshop, Lausanne, Sep. 1996, Nucl. Inst. & Meth. in Phys. Res. A 389 (1997) 81-86. See also https://root.cern/* (Apr. 1997). Paper published in the Linux Journal, Issue 51, July 1998. https://root.cern/ was accessed October 14th, 2023. DOI: 10.1016/S0168-9002(97)00048-X. URL: https://root.cern/download/lj.ps.gz.

[93] Sören Lange et al. *ONSEN System - Lessons from DESY testbeam 04/2016*. accessed January 4th, 2023. Belle II. June 2016. URL: https://kds.kek.jp/event/21740/contributions/60183/attachments/48106/57182/lange_b2gm_062016_pxd_v1.pdf.

[94] *JENNIFER*. accessed December 30th, 2022. URL: http://www.jennifer-project.eu/.

[95] *boost C++ Libraries*. accessed November 19th, 2023. URL: https://www.boost.org/doc/libs/1_83_0/libs/crc/crc.html.